ABSTRACT

VAN DYK, HERMANUS. Development of a Wood Fiber Composite using Nonwoven Textile Technology. (Under the direction of Dr. Ilona Peszlen and Dr. Perry Peralta.)

The feasibility of manufacturing engineered wood composites with nonwoven textile technology was investigated. Needlepunching is a nonwoven textile process which converts fiber mats into coherent fabric structures with a three dimensional character. This is done by means of barbed needles, which oscillate in a vertical or slanted direction with regards to the surface of the fiber mat. Hardwood fiber was blended with 10% urea formaldehyde and formed into mats (2.3, 4.6 and 6.9 mm thick) with target densities of 550 and 640 kg/m^3. The mats were then sandwiched with polypropylene / polyester bicomponent fiber webs and passed through a needleloom. The barbed needles mechanically bonded the bicomponent web to the wood fiber mat, and pulled some of the polymer fibers through the thickness direction of the mat. Bending and thickness swelling properties of the needlepunched wood composite were qualitatively assessed and compared to medium density fiberboard (MDF).

A macro-mechanical model predicting the elastic response of the wood-bicomponent fiber composite panel was developed. The strains at a given stress was determined by means of the model, and compared to strains determined experimentally. The model under predicted the strains along the fiber direction of the bicomponent fiber sheets by approximately 4.03 percent. A greater difference between predicted and measured values was observed in the lateral direction of 10 percent.

To further understand the behavior of the material, a hygro expansion model was developed for a wood-bicomponent fiber composite panel. The dimensional changes predicted by the model due to moisture fluctuation were compared to experimental data. No significant difference was found between the predicted and measured dimensions. However, significant differences were found between the state of strain predicted by the model and the measure state of strain in the x-direction in the panels.

The tensile behavior of the wood-bicomponent fiber composite under simulated long term load was studied. Short term creep tests were conducted at different temperatures and were shifted to a reference temperature to simulate long term creep tests. It was found that the shift factor used followed the WLF equation. Creep tests were conducted on bicomponent fiber sheets, MDF and the composite itself. It was observed that MDF creeped the least, with the greatest creep observed in the bicomponent fiber sheets. The wood-bicomponent fiber panel exhibited an intermediate creep.

Development of a Wood Fiber Composite using Nonwoven Textile Technology

by
Herman van Dyk

A dissertation submitted to the Graduate Faculty of
North Carolina State University
in partial fulfillment of the
requirements for the Degree of
Doctor of Philosophy

Wood and Paper Science

Raleigh, North Carolina
2008

APPROVED BY:

_____	_____
Dr. Pam Banks-Lee	Dr. Jag Kasichainula
_____	_____
Dr. Joel Pawlak	Dr. Perry Peralta Co Chair of Advisory Committee

_____
Dr. Ilona Peszlen
Chair of Advisory Committee

Dedication

To Semra.

Biography

Hermanus van Dyk completed his undergraduate degree in Forestry (Wood Science) at the University of Stellenbosch, Stellenbosch, South Africa in December, 2000. He worked at the Department of Physics at the University of Stellenbosch until June, 2002, after which he started his Masters degree in Wood Science at the University of Maine, Orono, ME. He completed his Masters degree in 2004. Upon completion of his Masters, he joined the Department of Wood and Paper Science at North Carolina State University, Raleigh, NC as a PhD student.

Table of Contents

List of Figures

List of Tables

Chapter 1: Development of a Wood-Bicomponent Fiber Composite

Abstract

The feasibility of manufacturing engineered wood composites with nonwoven textile technology was investigated. Needlepunching is a nonwoven textile process which converts fiber mats into coherent fabric structures with a three dimensional character. This is done by means of barbed needles, which oscillate in a vertical or slanted direction with regards to the surface of the fiber mat. Hardwood fiber was blended with 10% urea formaldehyde and formed into mats (2.3, 4.6 and 6.9 mm thick) with target densities of 550 and 640 kg/m^3. The mats were then sandwiched with polypropylene / polyester bicomponent fiber webs and passed through a needleloom. The barbed needles mechanically bonded the bicomponent web to the wood fiber mat, and pulled some of the polymer fibers through the thickness direction of the mat. The mats were then pressed until the urea formaldehyde was fully cured. Properties of the needlepunched wood composite were qualitatively assessed and compared to medium density fiberboard (MDF). An average increase in storage modulus of 40 percent was observed for the 640 kg/m^3 panels and 48 percent for the 550 kg/m^3 panels.

1.1) Introduction

Medium density fiberboard (MDF) is a wood based composite material that draws on the usage of wood fibres, rather than particles or veneers to produce board or sheet products (Guess et al. 2003). It is typically made as a board type product, replacing particleboard in

furniture manufacture, cabinet making, joinery, craft work and flooring. Its advantages include relatively high strength, ease of machining and the ability to be made from a wide variety of fibrous products. Its use as a structural product has, however, been limited by unacceptable weathering properties, particularly thickness swell as a result of moisture fluctuation.

Recently, technology has evolved for combining wood fiber and flour with plastics to make panel and molded products. Polypropylene and polyethylene are most commonly used due to cost, ease of processing and relative compatibility with wood fibers. According to Pirvu et al. (2004), fiber reinforced composites are found in a wide range of applications due to their high strength and stiffness. Recent studies have shown that fiber reinforced wood and wood-based materials show great promise as structural components in applications like bridge decking and beams. Attempts have also been made to incorporate stronger polymer fibers into a wood product, but these have been limited by problems associated with wood fiber and polymer adhesion (Gillahm et al., 2000; Park and Seo, 1993; Youngvist et al., 1992).

Fibers from polymer blends have been increasingly used to modify the physical properties of fabrics. These bicomponent fibers consist of at least two components, running parallel in the fiber throughout the length. Each of the components of the fiber retains its own characteristic properties. This research will focus on polypropylene / polyester bicomponent fibers used in the nonwoven textile industry and investigate the feasibility of incorporating these fibers into a wood panel product.

1.2) Background

1.2.1) Needlepunching

Needlepunching was developed in the late 1800s for producing carpet underlays and spring padding of mattresses and furniture from coarse animal hair and vegetable fibers (Hearle, 1972). The technology was adopted in the 1930's by the automotive industry, while it was widely adopted by the textile industry in the 1950's (Purdy, 1980).

Needlepunching is a process for converting fiber webs into coherent fabric structures (Krcma, 1971). This is done by means of barbed needles, which oscillate in a vertical or slanted direction with regards to the surface of the fiber web (Mrstina and Fejgl 1990). The barbed needles repeatedly penetrate or punch into the fiber web, reorienting fibers from the horizontal to the vertical plane (Figure 1.1). The vertical structure of the fabric consists of tufts of fiber pulled down through the web by the needles, while the horizontal structure consists of fibers following curved paths around these tufts (Lennox-Kerr 1972). This reorientation of some fibers in the vertical plane and the presence of fibers in both planes produce a coherent structure with improved mechanical properties (Mrstina and Fejgl 1990). The lateral disturbance of fibers not directly involved with needles is also an important factor in the formation of a fabric which is resistant to stressing (Purdy 1980). Both natural fibers, such as wool, cotton, jute and sisal, and synthetic fibers, such as polypropylene, polyethylene, rayon and nylon, have been used in manufacturing needle punched fabrics or panels.

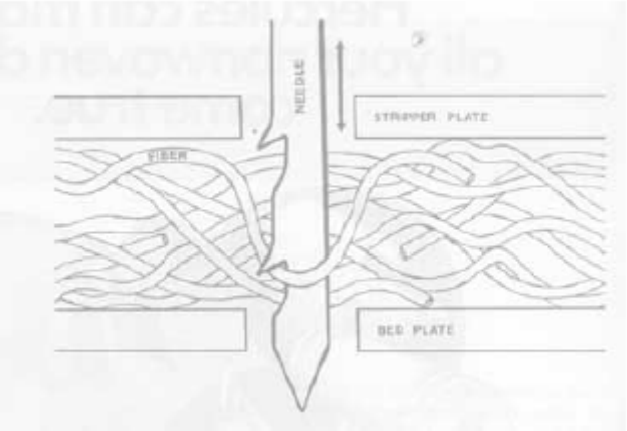

Figure 1.1: Action of the needle during needlepunching (Dedov 2008).

1.2.1.1) Components involved in needling

As illustrated in Figure 1.2 the web from a web forming system is fed into the loom by means of feed rolls. If the web is too bulky to fit into the working part of the loom, it is first passed through a converging channel or a pair of consolidating rollers to partially compress it (Batra et al. 2003). It is then passed through a horizontal channel formed by the bed and stripper plates, where the needles are passed through the web (Huntoon, 1990).

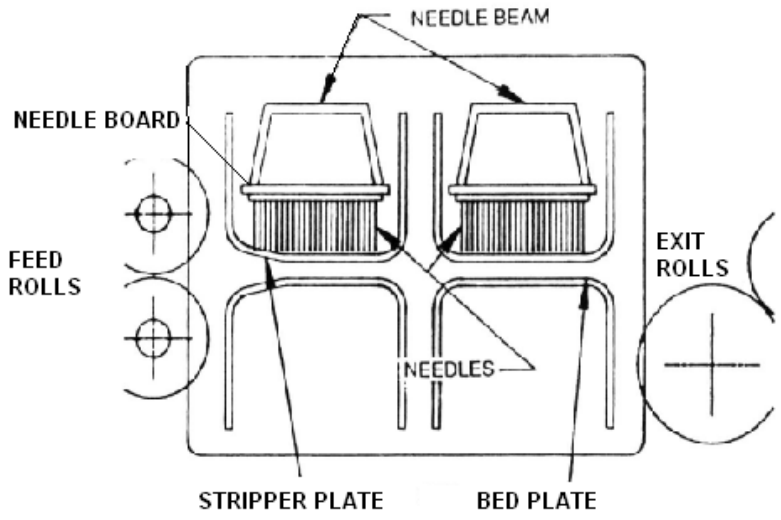

Figure 1.2: A diagram of a double arbor needle loom (Kamath et al. 2004).

The needles are inserted and held in a needle board. The needles are arranged in the needle board in rows extending along the width of the board (Batra et al. 2003). Spacing of the needles relative to each other in the board may differ depending on the nature of the needles and the products being produced. The needle board then fits into the needle beam that holds the needle board into place (Mcdonald, 1971). The vertical motion of the beam, which drives the needles in and out of the web, is applied by means of an eccentric crank mechanism (Batra et al. 2003). In the down stroke mode, the needles descend through the stripper plate, through the web and through the bed plate. Corresponding holes are located in each plate and it is through these holes the needles pass in and out (Hyungsup, 1998). The needles carry bundles of fiber through the bed plate holes. The stripper plate does what the

name implies; it strips the fibers from the needle so the material can advance through the needle loom (Batra et al. 2003).

According to Batra et al. (2003), the needling process can be done with a single or multiple beam looms. By placing multiple beams in a row on the same pass of the fabric, manufacturers can increase the needling density without decreasing the throughput speed. Another aspect to be considered is the formation of trumpet-shaped fiber arrangements caused by the action of the needles. During the descending action of the needle, the barbs pick up fibers from the surface as well as through the cross section of the web and push them towards the back. When the needles retract, the reoriented fibers are generally left undisturbed in their new position, creating a trumpet shape. If the web is only subjected to one-sided needling, one of the faces will be smooth, while the other will appear fuzzy. To overcome this problem, the web is needled from both sides (symmetric needling).

1.2.1.2) Needle design and choice

The choice of needle can make or break the needle punched product. The proper selection of gauge, barb, point type and blade shape (pinch blade, star blade, conical) is critical in both manufacturing and the final quality of the product (Kamath et al. 2004).

The gauge of the needles is defined as the number of needles that can be fitted in a square inch area. Thus, the finer the needles, the higher the gauge of the needles. Coarse fibers and crude products use lower gauge needles, and fine fibers and delicate fibers use higher gauge needles (Kamath et al. 2004).

According to Kamath et al. (2004), the major components of the basic felting needle are as follows (Figure 1.3):

- The crank: The crank is the 90 degree bend on the top of the needle. It seats the needle when inserted into the needle board.
- The shank: The shank is the thickest part of the needle. The shank is that part of the needle that fits directly in the needle board itself.
- The intermediate blade: The intermediate blade is put on fine gauge needles to make them more flexible and somewhat easier to put inside the needle board. This is typically put on 32 gauge needles and finer.
- The blade: The blade is the working part of the needle. The blade is what passes into the web and is where the all important barbs are placed.
- The barbs: The barbs are the most important part of the needle. It is the barb that carries and interlocks the fibers The shape and sized of the barbs can dramatically affect the needled product
- The point: The point is the very tip of the needle. It is important that the point is of correct proportion and design to ensure minimal needle breakage and maximize surface appearance.

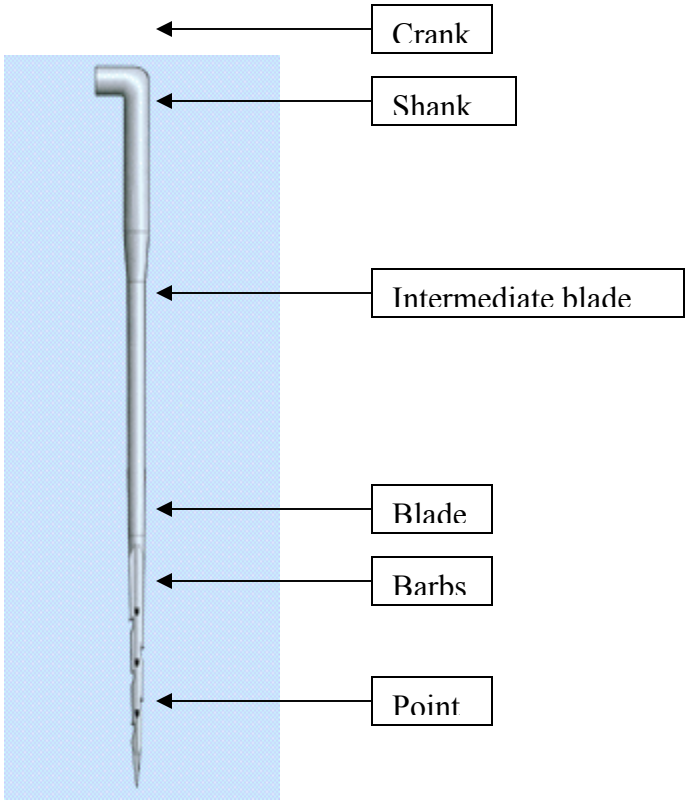

Figure 1.3: A representation of a needle used during needlepunching (Anon 2004)

The length of the working part (blade) of the needle may vary, as well as the amount and distance between the barbs. The barb shape can either be conventional, radius flow or rounded. In the past, needles were primarily triangular in shape. To meet the needs of specialty markets, new shapes such as tri-star, tear drop or crown needles have been developed (Batra et al. 2003; Kamath et al. 2004; Narejo and Collins, 2002; Mrstina and Fjeigl, 1990).

The choice of both the needle and needling parameters depend on a variety of factors. The amount of fiber rearrangement and entanglement that is needed to achieve the desired

end-properties needs to be considered in conjunction with fiber properties. Fiber properties such as fiber strength, surface qualities and friction, fiber dimensions and crimp all play a role in determining needling parameters and choice of needle. There is therefore no definitive guide to choosing the needle type and design characteristics if all the factors influencing the process are considered. Needle choice is therefore often determined by trial and error (Batra et al. 2003; Kamath et al. 2004; Narejo and Collins, 2002; Mrstina and Fjeigl, 1990).

1.2.1.3) Mechanical effect of needlepunching

Before needling, the fibers in the un-bonded web lie in layers parallel to the plane of the web and have very few intra-layer fiber entanglements (Batra et al, 2003). The mechanical properties of needle-punched nonwoven fabrics depend on the fiber entanglement effected by the needles. The needle barbs catch the fibers during punching and lead them into the thickness direction, creating fiber-to-fiber entanglement (Watanabe et al. 2005). The tensile properties of a needle-punched nonwoven are determined by its structural parameters and fiber properties. When a needlepunched web is subjected to in-plane tensile forces, the entangled fibers interlock due to frictional forces and resist slippage (Batra et al. 2003, Hearle, 1972). This mechanism is the primary source of the web strength.

According to Batra et al. (2003), it is well known that the larger the number of fibers caught by the needle, the greater entanglement of the fibers and the stronger the nonwoven. If the needle is extremely thick, the barbs catch too many fibers and lead them into the thickness direction, partially destroying the web structure. This is also a factor whenconsidering the punch density of the process, where a high punch density can lead to

excessive rearrangement of fibers in the web. Punch density is calculated as follows (Batra et al. 2003):

$$d = \frac{ns}{v} \qquad \text{Eq. 1.1}$$

Where: d = punch density (punches/m^2)

n = number of needles per unit length of the needle board (needles/m)

s = number of strokes per unit time (punches/minute)

v = rate of fabric delivery (m/minute)

In practice, the end use determines the desired fiber characteristics, basis weight of the web and the punch density required to obtain the optimal performance.

The process is used with webs made from both staple and continuous filament fibers. Depending on the fiber type and dimensions, the web basis weight and the processing parameters conventionally needled fabrics can display a range of strength characteristics, is generally quite resistant to tear or puncture damage.

Needlepunching a web inherently produces a structure that resists lateral (z-direction) crushing (Batra et al. 2003, Hearle, 1971). It also develops a graduation of fiber densities through the thickness. In a symmetrically needled fabric, the fiber density near the surface is quite high when compared to that in the center. This gives the final product the unique ability

to permit fluid flow in the plane of the fabric and makes needlepunched fabrics ideal for geotextile applications (Batra et al. 2003).

The following properties of needlepunched fabrics were listed by Mansfield (2005):

- Controlled fiber orientation in the machine or cross-machine direction, or at an intermediate angle
- Z-directional strength, which improves shear strength and reduces the potential for ply delamination
- High void volumes for easy absorption of resins
- Cost-effective thickness of composite structures by reducing the number of plies, weight, lay-up times and overall costs
- Ease of blending diverse fibers and fiber structures such as high-strength and thermoplastic fibers during the needlepunching process
- Distinct batt layering of two or more layers of distinct fiber types in one needlefelt, and the ability to incorporate lightweight woven fabrics, films and other fabric forms into the needlefelt structure
- Compressibility for easy molding or shaping, which allows for intricate design

1.2.1.4) Needle breakage

Needles can break due to a number of factors. Broken needles not only influence the quality of the final product due to the presence of needle tips in the material, but also the entire process performance. A large number of broken needles lead to maintenance downtime and additional costs in replacing the needles. It is therefore important to identify and rectify the causes of needles breaking. The following factors influence needle breakage (Anon 2004):

- Needle alignment: If the needle board is not aligned so the needles locate in the middle of the bed plate hole, breakage is likely
- The fiber quality can often cause needle breakage, especially when needlepunching waste and regenerated fibers.
- Unopened fiber particles can often break the needles or build up in the bed plate holes of the needle loom.
- Needling parameters, such as advance per stroke and punch density.
- Aggressive needling: If the barbs are too deep the load on the needle's blade can be too great and break the needles
- Old needle looms often cause vibration and or poor alignment that can lead to needle breakage, especially with fine gauge needles.
- Worn needle boards and worn inserts can cause the needles to be too loose in the needle boards. This can cause the needle to enter the fabric at an angle and break the felting needle and cause defects on the surface of the needled fabric.

- Uneven mass distribution in the web will lead to uneven stresses on the needle.

To minimize stresses and the resulting needle breakage, as well as to develop the desired structure of the finished product, proper size and shape of the needle is very important. There are now specialized needles available not only for different types of products, but also for different product weights (Narejo and Collins, 2002). Figure 1.4 illustrates a conical blade needle designed by Foster Needle Co. which is specifically designed for needling of coarser material where breakage is likely (http://www.fosterneedleusa.com/prd/ConicalBlade.html).

Figure 1.4: Conical shaped needle designed by Foster Needling Co.

As mentioned previously, needle breakage is also the result of uneven mass distribution across the roll width (Narejo and Collins, 2002). The higher the mass variation,

the greater the variation of stresses on the needle. Advances in fiber distribution control mechanisms have made it possible to manufacture products with uniform mass distribution which enable the manufacturer to control the stresses exerted on the needles during punching (Narejo and Collins, 2002).

Another important variable which influences the quality of the finish is the advance per stroke of the material (Narejo and Collins, 2002). The needles move in a vertical motion, while the web is pulled horizontally. The speed of the web through the loom is determined by how much distortion the web and the needles can absorb. In general, the higher the web penetration and web speed, the greater the stress on the needles. To compensate for this effect, needleboard manufacturers have developed an elliptical needle path (Narejo and Collins, 2002). The elliptical nature incorporates both a vertical and horizontal component in the stroke path, which allows the needle to move horizontally with the web. This leads to higher throughput speeds and less needle breakage.

1.2.2) Bicomponent Fiber

Bicomponent fibers are formed by extruding two polymers from the same spinneret with both polymers contained within the same filament. Bicomponent fibers were introduced by Dupont (Jangala and Kotra, 2004) in the mid 1960s. This was a side-by-side hosiery yarn called "cantrese" and was made from two nylon polymers, which, on retraction, formed a highly coiled elastic fiber. In the 1970s, various bicomponent fibers began to be made in Asia, notably in Japan. Very complex and expensive spin packs were used during the initial

phases of fiber production, limiting their use. In 1989, however, a novel approach was developed using thin flat plates with holes and grooves to route the polymers (Kikutani, et al., 1996). This process was very flexible and quite cost effective.

A wide range of polymers are used to manufacture bicomponents, including polyester, nylon 6,6, polypropylene and co-polyamides. The main objective of producing bicomponent fibers is to exploit capabilities not existing in either polymer alone. By this technique, it is possible to produce fibers of any cross sectional shape or geometry that can be imagined. Bicomponent fibers are commonly classified by their fiber cross-section structures as side-by-side, sheath-core, islands-in-the-sea and segmented-pie cross-section types.

Figure 1.5 illustrates examples of the four different fiber types. Side-by-side bicomponent fibers consist of two components divided along the length into two or more distinct regions. They are generally used as self-crimping fibers. Different melting points on the sides of the fiber are taken advantage of when fibers are used as bonding fibers in thermally bonded non-woven webs. Sheath-core bicomponent fibers are those fibers where one of the components (core) is fully surrounded by the second component (sheath). These fibers are widely used as bonding fibers in nonwoven industry. The sheath of the fiber is of a lower melting point than the core and so in an elevated temperature, the sheath melts, creating bonding pints with adjacent fibers - either bicomponent or monocomponent. Islands-in-the-sea bicomponent fibers contain areas of one polymer in a matrix of a second polymer. These types of bicomponent structure facilitate the generation of micro denier fibers.

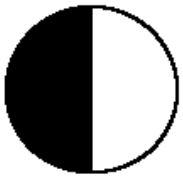

Figure 1.5a: Side-by-side bicomponent fiber

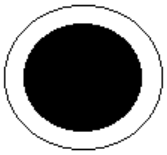

Figure 1.5b: Sheath-core bicomponent fiber

Figure 1.5c: Islands-in-the-sea bicomponent fiber

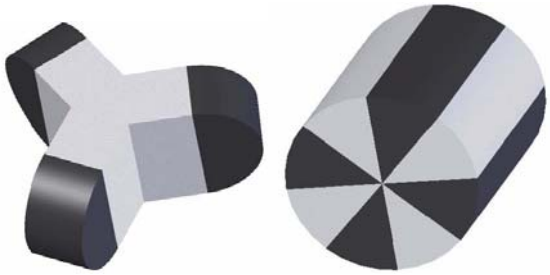

Figure 1.5d: Tipped trilobal and segmented pie bicomponent fibers

Figure 1.5: A representation of commonly used bicomponent fiber types (Hyungup 1998).

Polyester has a specific gravity which can range from 1.26 to 1.34, with a flexural modulus of 1400 to 2690 MPa, depending on the formulation used and the supplier. Polypropylene has a reported specific gravity of 0.899 to 0.901, with a flexural modulus of 694 to 2190 MPa (Perry and Green 1997). Glass transitions for the respective polymers are 69 and -18^{o}C respectively.

1.2.3) Medium Density Fiberboard (MDF)

MDF consists of wood fibers (including; tracheids in softwoods, and vessels, fibres, fiber-tracheids and parenchyma cells in hardwood (Evans, 1994)) blended with synthetic thermosetting formaldehyde based resins and then pressed into boards. MDF can be made from a wide variety of lignocellulosic materials and an important implication of this is the use of recycled materials and non-wood fibres in its manufacture. Many softwoods and even bamboo (Wang, 1991), rice husks and waste paper (Dube, 1995) have been used successfully in the manufacture of MDF, although the type of fiber used in its manufacture strongly influence board properties (Myers, 1983). Combinations of wood and non-wood materials are increasingly being used to enhance specific properties, particularly strength, density and sorption characteristics (Park, 1993). MDF is increasingly being used as a replacement for other wood products, and its use in engineering fields is increasing. Figure 1.6 illustrates the manufacturing process of MDF.

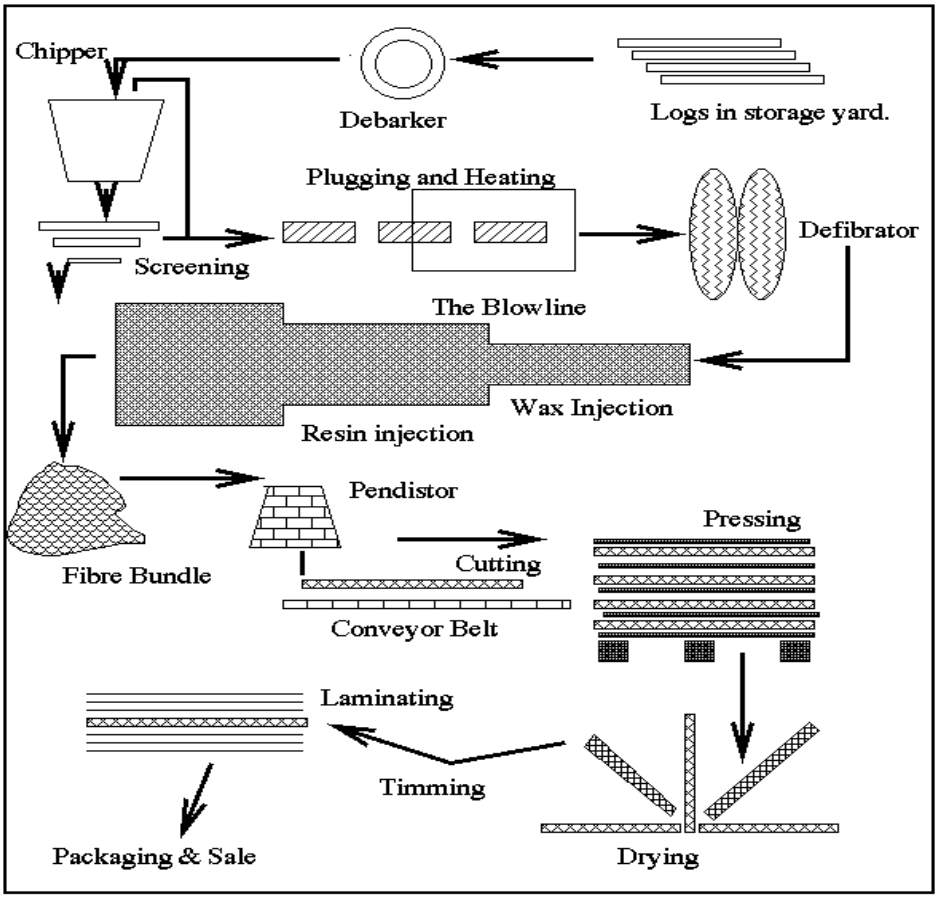

Figure 1.6: A schematic representation of an industrial MDF manufacturing process (Beutel, 1996)

Once the MDF plant has obtained suitable logs, the first process is debarking. The logs could be used with the bark, as could any fibrous material, but for optimisation of the final product the bark is removed to decrease equipment damaging grit, allow faster drainage of water during mat formation, decrease organic waste load by 10-15 %, stabilize pH levels (reduces corrosion of tools) and increase surface finish. Although some plants accept chips directly from other operations, chipping is typically done at the MDF plant. A disc chipper,

containing anything from four to sixteen blades, is used. The blades are arranged radially on a plate and the spinning plate is faced perpendicularly to the log feed. The feed speed of the logs, the radial speed of the knife plate, the protrusion distance of the knives and the angle of the knives, control the chip size. The chips are then screened and those that are oversized may be rechipped. The chips can be pulped using a Masonite gun process, atmospheric or pressurized disk refiner. After defibration fibers enter the blow line. The blow line is initially only 40mm in diameter with the fibers passing through at high velocity. Wax, used to improve the moisture resistance of the finished board, and resin are added in the blow line while the fibers are still wet, as dry fibers would form bundles, due to hydro bonding, and material consistency would be lost. The fibers are dried by heating coils warming the blowline to about 6-12 percent moisture content. After drying, mat formation is accomplished by means of airlaying. The mat can either be laterally cut to size as it leaves the pendistor or it can be cut half way through its run by a synchronised flying cut off saw. The density profile of the panel is critical to achieving satisfactory strength properties. Concentrating mass, and hence load bearing ability, at the top and bottom of the board means that inertial properties are maximized and the greatest strength can be obtained for minimal weight. This is achieved by the press acting at impacted pressure initially and then slower pressure application. As an example, for a 16mm board:

- Press closed. 20 seconds to bring mat to 28 mm.
- 28 seconds at 26mm.
- 23 seconds at 25mm.
- 125 seconds at 18.3

- Total time of 330 seconds to bring board to 16mm, then decompression time.

1.3) Materials and methods

Hardwood fibers and urea formaldehyde resin were obtained from DYNEA, Moncure, North Carolina. The resin mixture and resin/fiber ratios were calculated by means of the blending spreadsheet used by DYNEA in their in-house testing procedures. Fiber moisture content was established by oven drying.

Initial separation and blending of the wood fiber with the urea formaldehyde was done in a rotary drum blender designed and constructed at North Carolina State University. The blender drum has a diameter of 2 meters, with an atomizing spray nozzle attached in the center of the drum. After consultation with researchers at DYNEA, a 10 percent resin blend was decided on with board densities of 550 and 640 kg/m^3.

Fiber separation and randomization was accomplished by means of a C.S Bell Company 10HBML rotary hammermill with a cyclone attachment (Figure 1.7). The purpose of hammer milling was to break up any balls of fiber formed in blending with resin.

Figure 1.7: C.S. Bell 10HBML hammermill used during this research (http://www.csbellco.com/hammer.htm).

The cyclone attachment deposited fibers into a 0.61 by 0.30 m forming box. The fiber was manually fed into the hammermill, with each handful of fibers given adequate time to pass through the machine and into the forming box to avoid blockage. When all the fiber had been put into the forming box, the mats were manually precompressed. Figure 1.8 illustrates the forming box used during the course of this research.

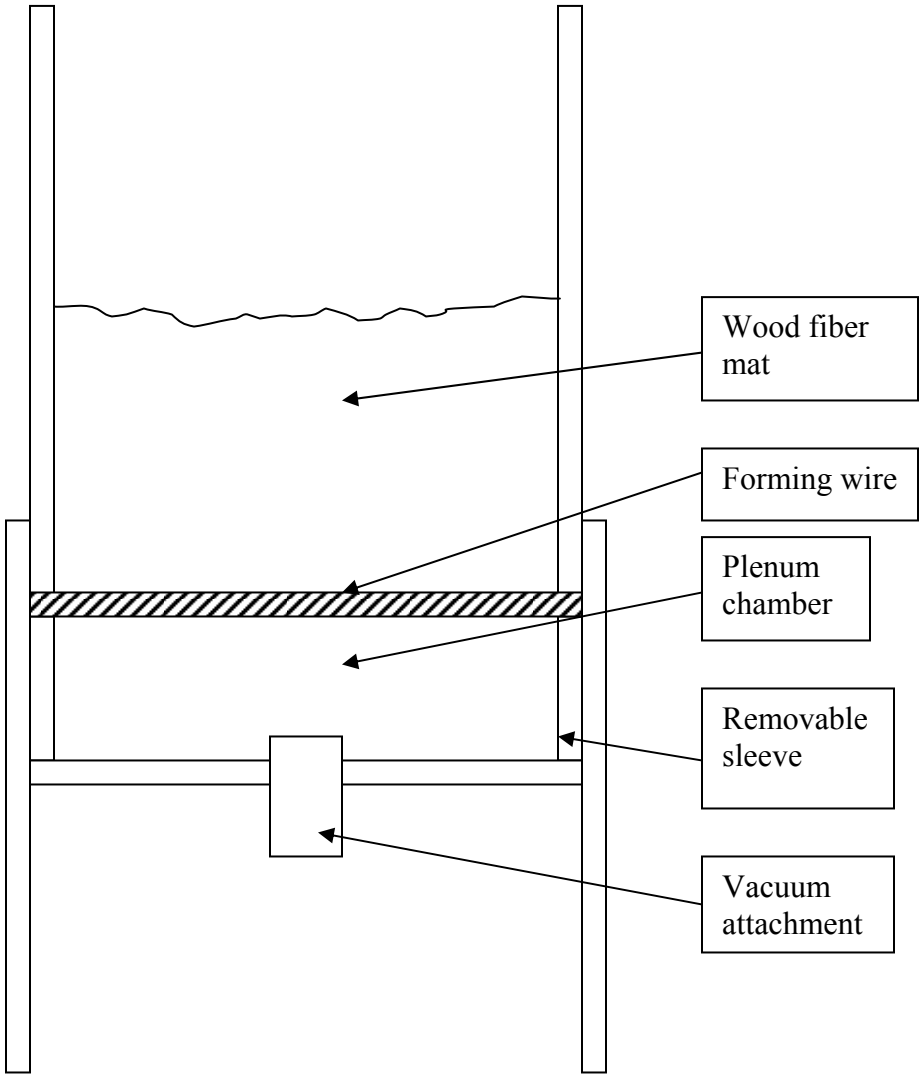

Figure 1.8: Design of the forming box used for mat formation.

Depending on the target thickness of the board, the average height of the mat was 100 to 250 mm. To reduce the mat height and to densify the mat, the mat was cold-pressed to approximately 20 to 100 mm using the Bryan 200 prepress. This allowed for easy handling and insertion into the hot press. Initially, the panels were consolidated using a steam-heated press. Later experiments were conducted using an electrically heated, manually controlled Carver 3912 press. The press temperature was approximately 177°C. Panels were pressed for 3 minutes at a minimum pressure of 68 MPa.

Internal bond strength tests were conducted on 50 by 50 mm samples to ensure that the MDF met industry requirements. A thermoplastic resin was applied to the surfaces of the samples, and heated aluminum testing fixtures were adhered. The testing fixtures were carefully aligned with the grip grooves on both surfaces kept parallel. Samples were tested to failure in an MTS testing machine in accordance with ASTM D1037 (ASTM 2006).

Due to inadequate bonding between the wood fiber and the PET, it was decided to switch to a polypropylene / PET bicomponent (BC) fiber, obtained from Fiber Innovation Technologies, Inc, Knoxville, Tennessee. The fiber length was 38 mm, with a fiber diameter of 3 denier (+- 0.3 denier). Fiber crimp was 11.0 percent (+- 1.5 %). The sheath melt temperature was listed as 165^{o}C. A DSC scan was conducted on the raw fiber by means of a TA Q100 differential scanning calorimeter.

The bicomponent fiber arrived in bale form, and was opened, carded and crosslapped to form fiber webs with a basis weight of 140 gsm in the laboratories of the Nonwoven Cooperative

Research Center at NCSU. Carding is a web forming process in which the fibers are opened and parallelized by means of rotating cylinders. The cylinders rotate at different speeds and have angled needles on the surface which combs the fibers to form a web with a distinct fiber orientation. The resultant bicomponent fiber web produced by the card had a very low basis weight, and it was decided to crosslap the material Crosslapping involves a pendulum conveyor which lays the web in to folds onto a conveyor belt. A low crosslapping angle was employed in order to maintain fiber orientation in the final product. A fiber orientation distribution analyses was conducted using a Fast Fourier Transform on backscattered light obtained from images of the nonwoven taken by a light microscope.

Initial experimentation involved the manufacture of a simple sandwich panel with the bicomponent fiber web on the surfaces, and wood fiber in the core. Adhesion between the polymer and wood fiber was found to be lower than desired and it was determined that the additional mechanical interlocking achieved with a needleloom was needed in order to ensure panel integrity. The needleloom used was James Hunter Machine Co. pilot scale loom. Needles were obtained from Foster Needle, Manitowoc WI.

Sample beams with dimensions of 12.5 by 50 mm were cut with a table saw from the different panels made in this study. These beams were tested in a TA Q800 Dynamic mechanical analyzer (DMA) with a double cantilever testing jig. A first set of samples were cut with the fiber alignment along the longitudinal axis (L) of the beams, and a second set was cut with fibers aligned perpendicular to the longitudinal access (C). Samples were conditioned to 9 percent moisture content for 10 days. Sample dimensions were carefully

measured and the samples were weighed. Three samples per panel falling within 3 percent of the target densities were selected for testing. A set strain of 0.5% was applied to the samples at a frequency of 1 Hz and the storage modulus was measured. The temperature in the chamber was kept constant at 26^{o}C. MDF panels were prepared and tested in conjunction with the laminate panels for comparison purposes.

1.4) Results and discussion

Experiments with MDF were conducted to determine the limitations of the experimental setup. Internal bond strength (IB) is a widely accepted industry standard to determine board properties. The boards manufactured during this research had an IB of 0.83 MPa (+- 0.2 MPa), which compared favorably with the results obtained by Xing et al. (2007) who listed IB values of between 0.67 and 1.2 MPa. The American National Standards Institute lists a minimum IB strength of 0.6 MPa for MDF (ANSI A208.2).

Figure 1.9 illustrates the results obtained from the fiber orientation distribution analyses conducted on the bicomponent fiber web. It can be seen that the web displays a higher degree of orientation with regards to the machine direction. The bimodal distribution is the result of crosslapping after the web is carded. This is in agreement with a fiber orientation analyses conducted by Ramal (2006) on webs produced with a 5^{o} cross lapping angle. This allowed control over the fiber orientation in the polymer webs when the bicomponent fiber webs were sandwiched with the wood fiber mats.

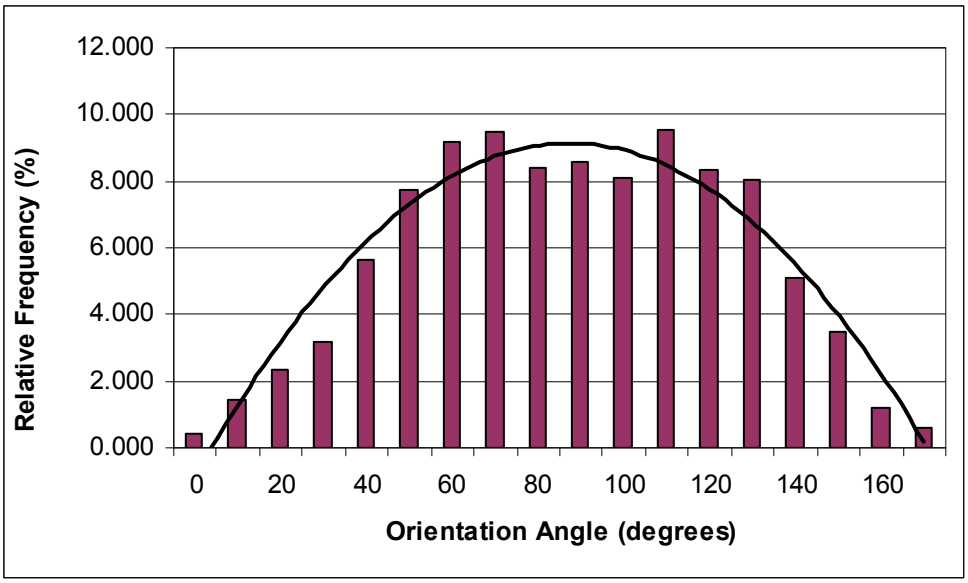

Figure 1.9: Fiber orientation distribution of the polypropylene / polyester bicomponent nonwoven fiber web used as reinforcement of a wood fiber composite.

Two panel products were considered for this research. The first consisted of wood / polymer fiber blend. This idea was discarded after initial attempts failed to obtain a homogenous blend in the rotary drum blending.

Initial experimentation involved determining whether the needlepunching process can successfully be applied to a wood fiber mat. It was quickly determined that wood fiber is two short to needlepunch. A longer carrier fiber was needed in order to insure the integrity of the fiber mat during the process and for adequate fiber entanglement.

The second panel product was a needlepunched composite laminate panel with a nonwoven web used in conjunction with resinated wood fiber. Initial experiments to

investigate the feasibility of the research method were conducted using polyester webs (PET) obtained from the Nonwoven Cooperative Research Center (NCRC) at NCSU. The webs used had basis weights of 60 and 100 grams per square meter (gsm) respectively. Figure 1.10 illustrates the panel obtained using a polyester web.

Figure 1.10: Wood-polyester fiber panels manufactured during initial phases of the project.

The biggest issue considered was to obtain the thickest possible final panel thickness at the desired panel density, while still adhering to the limitations of the needlepunching process. The needleloom used had a throat height of approximately 30 mm. Initial runs on the loom with approximately 7475 gsm wood fiber webs prepressed to less than 30 mm resulted in an excessive amount of needles breaking. In order to optimize the needle design and mat thickness, the needle types were changed and tested on wood fiber mats with basis

weights of 4485, 2990, 1495, 748 and 500 gsm respectively. Unfortunately, good records were not kept of the specific needles used, but the following will briefly describe how the needle choice was influenced.

The first runs on the loom were conducted using thin, 9 barb needles which were already present in the needleboard. The needle was only successful in punching the 500 gsm mats. To obtain the target densities of 550 and 640 kg/m^3 with a 500 gsm mat will result in a panel with final dimensions too thin for testing with conventional methods used in characterizing MDF. It was suggested that the needle damage might be caused by excess fibers being captured from the polyester webs on the surfaces. A thin 6 barb needle was tried, with similar results as observed with the 9 barb needle. An extremely thick carpeting needle managed to survive the punching process at all the basis weights, but, unfortunately, the fiber mats did not. Too much of the polyester fibers were captured, which resulted in the wood fiber breaking through the surfaces and the mat loosing integrity. Intermediate 9 and 6 barb needles failed as well. A stronger alloy needle used to punch kenaf fiber was investigated next. It performed well at 500 and 748 gsm, but both basis weights would still result in inadequate final panel thicknesses at the desired panel densities. An intermediate alloy needle was attempted with limited success up to 1495 gsm. A basis weight of 1495 gsm at 640kg/m^3 will result in a final panel thickness of 2.3 mm which was considered adequate. A conical blade 9 barb needle (F 20 9-20-3B) with a triangular crossection proved to be the most successful. hicker alloy needles were investigated, but they experienced similar problems as those observed with the carpeting needles.

Panels were differentiated according to punching depth. For the first panel type, the carded web was placed on top of 1495 gsm wood fiber and needlepunched (Figure 1.11). This provided adequate bonding for the surface laminate. Two of these needlepunched webs were then used to sandwich resinated wood fiber before consolidation in the press. The final panel thickness for this configuration was 6.9 mm.

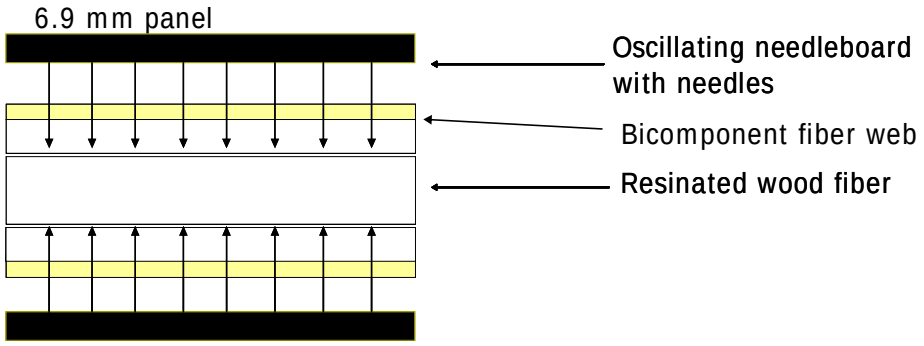

Figure 1.11: The 6.9 mm surface punched panels illustrating the different layers of the composite, and the areas affected by needling.

In the second panel type, a 1495 gsm wood fiber web was needlepunched in conjunction with a bicomponent web (Figure 1.12). Two needlepunched mats were placed on top of each other with the wood fiber facing the center. The final panel thickness after consolidation in the press was 4.6 mm.

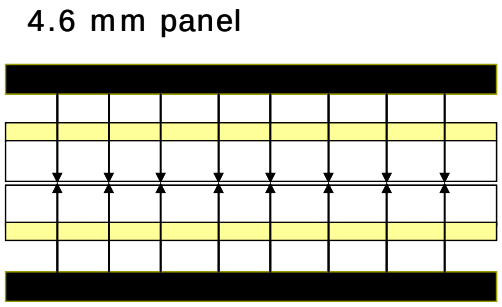

Figure 1.12: Illustration of a 4.6 mm half punched wood-bicomponent fiber panel.

The third was a sandwich panel containing a 1495 gsm wood fiber web punched all the way through with bicomponent fiber placed on both sides of the wood fiber mat (Figure 1.13). The panels were punched from both sides and had a final thickness after pressing of 2.3 mm.

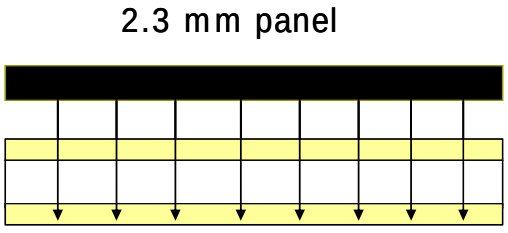

Figure 1.13: Illustration of the 2.3 mm punched through wood-bicomponent fiber panels.

The fiber alignment in the bicomponent webs were carefully noted and controlled during the formation of the panels with both surfaces of the panels having the same fiber alignment. Ten panels of each type were made at target densities of 550 and 640 kg/m^3. For the 550 kg/m^3 panels, 1285 gsm wood fiber webs were used. Figure 1.14 illustrates an unpressed and pressed sandwich panel with bicomponent fiber on the surfaces.

Figure 1.14a: Unconsolidated 4.3 mm half punched wood-bicomponent fiber panel.

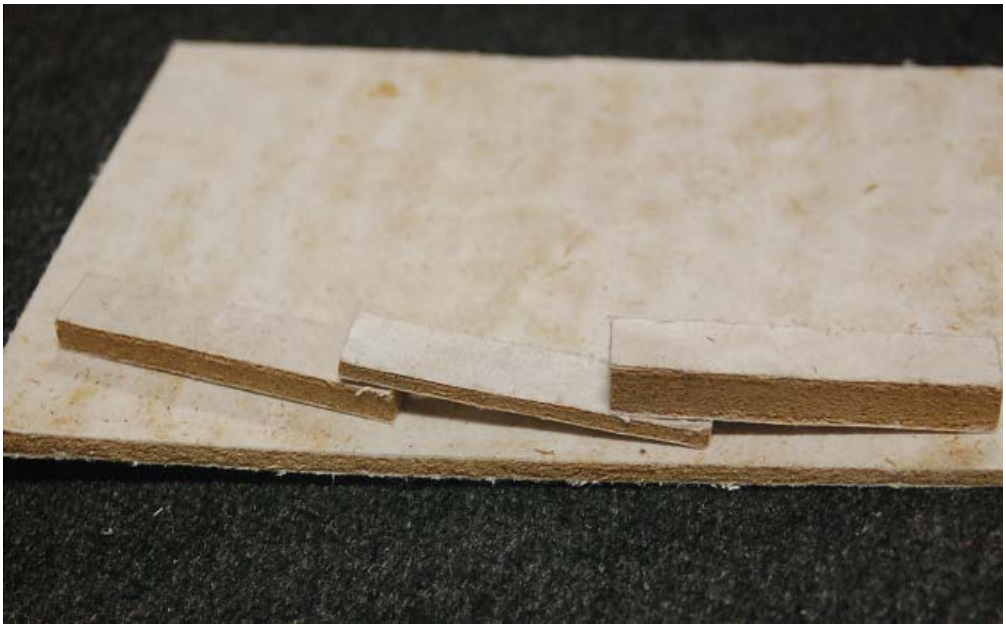

Figure 1.14b: Consolidated wood-bicomponent fiber panels.

Figure 1.14: Unconsolidated and consolidated wood-bicomponent fiber panels manufactured for this research.

To further investigate the interaction between the bicomponent and wood fibers, samples were prepared for imaging on a scanning electron microscope. The samples were first desiccated to a moisture content of 0 percent, prior to being sputter coated with gold. Figure 1.15 shows a bicomponent fiber tuft pulled from one surface through the wood fiber core, illustrating the action of the needles during punching. Figure 1.16 illustrates the interface between the surface reinforcement and the wood core. A wood fiber can be observed at the center of the scan, with a bicomponent fiber adjacent to it.

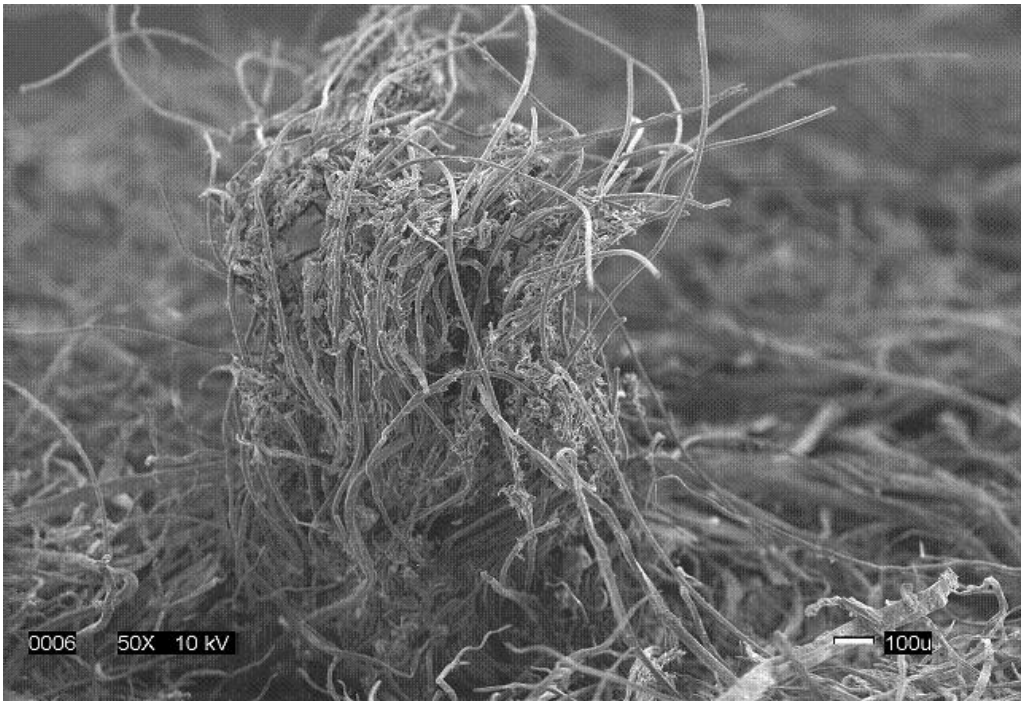

Figure 1.15: Fiber tuft protruding from the surface of the wood fiber core

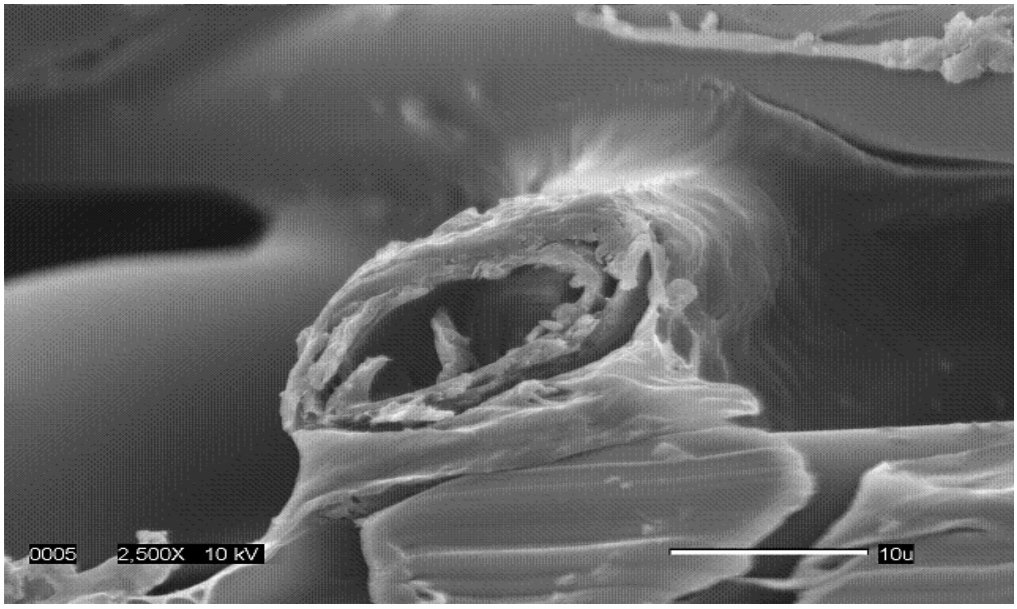

Figure 1.16: SEM scan of a wood fiber at the wood fiber / bicomponent fiber interface

Figure 1.17 illustrates a representative graph obtained from the DSC scan of the raw bicomponent fiber. The melting point of the polypropylene sheath can be observed at 165^{o}C, and that of the polyester core at 250^{o}C, which is in agreement with results publish by Perry and Green (1997). This shows that the polypropylene sheath will melt and fuse with the wood at the press temperature of 177^{o}C, while the polyester core will remain intact during pressing. A total of three samples were tested.

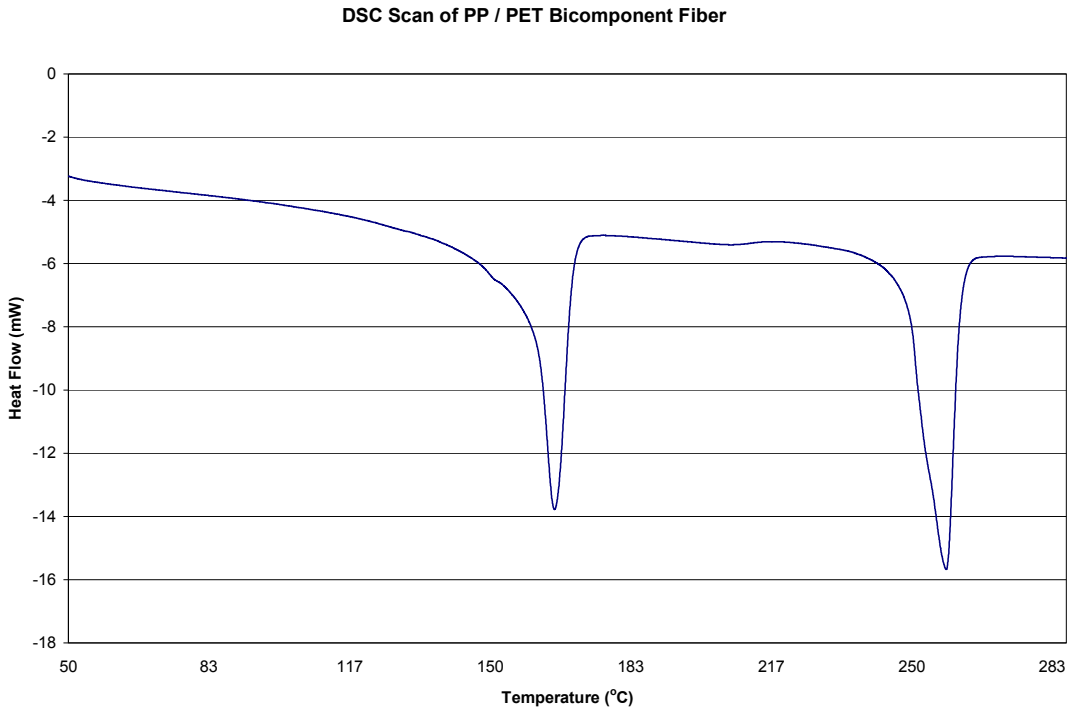

Figure 1.17: DSC scan of polypropylene / polyester bicomponent fiber showing the melting point of both polymer components.

Figure 1.18 illustrates the results obtained for the storage modulus of the 550 kg/ m^3 panels with the DMA. The mean storage modulus of all three MDF panel thicknesses were 392 MPa (Coefficient of variation (CV) 2.8 percent), while no significant difference in storage modulus was found between panel thicknesses. The mean storage modulus of the 2.3 mm punched through wood-bicomponent fiber laminate panel with the bicomponent fibers aligned along the longitudinal axis was found to be 563 MPa (CV 5.2 percent), while the storage modulus for the 4.6 half punched and 6.9 mm surface punched panels were 489 (CV

5.1 percent) and 501 (CV 4.5 percent) MPA respectively. All three values were significantly different from that obtained with MDF of the respective thicknesses. The storage modulus obtained from the 2.3 mm samples were, however, 11 percent higher than that obtained from the 4.6 and 6.9 mm samples. This can be attributed to the fact that the bicomponent fiber sheet is stiffer than MDF (see Chapter 3), and has a greater influence on the overall stiffness of the thin panels

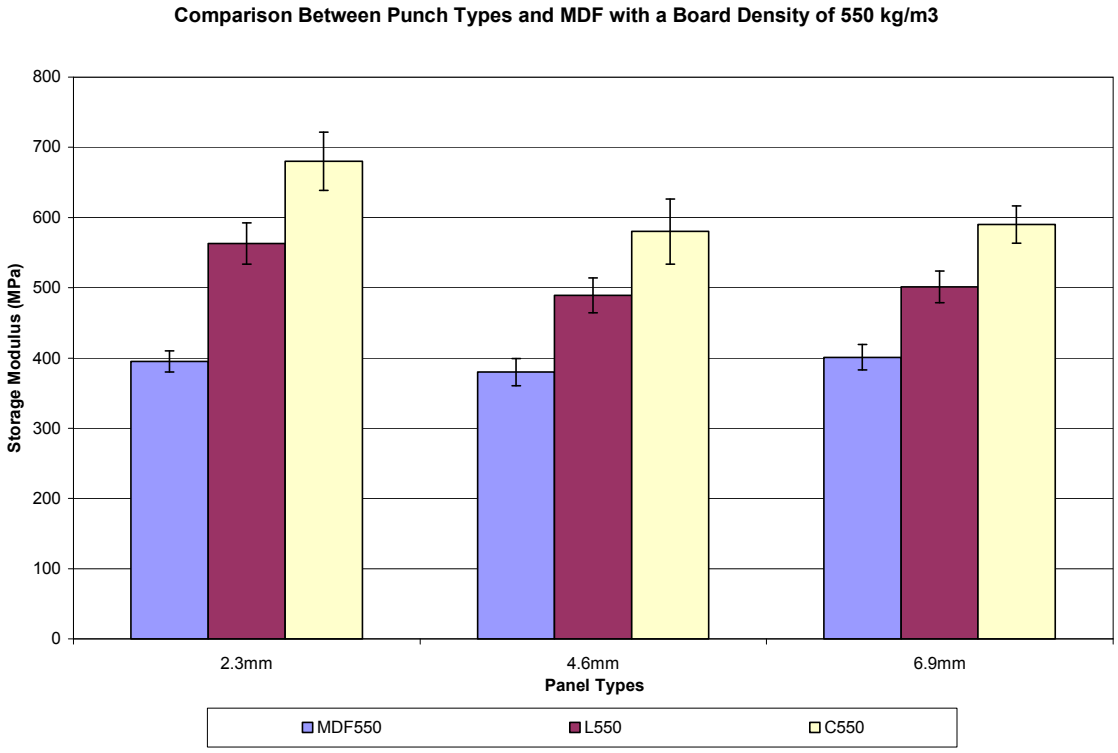

Figure 1.18: Storage modulus comparison of MDF with a board density of 550 kg/m3 (MDF550) and wood-bicomponent fiber panels with bicomponent fiber alignment along (L550) and across (C550) the testing beam length and for three punch types (2.3mm, 4.6mm and 6.9mm)

The storage modulus calculated when the bicomponent fibers aligned perpendicular to the longitudinal axis of the beams was found to be higher than that obtained from the longitudinally aligned fibers. Similar trends were observed with the cross-directional fibers, with the 2.3 mm panels having a significantly higher storage modulus than the 4.6 and 6.9 mm panels. The storage modulus for the 2.3, 4.6 and 6.9 mm panels were 683 (CV 5.8 percent), 581 (CV 8 percent) and 589 (CV 4.5 percent) MPa respectively. Further investigation is needed to determine why the longitudinal modulus is lower than the crossdirectional modulus.

Figure 1.19 illustrates the results of storage modulus measurements obtained from the 640 kg/m^3 panels. The results were similar as those obtained with the 550 kg/m^3 panels. An overall increase in storage modulus of 10 percent was observed due to the higher panel density. The relative difference between the storage modulus of the laminate panels and MDF was lower in the case of the 640 kg/m^3 panels than for the 550 kg/m^3 panels. This can be attributed to the greater influence of the lower stiffness wood fiber composite in the 640 kg/m^3 panels. Furthermore, there is an overall increase in the storage moduli with an increase in panel density. This is in agreement with Wu and Suchland (1998), who found that MOE increases linearly with an increase in panel density.

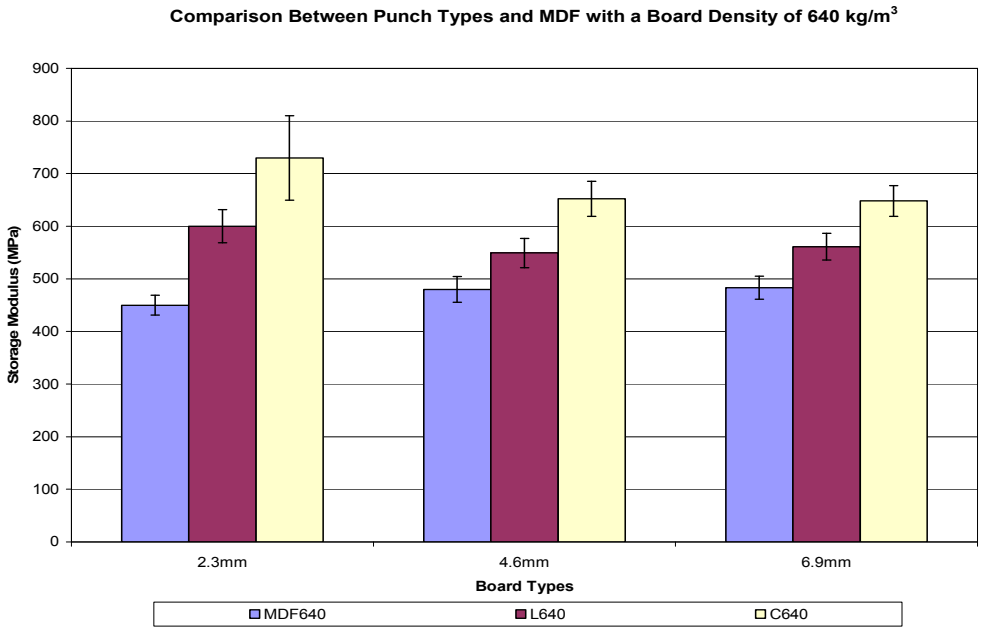

Figure 1.19: Storage modulus comparison of MDF with a board density of 640 kg/m^3 (MDF640) and wood-bicomponent fiber panels with bicomponent fiber alignment along (L640) and across (C640) the testing beam length and for three punch types (2.3mm, 4.6mm and 6.9mm)

1.5) Conclusion

Attempts have been made by the wood composites industry to blend a high strength fiber into a wood fiber panel product with some success. They are, however, limited by the difficulty of obtaining adequate wood fiber / polymer adhesion. Nonwoven textile technologies such as needlepunching and the use of bicomponent fibers could prove to be a viable option for incorporating high-end polymer fibers into an engineered wood fiber panel.

Polypropylene is commonly used to produce wood plastic composites and have been shown to form weak bond with wood flour. When hot-pressing the polypropylene / polyester (PP / PET) bicomponent fiber, the melt temperature of the polyester is not reached. PP, however, melts at approximately 165^{o}C. When incorporated into a wood fiber product, the PET component will remain intact, while the PP will melt and infuse into the wood fiber. This, along with the fiber rearrangement resulting from needlepunching, mechanically bonds the polyester fiber to the wood. The overall stiffnesses of the wood-bicomponent fiber laminate panels were found to be was significantly higher than that obtained from MDF.

The needlepunching process shows considerable promise for incorporation in an industrial setting. To overcome the problems of low final product thickness, minor adjustments need to be made to the needleloom machine parameters and the needle design.

1.6) References

American Society for Testing and Materials (ASTM). 2006. Standard methods for evaluating properties of wood-based fiber and particle panel materials. D1037. American Society for Testing and Materials, West Conshohocken, PA.

Anon. Why do needles break? Technical note, Foster Needles USA.

Batra, S.K., B. Pourdeyhimi and D. Shiffler. 2003. TT305: Fiberweb and nonwoven production. Classnotes.

Bosak, D.R., A.A. Ogale and J. van Dun. 2005. Bicomponent fibers derived from immiscible polymer blends. Textile Research Journal 75(1): 50-56.

Datla, V.M. 2002. The influence of fiber properties and processing conditions on the characeteristics of needlefelted fabrics. Masters thesis. North Carolina State University, Raleigh, North Carolina.

Dedov, A.V. 2008. Estimation of air permeability of needlepunch materials. Fiber Chemistry 39(6): 23-25

Gillahm P.R., M.A. Irle and S.A. Amartey, 2000. Development and production of laboratory scale novel MDF panels from composite and nonwoven mattresses of sisal and wood fiber mixtures. Holz Als Roh- und Werkstoff 58(5): 324-330.

Guess, F. M., D.J. Edwards, T.M Pickrell, and T.M. Young. 2003. Exploring graphically and statistically the reliability of medium density fiberboard. International Journal of Reliability and Applications 4(4): 97-110.

Hearle, J.W.S., 1972. A theory of the mechanics of needled fabrics. From: Needle-felted fabrics, Ed. P. Lennox-Kerr. W.R.C. Smith Publishing Co., Atlanta, Ga.

Hegde, R.R., A. Dahiya and M.G. Kamath. 2004. Bicomponent fibers. http://web.utk.edu/~mse/pages/Textiles/Bicomponent%20fibers.htm (2005).

Huntoon, R. 1990. The needlepunch handbook . NCINDA, Cary, NC.

Hyungsup, K. 1998. Study of needlepunching process and products. Ph.D thesis, North Carolina State University, Raleigh, North Carolina.

Kamath M.G., A. Dahiya and R.R. Hegde. 2004. Needlepunched nonwovens. http://web.utk.edu/~mse/pages/Textiles/Needle%20Punched%20Nonwovens.htm (2005).

Krcma, R., 1971. Manual of nonwovens. R.C. Smith Publishing Co., Atlanta, Ga.

Kiekens, P. and M. Zamfir. 2002. Non-wovens from cotton fibers for absorbent products obtained by the needle-punching process. AUTEX Research Journal 2(4): 166-174.

Lennox-Kerr, P. 1972. Needle felted fabrics. W. R. C. Smith Pub. Co, Atlanta, Ga.

Liu, J.Y. and J.D. McNatt. 1991. Thickness swelling and density variation in aspen flakeboards. Wood Science and Technology 25(1): 73-82.

Mansfield, R.G. 2005. Advancing needlepunched nonwovens. GFR Magazine 6.

Mcdonald, M., 1971. Nonwoven fabric technology. Noyes Data Corporation, New Jersey, NJ.

Mrstina, V., and F. Fejgl. 1990. Needle Punching Textile Technology . Textile Science and Technology 14(21):.44-68.

Narejo, D. and L. Collins. 2002. Advances in needlepunching. GFR Magazine 6.

National Particleboard Association. 1994. Medium density fiberboard. ANSI A208.2-1994. NPA, Gaithersburg, MD.

Park, J and S. Seo. 1993. Performances improvement of medium density fiberboard by combining with various non-wood materials. Research Reports of the Forestry Research Institute Seoul 47: 35-48.

Perry, R.H. and D.W. Green. 1997. Perry's Chemical Engineers Handbook. McGraw Hill, New York, NY.

Pirvu, A., D.J. Gardner and R. Lopez-Anido. 2004. Carbon fiber-vinyl ester reinforcement of wood using the VARTM/SCRIMP fabrication process. Composites Part A: Applied Science and Manufacturing 35(11): 1257-1265.

Purdy, A.T. 1980. Needle Punching. The Textile Institute, London.

Rawal, A. 2006. A modified micromechanical model for the prediction of tensile behavior of nonwoven structures. Journal of Industrial Textiles 36: 133-138.

Youngvist, J.A., A.M Krsysu, J.H. Muehl and C. Carll, 1992. Mechanical and physical properties of air-formed wood-fiber / polymer-fiber composites. Forest Products Journal 42(6): 42-48.

Xing, C., J. Deng and S.Y. Yang. 2007. Effect of thermo-mechanical refining on the properties of MDF. Wood Science and Technology 41: 329-338.

Xu, W., and O. Suchsland. 1998. Modulus of elasticity of wood composite panels with a uniform vertical density profile: A model. Wood and Fiber Science 30(3): 293–300.

Chapter 2: Thickness Swelling Characteristics of a Needlepunched Wood-Bicomponent Fiber Composite

Abstract

This study focused on the feasibility of incorporating a polypropylene / polyester bicomponent fiber web into a wood fiber panel, and the effect this will have on thickness swell characteristics. Thickness swelling properties were investigated for 3 panel configurations: a 2.3mm panel with a polypropylene / polyester bicomponent web placed on each surface and needlepunched from both surfaces with the needles passing through the entire thickness prior to pressing; a 4.6 mm panel with a polypropylene / polyester bicomponent web placed on each surface and needlepunched through both surfaces with the needles passing through half the thickness prior to pressing; and a 6.9 mm panel with a polypropylene / polyester bicomponent web placed on each surface and needlepunched from both surfaces with the needles passing through a third of the thickness prior to pressing. Results were compared to the thickness swelling characteristics of MDF panels with similar thicknesses as the wood-bicomponent fiber panels investigated. Improvements in thickness swelling over that of MDF was observed in the 2.3 mm punched through panels and the 4.6 mm half punched panels.

2.1) Introduction

Thickness swelling of wood composites in relation to moisture content (MC) change and panel manufacturing parameters has been extensively studied. It was shown (Wu and Piao, 1999; Halligan, 1970; Wu and Suchsland, 1997) that total thickness swelling has two components: recoverable thickness swell and non-recoverable thickness swell. Recoverable thickness swelling is due to MC change within the hygroscopic range, while non-recoverable thickness swell is a result of the combined effect of the compression stress release from the pressing operation and differential swelling potential due to inherent in-plane density variation. The latter results in normal swelling stresses between high and low density areas in the plane of the panel. These stresses are often large enough to break the adhesive bonds, leading to non-recoverable thickness swelling.

Dimensional stability has been one of the mostly investigated characteristics of wood and wood-based composites. The hygroscopic nature of the wood material comes from the hydroxyl groups of the cell wall polymers. Many efforts were made to replace the hydroxyl groups by less hygroscopic groups.

Rowell et al. (1995, 1989) studied extensively the chemical modification of wood and wood-based composites by esterification treatments, mainly acetylation (esterification using acetic anhydride). However, various reports mention that this treatment causes a decrease in the mechanical properties and other important properties of wood materials (Chow et al. 1996; Rowell et al. 1989; Subiyanto et al. 1989; Nishimoto and Imamura 1985).

Currently, the wood-based panel industry uses paraffin waxes to improve the dimensional stability of the panels. However, the hydrophobic properties of paraffin waxes have a short-time effect, resulting in a simple delay in water absorption.

Needlepunching utilizes barbed needles to rearrange fibers in a fiber mat from the horizontal to the vertical position. This mechanically interlocks the fibers and significantly changes the properties of a fiber web. Furthermore, polypropylene / polyester bicomponent fiber webs were used as surface reinforcement. Bicomponent fibers are formed by extruding two polymers from the same spinneret with both polymers contained within the same filament. The properties affected can be adapted by changing the process parameters and the polymers involved, resulting in the possibility of an engineered final product. The bicomponent fiber webs were needlepuched in conjunction with wood fiber mats to form sandwich panels.

This study focused on the effect of needlepunching on the thickness swell of MDF. It also investigated the feasibility of incorporating a polypropylene / polyester bicomponent fiber web into a wood fiber panel, and the effect this will have on thickness swell characteristics.

2.2) Materials and methods

Wood fibers were prepared and blended as described in Chapter 1. The needleloom used during the course of this research had a throat height of approximately 30 mm. It was therefore necessary to prepare the fiber mats with a prepressed thickness less than 25 mm.

The configurations investigated were a 2.3 mm punched through panel, a 4.6 mm half punched panel and a 6.9 mm surface panel descrived in Chapter 1.

Thickness swelling tests were performed according to ASTM D 1037 Method 23A (ASTM 2006). Eight samples of each panel type were made, in conjunction with 8 MDF panels as control. Samples were cut (152 mm by 152 mm) with a table saw and conditioned in a conditioning chamber set at 65 percent relative humidity and a temperature of 20°C for 30 days. Samples were weighed and measured 25.4 mm from the edges after the conditioning period. Measuring positions were marked prior to measurement. Samples were submersed horizontally on a plastic grid in 25.4 mm of water and weighed down with additional plastic grids for 2 hours. The grids allowed free movement of water on all surfaces of the specimens, while maintaining minimum contact with the samples. Samples were removed from the water and allowed to drain for 10 minutes prior to measurement of the dimensions and weight. The process was repeated after a further 22 hours. Samples were oven dried to determine the final moisture content. A completely randomized split plot design was used, with boards as whole plot units, treatment and panel thickness as whole plot factors and a subplot factor of time.

To determine the recoverable and unrecoverable thickness swell, the samples were conditioned at 65 percent relative humidity and a temperature of 20°C for 30 days. Samples were remeasured, and the nonrecoverable thickness swell was determined based on the original sample dimensions.

In order to determine what the contribution of the constituents of the composite were in overall panel thickness swelling, a thickness swelling test was conducted on manually delaminated bicomponent sheets.

2.3) Results and discussion

The bicomponent sheets were found to swell by approximately 2.7% after a two hour submersion test, with no increase in thickness swelling found after 24 hours (Table A2.1). Table A2.2 lists the dimensions observed for the 3 panel configurations described earlier, as well as MDF manufactured with corresponding thicknesses. A rule of mixtures was used to back out the contribution of the bicomponent sheets to the overall thickness swell:

$$S_p x_p = S_m x_m + S_b x_b \qquad \text{Eq. 2.1}$$

where: S_i = percentage thickness swell

x_i = thickness component of each composite lamina

p, m, b = laminate, wood component and bicomponent sheet component, respectively

Figure 2.1 illustrates the thickness swell of the wood component of the wood-bicomponent fiber panels after 2 hours (S_m) and the thickness swell observed in MDF (Table A2.2). It was found that thickness swell of the MDF decreased with an increase in panel thickness. The 2.3 mm panels, which were punched from both surfaces throughout the

thickness, showed the greatest difference in measured thickness swell when compared with the thickness swell of 2.3 mm MDF panels. The difference in thickness swell in the 4.3 mm needlepunched and MDF panels, which consisted of two fiber mats which were punched from one side only, essentially resulting in panels which were punched only half way through the thickness, was relatively smaller. No significant difference in MDF / needlepunched panel thickness swell was observed in the 6.9 mm panels, where only a surface layer was punched. The values obtained for MDF are in agreement with those observed by Hashim et al. (2008) and Widsten et al. (2004) who obtained values after 2 hours of 16.2 and 13.7 percent respectively. Both sets of researchers did not use any additives during their research. The addition of additives can significantly improve both 2 and 24 hour thickness swell, however. Ye et al. (2007) observed a value of 5% thickness swell at a resin content of 9% after addition of 1% wax emulsion to the furnish during blending. Wang et al. (2001) obtained mats with 9% resin content with 0.25% wax emulsion added from a commercial MDF mill. They observed thickness swell values of approximately 4%.

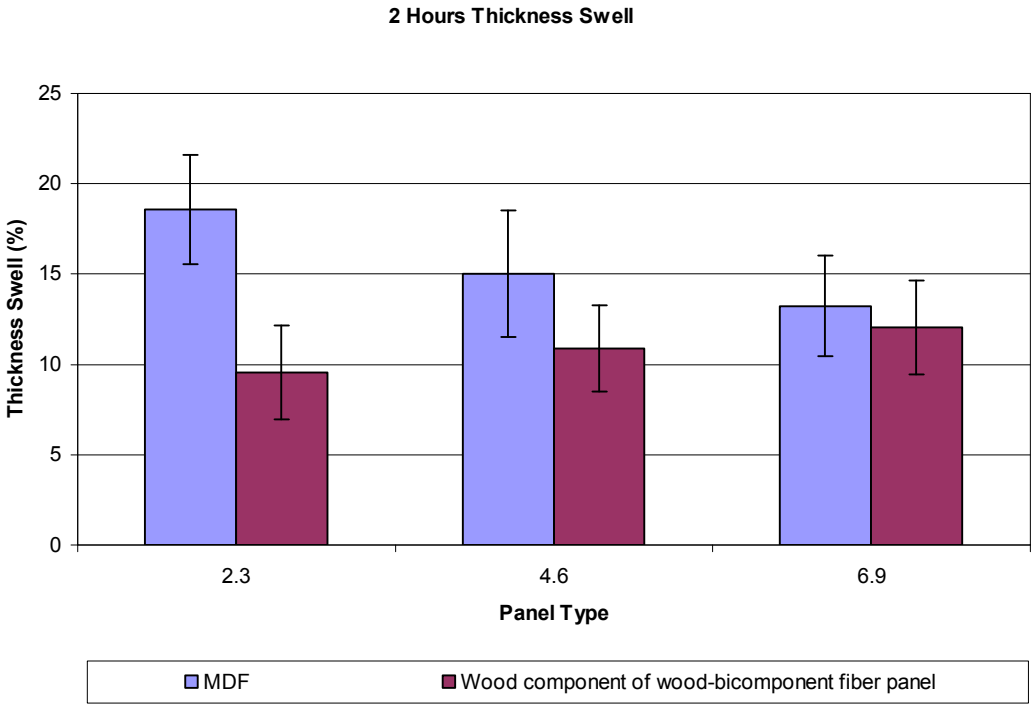

Figure 2.1: Thickness swell measured after 2 hours for the wood component of the three panel types (2.3mm punched through, 4.6mm half punched and 6.9mm surface punched) compared to MDF at the respective thicknesses.

Figure 2.2 illustrates the thickness swell of the wood component observed after an additional 22 hours of submersion. Similar trends were observed to the thickness swell measurement after 2 hours. As with the swelling observed after 2 hours, all differences were significant, except for the 6.9 mm surface punched panels (see SAS output in Table A2.4). The values for MDF were again in agreement with 24 hour thickness swelling observed when no additives are added to the furnish. Values of 33.7 and 44 percent were observed by Hashim et al. (2008) and Widsten et al. (2004) respectively. Wang et al. (2001) observed 24 hour thickness swell of 12 percent in the industrial mats.

Improvements in thickness swell obtained in this study by needlepunching a bicomponent web onto the surfaces of a MDF panel are not in range with improvements obtained by adding additives to the furnish. Further research is therefore needed to determine thickness swell in bicomponent fiber reinforced, needlepunched panels with moisture resistant additives added to the furnish to further evaluate the feasibility of using this method to improve thickness swelling.

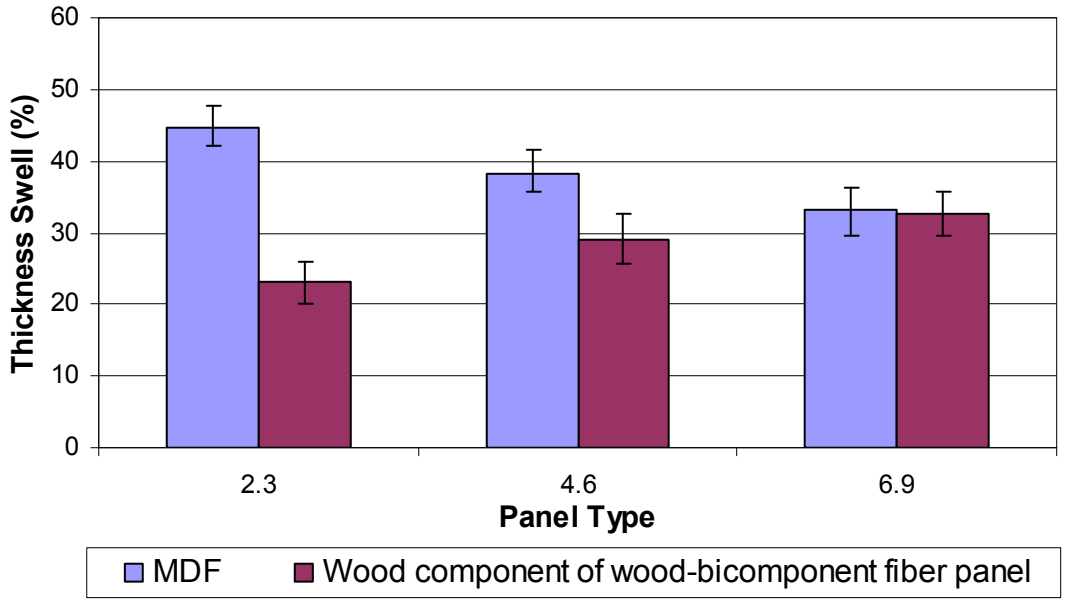

Figure 2.2: Thickness swell measured after 24 hours for the wood component of the three panel types (2.3mm punched through, 4.6mm half punched and 6.9mm surface punched) compared to MDF at the respective thicknesses.

Figure 2.3 illustrates the moisture absorption after 24 hours as a percentage of the oven dry weight. T-tests conducted for each thickness showed no significant difference. The wood-bicomponent fiber panels showed lower moisture absorption compared to MDF. These differences were not significant, however, except for the 4.6 mm panels. The bicomponent fiber therefore only has a marginal effect on water flow into the core of the panel. This is in contrast with the study of Cai (2006) who attribute decreases in moisture absorption of fiberglass reinforced MDF to a sealing effect of the reinforcement used. From this we can conclude that the differences observed in thickness swell between the needlepunched panels and MDF is mainly the result of the needlepunching process in conjunction with a constriction effect of the bicomponent fiber passing through the panel thickness.

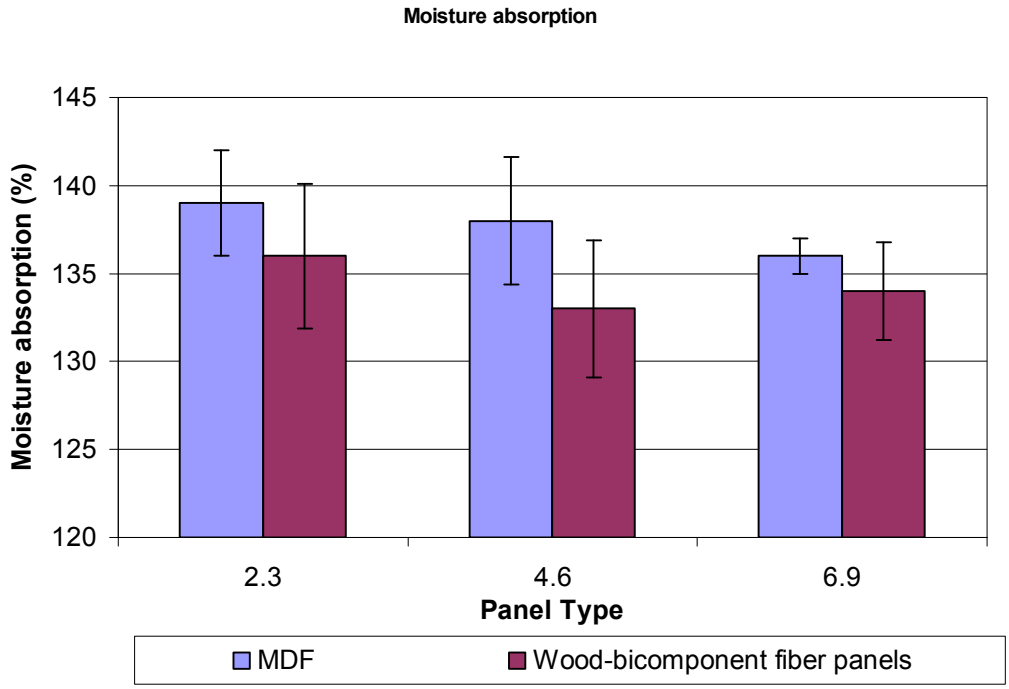

Figure 2.3: Moisture absorption after 24 hours of the three panels (2.3mm punched through, 4.6mm half punched and 6.9 mm surface punched) types compared to that of MDF

The action of the needles during needlepunching grabs fibers from the bicomponent webs on the top surface and forces them down through the thickness of the fiber web. It is proposed that the polymer fibers passing between the bicomponent webs on the surfaces holds the panels together and , in conjunction with the fiber web to which it is connected on the surface, mechanically prevents the panels from swelling. In the case of the 2.3 mm panels, they are mechanically interlocked and fused during pressing with the web placed on the opposite surface of the panels. The interaction of the bicomponent fiber passing through

the thickness and the surface webs are therefore greater, resulting in a decrease in overall thickness swell. In the case of the 4.3 mm panels, the fibers punched through from the surface only extend halfway into the panel thickness, resulting in a smaller effect on thickness swell. The smallest effect was observed in the 6.9 mm panels, where the unpunched fiber mat, sandwiched between the punched surface mats, is not prevented from swelling.

Figure 2.4 illustrates the mean unrecovered thickness swell of MDF and the wood-bicomponent fiber panels at the three panel thicknesses. It can be observed that the difference in unrecovered thickness swell in the 2.3 mm punched through panels is substantially greater than that obtained from the 4.6 mm half punched and 6.9 mm surface punched panels. This can again be attributed to the effect of the fibers passing through the thickness of the panels from the one bicomponent surface layer to the other, essentially applying pressure to the panels as they dry. The results obtained for unrecovered thickness swell of MDF are in agreement with those obtained by Cai (2006), who observed unrecovered thickness swell values of 9 percent for UF bonded MDF prepared with no additives.

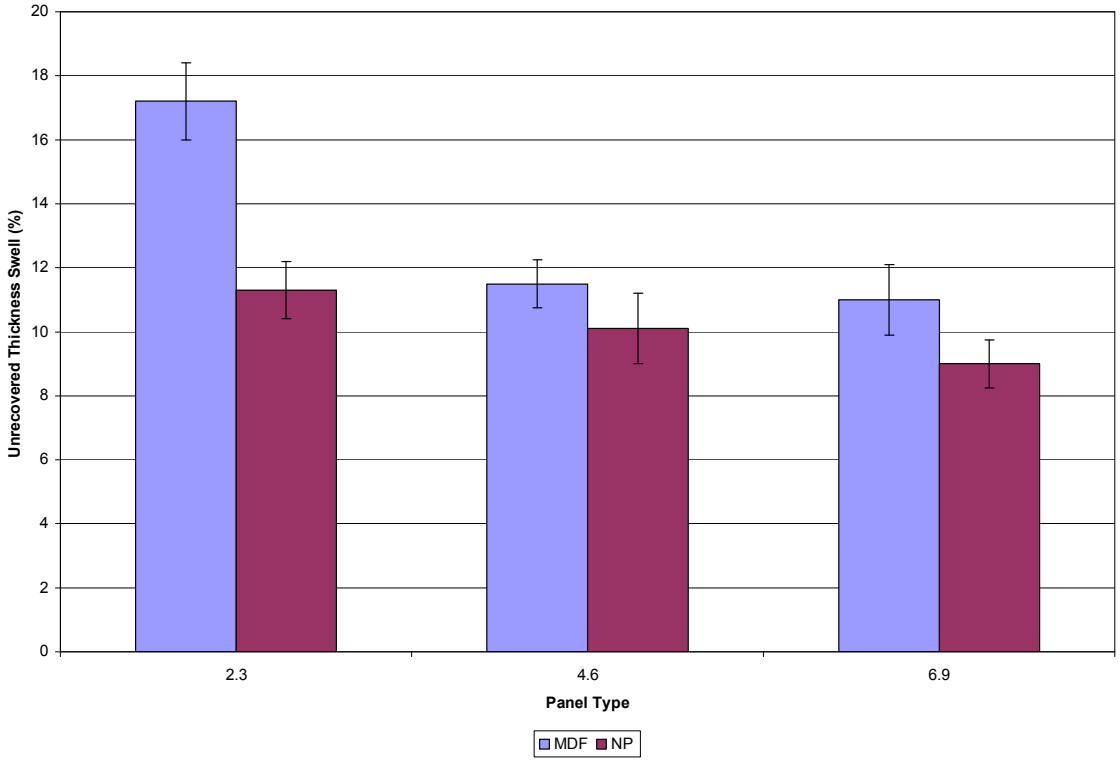

Figure 2.4 : Unrecovered thickness swell of MDF at three different thicknesses and the three panel treatments (2.3mm punched through, 4.6mm half punched and 6.9mm surface punched)

2.4) Conclusion

It was found that the three needlepunching panel treatments used in this study all significantly improved the thickness swell characteristics of wood fiber panels. The panels which were punched through the thickness showed the greatest improvement, both with regards to thickness swell and unrecovered thickness swell. It is proposed that this was due to the influence of the bicomponent fibers passing through the panel thickness from the bicomponent surface webs. It was also found that the effect of the bicomponent surface webs on overall panel moisture absorption was small.

2.5) References

American Society for Testing and Materials (ASTM). 2006. Standard methods for evaluating properties of wood-based fiber and particle panel materials. ASTM D1037. American Society for Testing and Materials, West Conshohocken, PA.

Cai, Z. 2006. Selected Properties of MDF and Flakeboard Overlaid With Fiberglass Mats. Forest Products Journal 56(11/12): 5-10.

Chow P, Bao Z, Youngquist JA, Rowell RM, Muehl JH, Krzysik AM (1996) Properties of hardboards made from acetylated aspen and southern pine. Wood and Fiber Science 28(2): 252–258.

Garcia, R.A., A. Cloutier and B. Riedle. 2005. Dimensional stability of MDF panels produced from fibres treated with maleated polypropylene wax. Wood Science and Technology 39(8): 630-650.

Guess, F. M., D.J. Edwards, T.M Pickrell, and T.M. Young. 2003. Exploring Graphically and Statistically the Reliability of Medium Density Fiberboard. International Journal of Reliability and Applications 4(4): 97-110.

Halligan, A.F. 1970. A review of thickness SPS swelling in particleboard. Wood Sci. Technology 4:301-312.

Hashim, R, O. Sulaiman, R.N. Kumar, P.F. Tamyez, R.J. Murphy and Z. Ali. 2002. Physical and mechanical properties of flame retardant urea formaldehyde medium density fiberboard. Journal of Material Processing Technology 20(6): 505-517.

Kazayawoko M, Balatinecz JJ, Woodhams RT, Sochi RNS (1998) X-ray photoelectron spectroscopy of lignocellulosic materials treated with maleated polypropylenes. Journal of Wood Chemistry and Technology 18(1):1–26

Liu, J.Y. and J.D. McNatt. 1991. Thickness swelling and density variation in aspen flakeboards. Wood Science and Technology 25: 73-82.

Mahlberg R, Paajanen L, Nurmi A, Kivistö A, Koskela K, Rowell RM (2001) Effect of chemical modification of wood on the mechanical and adhesion properties of wood fiber/polypropylene fiber and polypropylene/veneer composites. Holz als Roh und Werkstoff 59: 319–326

Nishimoto K, Imamura Y (1985) Mokuzai Kogyo (J Wood Technol Assoc, Jpn), 40, 414. In: Kajita H, Imamura Y (1993) Chemically modified particleboards. In: Shiraishi N, Kajita H, Norimoto M (eds) Recent research on wood and wood-based materials. The Society of Materials Science 11:67–74.

Rowell RM, Imamura Y, Kawai S, Norimoto M (1989) Dimensional stability, decay resistance, and mechanical properties of veneer-faced low-density particleboard made from acetylated wood. Wood and Fiber Science 21(1): 67–79.

Rowell RM, Kawai S, Inoue M (1995) Dimensional stabilized, very low density fiberboard. Wood and Fiber Science 27(4): 428–436

Sanadi AR, Caulfield DF, Jacobson RE (1997) Agro-fiber thermoplastic composites. In: Rowell RM, Young RA, Rowell JK (eds) Paper and composites from agro-based resouces. Inc. Lewis Publishers, CRC Press, Boca Raton, pp 377–401.

Wang, S., P. Winistorfer, T.M. Young and C. Helton. 2001. Step closing pressing of medium density fiberboard. Holz als Roh und Wekstoff 59(5): 311-318.

Wu, Q. and O. Suchsland. 1997. Effect of moisture on the flexural properties of commercial oriented strandboard. Wood and Fiber Science 29(1): 47-57.

Ye, P.X., J. Julson, M. Kuo, A. Womac, D. Myers. 2007. Properties of medium density fiberboards made from renewable biomass. Bioresource Technology 98(5): 1077-1084.

Appendix 2

Table A2.1: Thickness swell observed in bicomponent fiber sheets after 2 and 24 hour submersion tests.

Sample	Thickness (mm)			Thickness swell (%)
	Dry	after 2 hrs soaking	After 24 hrs soaking	
1	0.22	0.23	0.23	4.55
2	0.24	0.24	0.24	0.00
3	0.26	0.26	0.26	0.00
4	0.21	0.22	0.22	4.76
5	0.24	0.25	0.25	4.17
Mean				2.69

Table A2.2: Dimensions measured for 2 and 24 hour submersion swelling tests for MDF and the three configurations of wood-bicomponent fiber panels investigated in this Chapter.

2.3 mm										
Sample	**Oven Dry**		**2hrs**				**24hrs**			
	MDF (mm)	**Punched Through (mm)**	**MDF (mm)**	**MDF Swelling (%)**	**Punched Through (mm)**	**Swelling**	**MDF (mm)**	**Swelling (%)**	**Punched Through (mm)**	**Swelling (%)**
1	2.71	2.49	3.77	18.84	2.75	10.46	3.93	45.02	3.23	23.11
2	2.68	2.51	3.94	20.25	2.75	9.64	4.06	48.23	3.11	23.75
3	2.76	2.71	3.85	18.01	2.96	9.53	3.94	42.75	3.29	21.72
4	2.68	2.66	3.88	19.28	2.88	8.49	3.98	48.51	3.12	22.30
5	2.70	2.59	3.75	16.75	2.83	9.22	4.00	48.15	3.18	23.11
6	2.70	2.41	3.80	17.54	2.64	9.43	3.74	41.51	2.98	23.62
7	2.65	2.61	3.74	18.71	2.85	8.89	3.75	41.51	3.20	22.65
8	2.65	2.76	3.80	18.69	3.02	9.76	3.77	42.26	3.41	23.79
Mean	2.69	2.59	3.82	18.51	2.84	9.43	3.90	44.74	3.19	23.01
St dev.	0.03	0.11	0.06	1.01	0.11	0.55	0.12	2.94	0.12	0.69
4.6 mm										
1	5.40	5.29	6.25	15.74	5.95	10.19	7.44	37.78	6.70	26.65
2	5.46	5.31	6.25	14.47	6.05	10.81	7.55	38.28	6.71	26.37
3	5.46	5.27	6.36	16.48	6.01	10.07	7.45	36.45	6.67	26.57
4	5.52	5.34	6.40	15.94	6.15	11.41	7.69	39.31	6.93	29.78
5	5.15	5.25	5.90	14.56	5.80	12.62	7.09	37.67	6.63	26.29
6	5.16	5.10	5.95	15.31	5.70	10.47	7.15	38.57	6.46	26.67
7	5.20	5.12	5.95	14.42	5.75	10.58	7.18	38.10	6.54	27.73
8	5.22	5.15	6.00	15.00	5.79	10.92	7.21	38.12	6.55	27.18
Mean	5.32	5.23	6.13	15.24	5.90	10.88	7.35	38.03	6.65	27.15
St dev.	0.14	0.09	0.19	0.71	0.15	0.77	0.20	0.77	0.13	1.09
6.9 mm										
1	7.72	6.64	8.75	13.34	7.51	13.05	10.10	30.83	10.00	29.53
2	7.68	7.59	8.63	12.37	8.40	10.61	10.20	32.81	9.68	25.98
3	7.51	6.26	8.56	13.98	7.10	13.45	9.90	31.82	10.10	34.49
4	7.48	7.53	8.46	13.10	8.37	11.14	9.89	32.22	9.68	29.41
5	7.27	6.53	8.19	12.65	7.41	13.48	9.67	33.01	9.50	30.67
6	7.23	6.86	8.11	12.20	7.58	10.50	9.66	33.61	9.35	29.32
7	7.14	7.10	8.18	14.57	7.90	11.27	9.76	36.69	9.30	30.25
8	6.99	7.13	8.13	16.31	8.05	12.90	9.39	34.33	9.41	34.62
Mean	7.38	6.96	8.38	13.57	7.79	12.05	9.82	33.17	9.63	30.53
St dev.	0.24	0.44	0.24	1.28	0.44	1.21	0.24	1.67	0.28	2.67

Table A2.3: Final dimensions after redrying MDF and wood-bicomponent fiber panel samples.

Sample	Final dimensions (mm)		Unrecovered swelling (%)	
	MDF	Punched Through	MDF	Punched Through
2.3				
1	3.25	2.82	19.93	13.48
2	3.01	2.60	12.31	3.48
3	3.26	3.08	18.12	13.86
4	3.18	3.05	18.66	14.77
5	3.15	2.86	16.67	10.64
6	3.19	2.70	18.15	11.92
7	3.10	2.88	16.98	10.56
8	3.10	3.05	16.98	10.61
Mean	3.16	2.88	17.22	11.16
St dev.	0.08	0.16	2.11	3.28
4.6				
1	6.10	5.90	12.96	11.53
2	5.98	5.75	9.52	8.29
3	6.15	5.90	12.64	11.95
4	6.06	5.68	9.78	6.37
5	5.80	5.85	12.62	11.43
6	5.79	5.74	12.21	12.55
7	5.60	5.56	7.69	8.59
8	5.96	5.68	14.18	10.29
Mean	5.93	5.76	11.45	10.13
St dev.	0.17	0.11	2.05	2.02
6.9				
1	9.10	7.28	17.88	9.60
2	8.42	8.38	9.64	10.37
3	8.35	6.63	11.19	5.87
4	8.29	8.10	10.83	7.61
5	8.05	7.22	10.73	10.57
6	8.01	7.51	10.79	9.48
7	7.60	7.80	6.44	9.86
8	7.75	7.76	10.87	8.84
Mean	8.20	7.59	11.04	9.02
St. dev.	0.21	0.28	2.7	2.9

Table A2.4: SAS output for data obtained from thickness swelling tests of a wood-bicomponent fiber composite

The Mixed Procedure

Model Information

Data Set	WORK.ALL3
Dependent Variable	thickness
Covariance Structure	Variance Components
Estimation Method	Type 3
Residual Variance Method	Factor
Fixed Effects SE Method	Model-Based
Degrees of Freedom Method	Containment

Class Level Information

Class	Levels	Values
board	8	1 2 3 4 5 6 7 8
trt	2	MDF NP
pt	3	2.3 4.6 6.9
time	2	2 24

Dimensions

Covariance Parameters	2
Columns in X	36
Columns in Z	48
Subjects	1
Max Obs Per Subject	96

Number of Observations

Number of Observations Read	96
Number of Observations Used	96
Number of Observations Not Used	0

Type 3 Analysis of Variance

Source	DF	Sum of Squares	Mean Square	Expected Mean Square
time	1	10006	10006	Var(Residual) + Q(time,trt*time,pt*time,trt*pt*time)
trt	1	1004.726301	1004.726301	Var(Residual) + 2 Var(board(trt*pt)) + Q(trt,trt*time,trt*pt,trt*pt*time)
trt*time	1	144.967926	144.967926	Var(Residual) + Q(trt*time,trt*pt*time)

pt	2	103.748558	51.874279	Var(Residual) + 2 Var(board(trt*pt)) + Q(pt,pt*time,trt*pt,trt*pt*time)
pt*time	2	12.031558	6.015779	Var(Residual) + Q(pt*time,trt*pt*time)

The Mixed Procedure

Type 3 Analysis of Variance

Source	DF	Sum of Squares	Mean Square	Expected Mean Square
trt*pt	2	538.281033	269.140517	Var(Residual) + 2 Var(board(trt*pt)) + Q(trt*pt,trt*pt*time)
trt*pt*time	2	96.442608	48.221304	Var(Residual) + Q(trt*pt*time)
board(trt*pt)	42	147.328506	3.507822	Var(Residual) + 2 Var(board(trt*pt))
Residual	42	77.416006	1.843238	Var(Residual)

Type 3 Analysis of Variance

Source	Error Term	Error DF	F Value	Pr > F
time	MS(Residual)	42	5428.49	<.0001
trt	MS(board(trt*pt))	42	286.42	<.0001
trt*time	MS(Residual)	42	78.65	<.0001
pt	MS(board(trt*pt))	42	14.79	<.0001
pt*time	MS(Residual)	42	3.26	0.0481
trt*pt	MS(board(trt*pt))	42	76.73	<.0001
trt*pt*time	MS(Residual)	42	26.16	<.0001
board(trt*pt)	MS(Residual)	42	1.90	0.0199
Residual	.	.	.	.

Covariance Parameter Estimates

Cov Parm	Estimate
board(trt*pt)	0.8323
Residual	1.8432

Fit Statistics

-2 Res Log Likelihood	341.7
AIC (smaller is better)	345.7
AICC (smaller is better)	345.9
BIC (smaller is better)	349.5

Type 3 Tests of Fixed Effects

Effect	Num DF	Den DF	F Value	Pr > F
time	1	42	5428.49	<.0001
trt	1	42	286.42	<.0001

The Mixed Procedure

Type 3 Tests of Fixed Effects

Effect	Num DF	Den DF	F Value	Pr > F
trt*time	1	42	78.65	<.0001
pt	2	42	14.79	<.0001
pt*time	2	42	3.26	0.0481
trt*pt	2	42	76.73	<.0001
trt*pt*time	2	42	26.16	<.0001

Estimates

Label	Estimate	Standard Error	DF	t Value	Pr > |t|
linear pt for MDF	-8.2606	0.6622	42	-12.47	<.0001
nonlinear pt for MDF	-1.7156	1.1469	42	-1.50	0.1422
linear pt for NP	3.3144	0.6622	42	5.01	<.0001
nonlinear pt for NP	-0.3856	1.1469	42	-0.34	0.7384

Least Squares Means

Effect	trt	pt	time	Estimate	Standard Error	DF	t Value	Pr > |t|
trt*pt*time	MDF	2.3	2	18.5088	0.5783	42	32.00	<.0001
trt*pt*time	MDF	2.3	24	44.7425	0.5783	42	77.37	<.0001
trt*pt*time	MDF	4.6	2	15.2400	0.5783	42	26.35	<.0001
trt*pt*time	MDF	4.6	24	38.0350	0.5783	42	65.77	<.0001
trt*pt*time	MDF	6.9	2	13.5650	0.5783	42	23.46	<.0001
trt*pt*time	MDF	6.9	24	33.1650	0.5783	42	57.35	<.0001
trt*pt*time	NP	2.3	2	10.9275	0.5783	42	18.90	<.0001
trt*pt*time	NP	2.3	24	27.3650	0.5783	42	47.32	<.0001
trt*pt*time	NP	4.6	2	11.7000	0.5783	42	20.23	<.0001
trt*pt*time	NP	4.6	24	29.5212	0.5783	42	51.05	<.0001
trt*pt*time	NP	6.9	2	12.6488	0.5783	42	21.87	<.0001
trt*pt*time	NP	6.9	24	32.2725	0.5783	42	55.80	<.0001

Differences of Least Squares Means

Effect	trt	pt	time	_trt	_pt	_time	Estimate	Standard Error	DF	t Value	Pr > |t|
trt*pt*time	MDF	2.3	2	MDF	2.3	24	-26.2337	0.6788	42	-38.65	<.0001
trt*pt*time	MDF	2.3	2	MDF	4.6	2	3.2687	0.8179	42	4.00	0.0003
trt*pt*time	MDF	2.3	2	MDF	4.6	24	-19.5263	0.8179	42	-23.88	<.0001
trt*pt*time	MDF	2.3	2	MDF	6.9	2	4.9438	0.8179	42	6.04	<.0001

The Mixed Procedure

Differences of Least Squares Means

Effect	trt	pt	time	_trt	_pt	_time	Estimate	Standard Error	DF	t Value	Pr > |t|
trt*pt*time	MDF	2.3	2	MDF	6.9	24	-14.6562	0.8179	42	-17.92	<.0001
trt*pt*time	MDF	2.3	2	NP	2.3	2	7.5812	0.8179	42	9.27	<.0001
trt*pt*time	MDF	2.3	2	NP	2.3	24	-8.8563	0.8179	42	-10.83	<.0001
trt*pt*time	MDF	2.3	2	NP	4.6	2	6.8087	0.8179	42	8.33	<.0001
trt*pt*time	MDF	2.3	2	NP	4.6	24	-11.0125	0.8179	42	-13.47	<.0001
trt*pt*time	MDF	2.3	2	NP	6.9	2	5.8600	0.8179	42	7.17	<.0001
trt*pt*time	MDF	2.3	2	NP	6.9	24	-13.7638	0.8179	42	-16.83	<.0001
trt*pt*time	MDF	2.3	24	MDF	4.6	2	29.5025	0.8179	42	36.07	<.0001
trt*pt*time	MDF	2.3	24	MDF	4.6	24	6.7075	0.8179	42	8.20	<.0001
trt*pt*time	MDF	2.3	24	MDF	6.9	2	31.1775	0.8179	42	38.12	<.0001
trt*pt*time	MDF	2.3	24	MDF	6.9	24	11.5775	0.8179	42	14.16	<.0001
trt*pt*time	MDF	2.3	24	NP	2.3	2	33.8150	0.8179	42	41.35	<.0001
trt*pt*time	MDF	2.3	24	NP	2.3	24	17.3775	0.8179	42	21.25	<.0001
trt*pt*time	MDF	2.3	24	NP	4.6	2	33.0425	0.8179	42	40.40	<.0001
trt*pt*time	MDF	2.3	24	NP	4.6	24	15.2213	0.8179	42	18.61	<.0001
trt*pt*time	MDF	2.3	24	NP	6.9	2	32.0937	0.8179	42	39.24	<.0001
trt*pt*time	MDF	2.3	24	NP	6.9	24	12.4700	0.8179	42	15.25	<.0001
trt*pt*time	MDF	4.6	2	MDF	4.6	24	-22.7950	0.6788	42	-33.58	<.0001
trt*pt*time	MDF	4.6	2	MDF	6.9	2	1.6750	0.8179	42	2.05	0.0468
trt*pt*time	MDF	4.6	2	MDF	6.9	24	-17.9250	0.8179	42	-21.92	<.0001
trt*pt*time	MDF	4.6	2	NP	2.3	2	4.3125	0.8179	42	5.27	<.0001
trt*pt*time	MDF	4.6	2	NP	2.3	24	-12.1250	0.8179	42	-14.83	<.0001
trt*pt*time	MDF	4.6	2	NP	4.6	2	3.5400	0.8179	42	4.33	<.0001
trt*pt*time	MDF	4.6	2	NP	4.6	24	-14.2812	0.8179	42	-17.46	<.0001
trt*pt*time	MDF	4.6	2	NP	6.9	2	2.5912	0.8179	42	3.17	0.0029
trt*pt*time	MDF	4.6	2	NP	6.9	24	-17.0325	0.8179	42	-20.83	<.0001
trt*pt*time	MDF	4.6	24	MDF	6.9	2	24.4700	0.8179	42	29.92	<.0001
trt*pt*time	MDF	4.6	24	MDF	6.9	24	4.8700	0.8179	42	5.95	<.0001

trt*pt*time	MDF	4.6	24	NP	2.3	2	27.1075	0.8179	42	33.14	<.0001
trt*pt*time	MDF	4.6	24	NP	2.3	24	10.6700	0.8179	42	13.05	<.0001
trt*pt*time	MDF	4.6	24	NP	4.6	2	26.3350	0.8179	42	32.20	<.0001
trt*pt*time	MDF	4.6	24	NP	4.6	24	8.5138	0.8179	42	10.41	<.0001
trt*pt*time	MDF	4.6	24	NP	6.9	2	25.3862	0.8179	42	31.04	<.0001
trt*pt*time	MDF	4.6	24	NP	6.9	24	5.7625	0.8179	42	7.05	<.0001
trt*pt*time	MDF	6.9	2	MDF	6.9	24	-19.6000	0.6788	42	-28.87	<.0001
trt*pt*time	MDF	6.9	2	NP	2.3	2	2.6375	0.8179	42	3.22	0.0024
trt*pt*time	MDF	6.9	2	NP	2.3	24	-13.8000	0.8179	42	-16.87	<.0001
trt*pt*time	MDF	6.9	2	NP	4.6	2	1.8650	0.8179	42	2.28	0.0277
trt*pt*time	MDF	6.9	2	NP	4.6	24	-15.9562	0.8179	42	-19.51	<.0001
trt*pt*time	MDF	6.9	2	NP	6.9	2	0.9162	0.8179	42	1.12	0.2689
trt*pt*time	MDF	6.9	2	NP	6.9	24	-18.7075	0.8179	42	-22.87	<.0001
trt*pt*time	MDF	6.9	24	NP	2.3	2	22.2375	0.8179	42	27.19	<.0001
trt*pt*time	MDF	6.9	24	NP	2.3	24	5.8000	0.8179	42	7.09	<.0001
trt*pt*time	MDF	6.9	24	NP	4.6	2	21.4650	0.8179	42	26.25	<.0001
trt*pt*time	MDF	6.9	24	NP	4.6	24	3.6437	0.8179	42	4.46	<.0001
trt*pt*time	MDF	6.9	24	NP	6.9	2	20.5162	0.8179	42	25.09	<.0001

The Mixed Procedure

Differences of Least Squares Means

Effect	trt	pt	time	_trt	_pt	_time	Estimate	Standard Error	DF	t Value	Pr > |t|
trt*pt*time	MDF	6.9	24	NP	6.9	24	0.8925	0.8179	42	1.09	0.2814
trt*pt*time	NP	2.3	2	NP	2.3	24	-16.4375	0.6788	42	-24.21	<.0001
trt*pt*time	NP	2.3	2	NP	4.6	2	-0.7725	0.8179	42	-0.94	0.3503
trt*pt*time	NP	2.3	2	NP	4.6	24	-18.5937	0.8179	42	-22.73	<.0001
trt*pt*time	NP	2.3	2	NP	6.9	2	-1.7213	0.8179	42	-2.10	0.0414
trt*pt*time	NP	2.3	2	NP	6.9	24	-21.3450	0.8179	42	-26.10	<.0001
trt*pt*time	NP	2.3	24	NP	4.6	2	15.6650	0.8179	42	19.15	<.0001
trt*pt*time	NP	2.3	24	NP	4.6	24	-2.1562	0.8179	42	-2.64	0.0117
trt*pt*time	NP	2.3	24	NP	6.9	2	14.7162	0.8179	42	17.99	<.0001
trt*pt*time	NP	2.3	24	NP	6.9	24	-4.9075	0.8179	42	-6.00	<.0001
trt*pt*time	NP	4.6	2	NP	4.6	24	-17.8212	0.6788	42	-26.25	<.0001
trt*pt*time	NP	4.6	2	NP	6.9	2	-0.9488	0.8179	42	-1.16	0.2526
trt*pt*time	NP	4.6	2	NP	6.9	24	-20.5725	0.8179	42	-25.15	<.0001
trt*pt*time	NP	4.6	24	NP	6.9	2	16.8725	0.8179	42	20.63	<.0001
trt*pt*time	NP	4.6	24	NP	6.9	24	-2.7513	0.8179	42	-3.36	0.0016
trt*pt*time	NP	6.9	2	NP	6.9	24	-19.6237	0.6788	42	-28.91	<.0001

The Mixed Procedure

Model Information

Data Set	WORK.ALL3
Dependent Variable	thickness
Covariance Structure	Variance Components
Estimation Method	Type 3
Residual Variance Method	Factor
Fixed Effects SE Method	Model-Based
Degrees of Freedom Method	Containment

Class Level Information

Class	Levels	Values
board	8	1 2 3 4 5 6 7 8
time	2	2 24
trt	2	MDF NP
pt	3	2.3 4.6 6.9

Dimensions

Covariance Parameters	2
Columns in X	36
Columns in Z	48
Subjects	1
Max Obs Per Subject	96

Number of Observations

Number of Observations Read	96
Number of Observations Used	96
Number of Observations Not Used	0

Type 3 Analysis of Variance

Source	DF	Sum of Squares	Mean Square	Expected Mean Square
time	1	10006	10006	Var(Residual) + Q(time,time*trt,time*pt,time*trt*pt)
trt	1	1004.726301	1004.726301	Var(Residual) + 2 Var(board(trt*pt)) + Q(trt,time*trt,trt*pt,time*trt*pt)
time*trt	1	144.967926	144.967926	Var(Residual) + Q(time*trt,time*trt*pt)
pt	2	103.748558	51.874279	Var(Residual) + 2 Var(board(trt*pt)) + Q(pt,time*pt,trt*pt,time*trt*pt)
time*pt	2	12.031558	6.015779	Var(Residual) + Q(time*pt,time*trt*pt)

The Mixed Procedure

Type 3 Analysis of Variance

Source	DF	Sum of Squares	Mean Square	Expected Mean Square
trt*pt	2	538.281033	269.140517	Var(Residual) + 2 Var(board(trt*pt)) + Q(trt*pt,time*trt*pt)
time*trt*pt	2	96.442608	48.221304	Var(Residual) + Q(time*trt*pt)
board(trt*pt)	42	147.328506	3.507822	Var(Residual) + 2 Var(board(trt*pt))
Residual	42	77.416006	1.843238	Var(Residual)

Type 3 Analysis of Variance

Source	Error Term	Error DF	F Value	Pr > F
time	MS(Residual)	42	5428.49	<.0001
trt	MS(board(trt*pt))	42	286.42	<.0001
time*trt	MS(Residual)	42	78.65	<.0001
pt	MS(board(trt*pt))	42	14.79	<.0001
time*pt	MS(Residual)	42	3.26	0.0481
trt*pt	MS(board(trt*pt))	42	76.73	<.0001
time*trt*pt	MS(Residual)	42	26.16	<.0001
board(trt*pt)	MS(Residual)	42	1.90	0.0199
Residual	.	.	.	.

Covariance Parameter Estimates

Cov Parm	Estimate
board(trt*pt)	0.8323
Residual	1.8432

Fit Statistics

-2 Res Log Likelihood	341.7
AIC (smaller is better)	345.7
AICC (smaller is better)	345.9
BIC (smaller is better)	349.5

Type 3 Tests of Fixed Effects

Effect	Num DF	Den DF	F Value	Pr > F
time	1	42	5428.49	<.0001
trt	1	42	286.42	<.0001

The Mixed Procedure

Type 3 Tests of Fixed Effects

Effect	Num DF	Den DF	F Value	Pr > F
time*trt	1	42	78.65	<.0001
pt	2	42	14.79	<.0001
time*pt	2	42	3.26	0.0481
trt*pt	2	42	76.73	<.0001
time*trt*pt	2	42	26.16	<.0001

Least Squares Means

Effect	time	trt	pt	Estimate	Standard Error	DF	t Value	Pr > |t|
time*trt*pt	2	MDF	2.3	18.5088	0.5783	42	32.00	<.0001
time*trt*pt	2	MDF	4.6	15.2400	0.5783	42	26.35	<.0001
time*trt*pt	2	MDF	6.9	13.5650	0.5783	42	23.46	<.0001
time*trt*pt	2	NP	2.3	10.9275	0.5783	42	18.90	<.0001
time*trt*pt	2	NP	4.6	11.7000	0.5783	42	20.23	<.0001
time*trt*pt	2	NP	6.9	12.6488	0.5783	42	21.87	<.0001
time*trt*pt	24	MDF	2.3	44.7425	0.5783	42	77.37	<.0001
time*trt*pt	24	MDF	4.6	38.0350	0.5783	42	65.77	<.0001
time*trt*pt	24	MDF	6.9	33.1650	0.5783	42	57.35	<.0001
time*trt*pt	24	NP	2.3	27.3650	0.5783	42	47.32	<.0001
time*trt*pt	24	NP	4.6	29.5212	0.5783	42	51.05	<.0001
time*trt*pt	24	NP	6.9	32.2725	0.5783	42	55.80	<.0001
time*trt	2	MDF		15.7712	0.3339	42	47.24	<.0001
time*trt	2	NP		11.7588	0.3339	42	35.22	<.0001
time*trt	24	MDF		38.6475	0.3339	42	115.75	<.0001
time*trt	24	NP		29.7196	0.3339	42	89.01	<.0001
time*pt	2		2.3	14.7181	0.4089	42	35.99	<.0001
time*pt	2		4.6	13.4700	0.4089	42	32.94	<.0001
time*pt	2		6.9	13.1069	0.4089	42	32.05	<.0001
time*pt	24		2.3	36.0538	0.4089	42	88.17	<.0001
time*pt	24		4.6	33.7781	0.4089	42	82.60	<.0001
time*pt	24		6.9	32.7187	0.4089	42	80.01	<.0001

Tests of Effect Slices

Effect	time	Num DF	Den DF	F Value	Pr > F
time*trt*pt	2	5	42	22.89	<.0001
time*trt*pt	24	5	42	119.15	<.0001
time*trt	2	1	42	72.21	<.0001
time*trt	24	1	42	357.50	<.0001
time*pt	2	2	42	4.27	0.0205

The Mixed Procedure

Tests of Effect Slices

Effect	time	Num DF	Den DF	F Value	Pr > F
time*pt	24	2	42	17.37	<.0001

Chapter 3: Modeling of the mechanical properties of a wood fiber / bicomponent fiber composite

Abstract

A macro-mechanical model predicting the elastic response of a wood-bicomponent fiber composite panel was developed. The strains at a given stress was determined by means of the model, and compared to strains determined experimentally. The model under predicted the strains along the fiber direction of the bicomponent fiber sheets by approximately 11.6 percent, with one sample differing by only 5.9 percent. A greater difference between predicted and measured values was observed in the lateral direction of 19 percent.

3.1) Introduction

A composite in engineering sense is any materials that have been physically assembled to form one single bulk without physical blending to form a homogeneous material. The resulting material would still have components identifiable as the constituent of the different materials (Rusmee 2005). One of the advantages of composite is that two or more materials could be combined to take advantage of the characteristics of each of the materials.

Usually, composite materials will consist of two separate components, the matrix and the filler. According to Rusmee (2005) the matrix is the component that holds the filler together to form the bulk of the material. It usually consists of various epoxy type polymers but other materials may be used. Metal matrix composite and thermoplastic matrix

composites are some of the possibilities. The filler is the material that has been impregnated in the matrix to lend its advantage (usually strength) to the composite.

Composite materials have been widely utilized in the field of civil engineering, both in new constructions as well as in the reinforcement of existing reinforced concrete structures (Corradi et al., 2006). Most recently, fiber reinforced polymers have also become popular in the forest products industry. Carbon and glass fiber reinforcement, in conjunction with an epoxy matrix, have been used as reinforcement of wood and glulam beams (Triantafillou 1997, Triantafillou et al., 1992, Gentile et al., 2000). These types of reinforcement, called fiber reinforced polymers (FRP's), are characterized by excellent mechanical properties, but the cost of both the fiber and the resin material can be prohibitive. Incompatible thickness swell characteristics also cause problems with regards to delamination (Lopez-Anido et al., 2005; Prian and Barkatt, 1999).

There is currently no feasible method for efficiently reinforcing wood fiber products other than extruding the wood fiber with a polymer to form a wood plastic composite. Bicomponent fiber sheets offer the potential of reinforcing a wood fiber composite. Bicomponent fibers consist of at least two components, running parallel in the fiber throughout the length (Hegde et al. 2004). Each of the components of the fiber retains its own characteristic properties. With sheath-core fibers the core component is completely surrounded by the sheath component. The sheath component has areas of interaction with the core and the surrounding medium. Commonly, the sheath polymer has a lower melting temperature than the core.

During heating, the sheath will melt and diffuse through the surrounding fibers, acting as a binder (Bosak et al. 2005). One method of reinforcing a wood fiber panel is the use of polypropylene / polyester bicomponent fiber sheets in conjunction with needlepunching to form a sandwich laminate composite panel. Based on the data obtained in Chapters 1 and 2, it was decided to focus on the 2.3 mm panels. The panel in question was manufactured by needlepunching a 1495 gsm wood fiber web in conjunction with bicomponent fiber sheets placed on both sides of the wood fiber mat. The panels were punched from both sides and had a final thickness after pressing of 2.3 mm. In order to fully understand the mechanical behavior of these panels, the elastic response of each of the laminae needs to be investigated, along with the response of the laminate.

This study will present a method for quantifying the engineering constants of a bicomponent / wood fiber composite, as well as the constants of each of the composite's constituent lamina. Furthermore, modeling of the behavior of the laminate formed with the different materials in question will be discussed.

3.2) Background

3.2.1) Model to Predict Elastic Constants of a Lamina

The stress-strain relationship for an anisotropic material is given by Hooke's law, which states that (Daniel and Ishai, 2005):

$$\sigma_{ij} = C_{ijkl}\varepsilon_{kl} \qquad \text{Eq. 3.1}$$

where: i, j, k, l = 1, 2, 3

σ_{ij} = stress

C_{ijkl} = stiffness matrix

ε_{kl} = strain

To characterize a material like this, 81 stiffness coefficients are needed. However, this number can be reduced to 36 since there are only six independent stresses and six independent strains. The stress-strain relationship for an anisotropic material can be written in contracted notation as:

$$\begin{bmatrix} \sigma_1 \\ \sigma_2 \\ \sigma_3 \\ \tau_{23} \\ \tau_{13} \\ \tau_{12} \end{bmatrix} = \begin{bmatrix} C_{11} & C_{12} & C_{13} & C_{14} & C_{15} & C_{16} \\ C_{21} & C_{22} & C_{23} & C_{24} & C_{25} & C_{26} \\ C_{31} & C_{32} & C_{33} & C_{34} & C_{35} & C_{36} \\ C_{41} & C_{42} & C_{43} & C_{44} & C_{45} & C_{46} \\ C_{51} & C_{52} & C_{53} & C_{54} & C_{55} & C_{56} \\ C_{61} & C_{62} & C_{63} & C_{64} & C_{65} & C_{66} \end{bmatrix} \begin{bmatrix} \varepsilon_1 \\ \varepsilon_2 \\ \varepsilon_3 \\ \gamma_{23} \\ \gamma_{13} \\ \gamma_{12} \end{bmatrix} \qquad \text{Eq.3.2}$$

where: τ_{ij} = Shear stress

γ_{ij} = Engineering shear strain

i, j = (1, 2, 3)

Since the stiffness matrix is symmetric, only 21 independent stiffness constants are required to characterize this material.

An orthotropic material has 3 mutually perpendicular planes of symmetry. The stress-strain relationship for an orthotropic material is reduced to the following form, with 9 independent stiffness coefficients:

$$\begin{bmatrix} \sigma_1 \\ \sigma_2 \\ \sigma_3 \\ \tau_{23} \\ \tau_{13} \\ \tau_{12} \end{bmatrix} = \begin{bmatrix} C_{11} & C_{12} & C_{13} & 0 & 0 & 0 \\ C_{21} & C_{22} & C_{23} & 0 & 0 & 0 \\ C_{31} & C_{32} & C_{33} & 0 & 0 & 0 \\ 0 & 0 & 0 & C_{44} & 0 & 0 \\ 0 & 0 & 0 & 0 & C_{55} & 0 \\ 0 & 0 & 0 & 0 & 0 & C_{66} \end{bmatrix} \begin{bmatrix} \varepsilon_1 \\ \varepsilon_2 \\ \varepsilon_3 \\ \gamma_{23} \\ \gamma_{31} \\ \gamma_{12} \end{bmatrix} \qquad \text{Eq.3.3}$$

In terms of the compliance coefficient (S_{ij}), Hooke's law in 3 dimensions for an orthotropic material may be also be written as:

$$\begin{bmatrix} \varepsilon_1 \\ \varepsilon_2 \\ \varepsilon_3 \\ \gamma_{23} \\ \gamma_{13} \\ \gamma_{12} \end{bmatrix} = \begin{bmatrix} S_{11} & S_{12} & S_{13} & 0 & 0 & 0 \\ S_{21} & S_{22} & S_{23} & 0 & 0 & 0 \\ S_{31} & S_{32} & S_{33} & 0 & 0 & 0 \\ 0 & 0 & 0 & S_{44} & 0 & 0 \\ 0 & 0 & 0 & 0 & S_{55} & 0 \\ 0 & 0 & 0 & 0 & 0 & S_{66} \end{bmatrix} \begin{bmatrix} \sigma_1 \\ \sigma_2 \\ \sigma_3 \\ \tau_{23} \\ \tau_{31} \\ \tau_{12} \end{bmatrix} \qquad \text{Eq.3.4}$$

For plane stress in the 1,2 – plane:

$\sigma_3 = 0$, $\tau_{23} = 0$ and $\tau_{13} = 0$

The compliance form for Hooke's law in this case reduces to:

$$\begin{bmatrix} \varepsilon_1 \\ \varepsilon_2 \\ \gamma_{12} \end{bmatrix} = \begin{bmatrix} S_{11} & S_{12} & 0 \\ S_{12} & S_{22} & 0 \\ 0 & 0 & S_{66} \end{bmatrix} \begin{bmatrix} \sigma_1 \\ \sigma_2 \\ \tau_{12} \end{bmatrix} \qquad \text{Eq.3.5}$$

In terms of engineering constants, Equation 3.5 can be rewritten as:

$$\begin{bmatrix} \varepsilon_1 \\ \varepsilon_2 \\ \gamma_{12} \end{bmatrix} = \begin{bmatrix} \frac{1}{E_1} & -\frac{\nu_{12}}{E_1} & 0 \\ -\frac{\nu_{21}}{E_2} & \frac{1}{E_2} & 0 \\ 0 & 0 & \frac{1}{G_{12}} \end{bmatrix} \begin{bmatrix} \sigma_1 \\ \sigma_2 \\ \tau_{12} \end{bmatrix} \qquad \text{Eq.3.6}$$

where: υ_{12}, ν_{21} = Poisson's ratio

E_1, E_2 = Modulus of elasticity

G_{12} = Shear modulus

It can be seen that five elastic constants are needed to characterize the material. The bicomponent layer of the laminate will be considered as an orthotropic material subjected to plane stresses. The medium density fiberboard (MDF) layer will be considered to be an isotropic material. Only three elastic constants are needed for an isotropic material, i.e. E, υ and G.

3.2.2) Macromechanical model to determine elastic behavior of a laminate

If an assumed deformation is introduced through the thickness of a three dimensional laminate, its behavior can be described by a two dimensional model. The simplest assumption is the Love-Kirchhoff assumption widely used in the conventional theory of plates and shells. The strains in a plate can be written as:

$$\begin{bmatrix} \varepsilon_x \\ \varepsilon_y \\ \gamma_{xy} \end{bmatrix} = \begin{bmatrix} \varepsilon_x^o \\ \varepsilon_y^o \\ \gamma_{xy}^o \end{bmatrix} + z \begin{bmatrix} \kappa_x^o \\ \kappa_y^o \\ \kappa_{xy}^o \end{bmatrix} \qquad \text{Eq.3.7}$$

where:

ε_x^o = extensional strain of the reference surface (midplane) in the x direction
ε_y^o = extensional strain of the reference surface (midplane) in the y direction
γ_{xy}^o = inplane shear strain of the reference surface (midplane)
z = distance of a point from the midplane
κ_x^o = curvature of the reference surface (midplane) in the x direction
κ_y^o = curvature of the reference surface (midplane) in the y direction
κ_{xy}^o = twisting curvature of the reference surface (midplane)

It can be seen from equation 3.7 that the strain varies linearly through the laminate thickness. Once the strains are known, the following stress-strain equation can be used to calculate the global stresses in the lamina:

$$\begin{bmatrix} \sigma_x \\ \sigma_y \\ \tau_{xy} \end{bmatrix} = \begin{bmatrix} \overline{Q}_{11} & \overline{Q}_{12} & \overline{Q}_{16} \\ \overline{Q}_{12} & \overline{Q}_{22} & \overline{Q}_{26} \\ \overline{Q}_{16} & \overline{Q}_{26} & \overline{Q}_{66} \end{bmatrix} \begin{bmatrix} \varepsilon_x \\ \varepsilon_y \\ \gamma_{xy} \end{bmatrix} \qquad \text{Eq.3.8}$$

where $\overline{Q}$ is the transformed reduced stiffness matrix. Combining equations 3.7 and 3.8 and simplifying, the stresses in the different layers of the laminate can be expressed in terms of the laminate midplane strains and curvatures as follows:

$$\begin{bmatrix} \sigma_x \\ \sigma_y \\ \tau_{xy} \end{bmatrix} = \begin{bmatrix} \overline{Q}_{11} & \overline{Q}_{12} & \overline{Q}_{16} \\ \overline{Q}_{12} & \overline{Q}_{22} & \overline{Q}_{26} \\ \overline{Q}_{16} & \overline{Q}_{26} & \overline{Q}_{66} \end{bmatrix} \begin{bmatrix} \varepsilon_x^o + z\kappa_x^o \\ \varepsilon_y^o + z\kappa_y^o \\ \gamma_{xy}^o + z\kappa_{xy}^o \end{bmatrix} \qquad \text{Eq.3.9}$$

This equation shows that the stresses vary linearly only through the thickness of each lamina. The stresses may change in magnitude from lamina to lamina because the transformed reduced stiffness matrix is dependent on the material and orientation of the ply. The stresses can be integrated in the thickness direction to yield the force resultants (N) and the moment resultants (M).

The strain and stress equations shown previously allow us to calculate the strains and stresses in terms of midplane strains and curvatures. However, if the midplane strains and curvatures are unknown, they can be determined from the applied forces and moment resultants. The following notation will be used in the equations:

n = number of layers

k = index for the ply number

h_k = thickness of each ply (where k=1 to n)

$h = \sum_{k=1}^{n} h_k$ = thickness of the laminate

z_i = z coordinate of each ply (where i=0 to n)

Layer 1 is bounded by z_0 and z_1

Layer k is bounded by z_{k-1} and z_k

Layer n is bounded by z_{n-1} and z_n

N = force per unit width of the laminate cross section

M = moment per unit width of the laminate cross section

The force and moment resultants can be combined in matrix form as follows:

$$\begin{bmatrix} N_x \\ N_y \\ N_{xy} \end{bmatrix} = \int_{-h/2}^{h/2} \begin{bmatrix} \sigma_x \\ \sigma_y \\ \tau_{xy} \end{bmatrix} dz = \sum_{k=1}^{n} \int_{z_{k-1}}^{z_z} \begin{bmatrix} \sigma_x \\ \sigma_y \\ \tau_{xy} \end{bmatrix} dz \qquad \text{Eq.3.10}$$

$$\begin{bmatrix} M_x \\ M_y \\ M_{xy} \end{bmatrix} = \int_{-h/2}^{h/2} \begin{bmatrix} \sigma_x \\ \sigma_y \\ \tau_{xy} \end{bmatrix} z\,dz = \sum_{k=1}^{n} \int_{z_{k-1}}^{z_z} \begin{bmatrix} \sigma_x \\ \sigma_y \\ \tau_{xy} \end{bmatrix} z\,dz \qquad \text{Eq.3.11}$$

Combining Equations 3.10 and 3.11 with Equation 3.9, gives us:

$$\begin{bmatrix} N_x \\ N_y \\ N_{xy} \end{bmatrix} = \sum_{k=1}^{n} \begin{bmatrix} \overline{Q}_{11} & \overline{Q}_{12} & \overline{Q}_{16} \\ \overline{Q}_{12} & \overline{Q}_{22} & \overline{Q}_{26} \\ \overline{Q}_{16} & \overline{Q}_{26} & \overline{Q}_{66} \end{bmatrix}_k \left\{ \int_{z_{k-1}}^{z_z} \begin{bmatrix} \varepsilon_x^o \\ \varepsilon_y^o \\ \gamma_{xy}^o \end{bmatrix} dz + \int_{z_{k-1}}^{z_k} \begin{bmatrix} \kappa_x^o \\ \kappa_y^o \\ \kappa_{xy}^o \end{bmatrix} z\,dz \right\} \qquad \text{Eq.3.12}$$

and

$$\begin{bmatrix} M_x \\ M_y \\ M_{xy} \end{bmatrix} = \sum_{k=1}^{n} \begin{bmatrix} \overline{Q}_{11} & \overline{Q}_{12} & \overline{Q}_{16} \\ \overline{Q}_{12} & \overline{Q}_{22} & \overline{Q}_{26} \\ \overline{Q}_{16} & \overline{Q}_{26} & \overline{Q}_{66} \end{bmatrix}_k \left\{ \int_{z_{k-1}}^{z_z} \begin{bmatrix} \varepsilon_x^o \\ \varepsilon_y^o \\ \gamma_{xy}^o \end{bmatrix} z\,dz + \int_{z_{k-1}}^{z_k} \begin{bmatrix} \kappa_x^o \\ \kappa_y^o \\ \kappa_{xy}^o \end{bmatrix} z^2\,dz \right\} \qquad \text{Eq.3.13}$$

In compact form, Equations 3.12 and 3.13 can be rewritten as:

$$\begin{bmatrix} N_x \\ N_y \\ N_{xy} \end{bmatrix} = \begin{bmatrix} A_{11} & A_{12} & A_{16} \\ A_{12} & A_{22} & A_{26} \\ A_{16} & A_{26} & A_{66} \end{bmatrix} \begin{bmatrix} \varepsilon_x^o \\ \varepsilon_y^o \\ \gamma_{xy}^o \end{bmatrix} + \begin{bmatrix} B_{11} & B_{12} & B_{16} \\ B_{12} & B_{22} & B_{26} \\ B_{16} & B_{26} & B_{66} \end{bmatrix} \begin{bmatrix} \kappa_x^o \\ \kappa_y^o \\ \kappa_{xy}^o \end{bmatrix} \qquad \text{Eq.3.14}$$

and:

$$\begin{bmatrix} M_x \\ M_y \\ M_{xy} \end{bmatrix} = \begin{bmatrix} B_{11} & B_{12} & B_{16} \\ B_{12} & B_{22} & B_{26} \\ B_{16} & B_{26} & B_{66} \end{bmatrix} \begin{bmatrix} \varepsilon_x^o \\ \varepsilon_y^o \\ \gamma_{xy}^o \end{bmatrix} + \begin{bmatrix} D_{11} & D_{12} & D_{16} \\ D_{12} & D_{22} & D_{26} \\ D_{16} & D_{26} & D_{66} \end{bmatrix} \begin{bmatrix} \kappa_x^o \\ \kappa_y^o \\ \kappa_{xy}^o \end{bmatrix} \qquad \text{Eq.3.15}$$

where:

$$A_{ij} = \sum_{k=1}^{n} \left[\overline{Q}_{ij}\right]_k \left(z_k - z_{k-1}\right)$$

$$B_{ij} = \frac{1}{2} \sum_{k=1}^{n} \left[\overline{Q}_{ij}\right]_k \left(z_k^2 - z_{k-1}^2\right)$$

$$D_{ij} = \frac{1}{3} \sum_{k=1}^{n} \left[\overline{Q}_{ij}\right]_k \left(z_k^3 - z_{k-1}^3\right)$$

The [A] matrix, called the extensional stiffness matrix, relates the resultant in-plane forces to the in-plane strains. The [D] matrix, called the bending stiffness matrix, relates the resultant bending moments to the plate curvatures. The [B] matrix, called the bending-extension coupling stiffness matrix, couples the force and moment terms to the midplane curvatures and midplane strains.

The two equations can be combined to give a single equation:

$$\begin{bmatrix} N_x \\ N_y \\ N_{xy} \\ M_x \\ M_y \\ M_{xy} \end{bmatrix} = \begin{bmatrix} A_{11} & A_{12} & A_{16} & B_{11} & B_{12} & B_{16} \\ A_{12} & A_{22} & A_{26} & B_{12} & B_{22} & B_{26} \\ A_{16} & A_{26} & A_{66} & B_{16} & B_{26} & B_{66} \\ B_{11} & B_{12} & B_{16} & D_{11} & D_{12} & D_{16} \\ B_{12} & B_{22} & B_{26} & D_{12} & D_{22} & D_{26} \\ B_{16} & B_{26} & B_{66} & D_{16} & D_{26} & D_{66} \end{bmatrix} \begin{bmatrix} \varepsilon_x^o \\ \varepsilon_y^o \\ \gamma_{xy}^o \\ \kappa_x^o \\ \kappa_y^o \\ \kappa_{xy}^o \end{bmatrix} \qquad \text{Eq.3.16}$$

The 6 x 6 matrix consisting of the components of [A], [B], and [D] is called the laminate stiffness matrix or the ABD matrix.

In order to calculate the strains and curvatures at the reference surface in terms of the force and moment resultants, we must take the inverse of the ABD matrix shown in Equation 3.16:

$$\begin{bmatrix} \varepsilon_x^o \\ \varepsilon_y^o \\ \gamma_{xy}^o \\ \kappa_x^o \\ \kappa_y^o \\ \kappa_{xy}^o \end{bmatrix} = \begin{bmatrix} A_{11} & A_{12} & A_{16} & B_{11} & B_{12} & B_{16} \\ A_{12} & A_{22} & A_{26} & B_{12} & B_{22} & B_{26} \\ A_{16} & A_{26} & A_{66} & B_{16} & B_{26} & B_{66} \\ B_{11} & B_{12} & B_{16} & D_{11} & D_{12} & D_{16} \\ B_{12} & B_{22} & B_{26} & D_{12} & D_{22} & D_{26} \\ B_{16} & B_{26} & B_{66} & D_{16} & D_{26} & D_{66} \end{bmatrix}^{-1} \begin{bmatrix} N_x \\ N_y \\ N_{xy} \\ M_x \\ M_y \\ M_{xy} \end{bmatrix} \qquad \text{Eq.3.17}$$

3.3) Materials and Methods

One method for measuring the elastic constants and the shear modulus needed for the model described in Section 3.2.2 involves the use of two tensile test specimens, one with the primary material axis orientated along the longitudinal axis of a specimen and the second with the primary material axis orientated at 10 degrees to the longitudinal axis of the specimen (Chamis and Sinclair, 1977). A T-rosette is installed on the on-axis specimen to measure the Poisson's ratio, while a three element rectangular rosette is installed on the off-axis specimen (See Figure 3.1).

The following paragraph describes strain gauge application techniques. Samples were prepared for the application of the strain gauge by lightly scuffing the surfaces with a high grade sand paper. A placement grid was measured out on opposite faces to align the gauges.

The gauges were placed face up in the centre of a 25mm by approximately 75 mm piece clear adhesive tape to assist and maintain gauge alignment during gluing. Gauges were then held in place on the sample with the correct alignment by means of the tape, and partially lifted off prior to gluing leaving 35 mm of the tape in contact with the sample. An epoxy adhesive was prepared (Vishay M-Bond AE-10) in accordance with the supplier's specifications, and applied lightly to the surface of the gauge and the sample with a glass applicator. The adhesive tape was gently rolled down from the still attached end by means of the applicator, squeezing out any excess resin. If done correctly, the gauge alignment is maintained through the entire process. A 25 mm by 25 mm silicon rubber pad was then placed on the gauge to evenly distribute the pressure, followed by a 25 mm by 25 mm block of wood. An 11 kg weight was placed on top of the entire assembly. The resin was left to dry overnight.

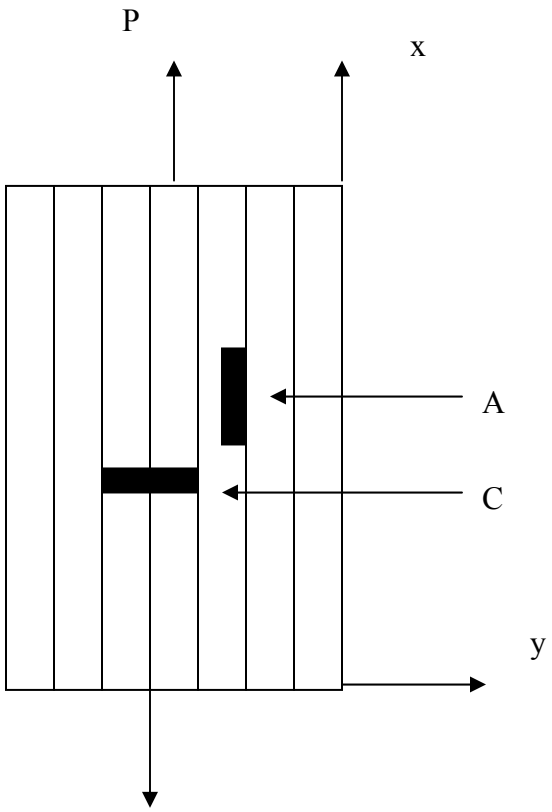

Figure 3.1a**:** T-rosette

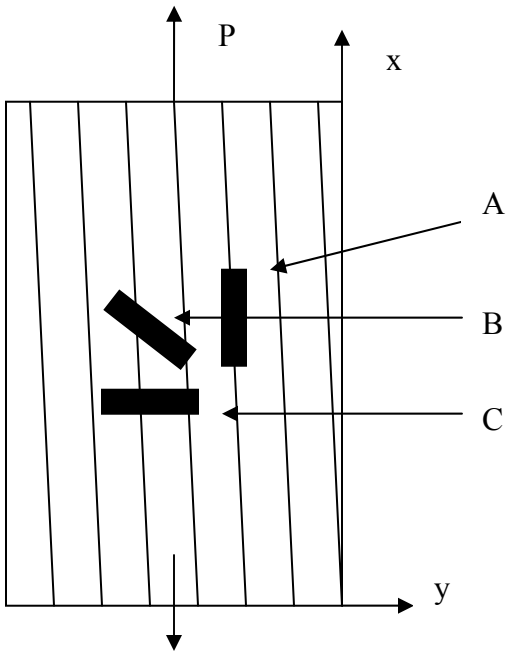

Figure 3.1b**:** Rectangular rosette

Figure 3.1: Layout of the T-rosette (Figure 3.1a) and rectangular rosette (Figure 3.1b) strain gauge in the on-axis and 10 degree off-axis test specimens respectively. P denotes the applied force. A, B and C indicates the x, 45 degree and y gages found on the rosettes respectively.

The Poisson's ratio, υ_{12}, can be calculated from the strain measurements made with the T-rosette on the on-axis specimen with Equation 3.18:

$$\nu_{12} = \left| \frac{\varepsilon_2}{\varepsilon_1} \right| \qquad \text{Eq. 3.18}$$

Where ε_1 is the normal strain along the principal material axis which has the highest elastic moduls and ε_2 is the strain along the material axis with the lowest elastic modulus. The

remaining calculations are based on υ_{12} and the strain measurements obtained from the off-axis tensile test.

The strain gauge data obtained with the rosette shown in Figure 3.1 can be rewritten as:

$$\varepsilon_A = \varepsilon_x \qquad \text{Eq. 3.19}$$

$$\varepsilon_C = \varepsilon_y \qquad \text{Eq. 3.20}$$

$$\varepsilon_B = \varepsilon_{45} \qquad \text{Eq. 3.21}$$

from which the shear strain, γ_{xy}, can be calculated as follows:

$$\varepsilon_{45} = \varepsilon_x \cos^2 45 + \varepsilon_y \sin^2 45 + \gamma_{xy} \sin 45 \cos 45 \qquad \text{Eq. 3.22}$$

$$\gamma_{xy} = \frac{\varepsilon_{45} - \varepsilon_x \cos^2 45 + \varepsilon_y \sin^2 45}{\sin 45 \cos 45} \qquad \text{Eq. 3.23}$$

Equations 3.22 and 3.23 can then be used to determine the direction of the minimum and maximum principle strains ($\theta_{p,q}$).

$$\theta_p = \frac{1}{2} \tan^{-1} \frac{\gamma_{xy}}{\varepsilon_x - \varepsilon_y} \qquad \text{Eq. 3.24}$$

$$\theta_q = \theta_p + 90 \qquad \text{Eq. 3.25}$$

The magnitude of the maximum and minimum principal strains can be calculated with:

$$\varepsilon_{p,q} = \frac{\varepsilon_x + \varepsilon_y}{2} \pm \sqrt{\left(\frac{\varepsilon_x - \varepsilon_y}{2}\right)^2 + \left(\frac{\gamma_{xy}}{2}\right)^2} \qquad \text{Eq. 3.26}$$

Using the standard strain transformations, the normal strains in the principal material axis (ε_1 and ε_2) and the shear strain (γ_{12}) can be calculated with:

$$\varepsilon_1 = \varepsilon_p \cos^2 \beta + \varepsilon_q \sin^2 \beta \qquad \text{Eq. 3.27}$$

$$\varepsilon_2 = \varepsilon_p \sin^2 \beta + \varepsilon_q \cos^2 \beta \qquad \text{Eq. 3.28}$$

$$\gamma_{12} = -2(\varepsilon_p - \varepsilon_q) \sin \beta \cos \beta \qquad \text{Eq. 3.29}$$

Where: β = the counterclockwise rotation of the primary material axis from ε_p.

The normal stresses and shear stress for the principal material axis can be calculated with:

$$\sigma_1 = \frac{P \cos^2 \theta}{bt} \qquad \text{Eq. 3.30}$$

$$\sigma_2 = \frac{P \sin^2 \theta}{bt} \qquad \text{Eq. 3.31}$$

$$\tau_{12} = \frac{-P \sin \theta \cos \theta}{bt} \qquad \text{Eq. 3.32}$$

where: P = applied load

b = specimen width

t = specimen thickness

θ = off-axis angle

The elastic moduli, the shear modulus and the remaining Poisson's ratio can then be calculated from:

$$E_1 = \frac{\sigma_1 - (\nu_{12}\sigma_2)}{\varepsilon_1} \qquad \text{Eq. 3.33}$$

$$E_2 = \frac{E_1 \sigma_2}{E_1 \varepsilon_2 + \sigma_1 \nu_{12}} \qquad \text{Eq. 3.34}$$

$$\nu_{21} = \nu_{12} \frac{E_2}{E_1} \qquad \text{Eq. 3.35}$$

$$G_{12} = \frac{\tau_{12}}{\gamma_{12}} \qquad \text{Eq. 3.36}$$

The experimental procedure was initially tested using radially sawn sassafras (*Sassafras albidum*) samples. The boards were selected according to straightness of grain. Sample beams with dimensions of 400x25x12.5 mm were cut with the grain aligned along the longitudinal axis of the beams for the on-axis tests. A T-rosette (Vishay 125LT) was adhered in the centre of the 25 mm face, with a second linear strain gauge (Vishay 125LW) placed on the opposite face. For the 10 degree off-axis test, beams were cut from the boards by means of a tapering jig adjusted to 10 degrees. A triangular rosette gauge (Vishay 125LR) was used. Seven mm holes were drilled in the ends of the beams. The stress was applied with a pin jig in an MTS testing machine. Strains were recorded with a Vishay Micro Measurements P3 strain indicator and recorder. The resultant elastic moduli were compared to data obtained from the literature. In order to ascertain whether the gauge application was consistent, a T- and angular rosette gauge were applied to the same sample and the data obtained from the linear component of the gauges were compared. No significant differences were observed between the two results, which indicate that the gauge application technique worked adequately.

Wood-bicomponent fiber panels and MDF were prepared according to the techniques described in Chapter 1. It was decided to limit the tests conducted in this section to the 2.3 mm panels, due to the comparatively large differences observed in bending modulus between the 2.3 mm wood-bicomponent panels and the MDF control in the DMA. Furthermore, the sample dimensions were limited by the length of the panels produced to 200 mm by 18 mm by 2.3mm. Samples were cut with a fiber orientation of the bicomponent sheets along the

longitudinal axis of the beams, as well as at 10 degrees with respect to the beam axis.

To ensure that the stress distribution was even in the centre of the beams where the gauges were placed, the ends were reinforced with an epoxy reinforced paper sheet. The gauges were applied according to the procedure described previously.

Samples were preloaded in the MTS at 2.5 mm/min until a load of 8.9 N was reached, after which the test proceeded at 1.25 mm/min. The tests were stopped when a reading of at least 600 microstrains was reached on the longitudinal component of the strain gauge.

After conducting the tensile tests on the laminates, the bicomponent lamina was carefully removed from the surfaces by means of a paring knife. Care was taken to ensure that the gauges were not bent or otherwise damaged during removal. The delaminated bicomponent lamina was then retested in the MTS according to the procedure described above. Strain gauges were also attached to the delaminated wood fiber core after removal. The ends of these sections were also reinforced with the epoxy-infused paper sheets, and tested in the MTS.

A total of 15 bicomponent laminate panels were tested.

3.4) Results and discussion

Based on the techniques used during the forming of the laminate panels, and data obtained for thickness swell, it was decided that the wood fiber core of the wood-bicomponent laminate panels were isotropic, and it was treated as such in the model.

The stress-strain curve for a representative sample (MDF1) of the delaminated wood fiber core is shown in Figure 3.2. The slope of this curve gives the modulus of elasticity (681.16 MPa). The axial and lateral strain readings from the T-rosette strain gage were used to determine the Poisson's ratio (0.29 in the case of MDF1). From the MOE and ν values, the shear modulus was calculated using the following equation:

$$G = \frac{E}{2(1+\nu)} \qquad \text{Eq. 3.36}$$

For MDF1, the shear modulus was 264 MPa. The slope of the stress strain curves, Poisson's ratios and calculated shear modulus for the fiber board cores are shown in Table A3.1 in the appendix. . The core had a mean modulus of elasticity of 689.13 MPa (St. dev. 45 MPa) with a mean Poisson's ratio of 0.288 (St. dev. 0.026). The calculated mean shear modulus was 267.7 MPa (St. dev. 19.1 MPa). Cai (2006) obtained values for MOE in tension for MDF of 2000 MPa. This large discrepancy between the values obtained during this research and those cited in the literature can be attributed to the long press times used in this study to ensure that the bicomponent fiber surface reinforcement has adequate time at high temperature to melt the polypropylene sheath. UF resin degrades when it is exposed to high temperature for long periods of time. Furthermore, the blender used during this research was specifically designed to process particleboard, and it is suspected that resin blending during furnish processing was non-uniform.

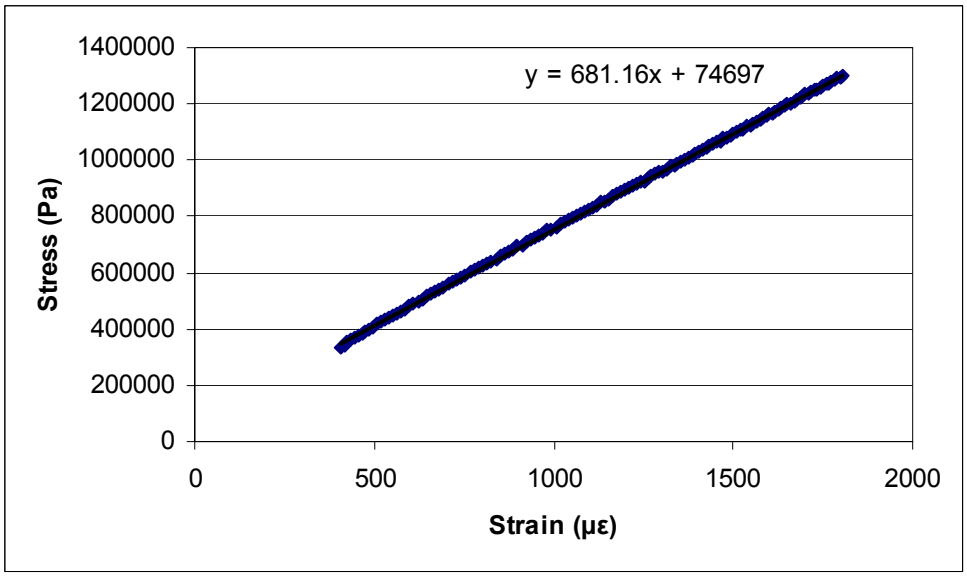

Figure 3.2: Stress strain curve for a representative sample of the wood fiber core obtained from the wood-bicomponent fiber panels

Similarly, the Poisson's ratio (ν_{12}) for the delaminated bicomponent fiber sheets was obtained from an on-axis tensile test. The values for ε_x, ε_y and ε_{45}, as well as the corresponding stress, were obtained from the data produced by the off-axis tensile tests conducted on the bicomponent sheets. Values were obtained 2 minutes after the tests started. The strain values, along with the corresponding stresses and the Poisson's ratios are shown in Table A3.2 in the appendix. These values, in conjunction with Equations 3.19 through 3.36 were then used to calculate the elastic moduli in the 1 and 2 directions, as well as the resultant shear moduli and the Poisson's ratio (ν_{21}) (Table 3.1). Two samples were rejected after completion of the experiments. Bicosheet3 was rejected after issues were observed with the strain gage adhesion to the wood fiber core, and bicosheet13 was rejected due to one of

the lead wires detaching during the testing procedure. A mean E_1 of 2178.2 MPa (St. dev. 118.7 MPa) and an E_2 of 1051.6 MPa (St. dev. 143.7 MPa) was observed. G_{12} and ν_{21} was 726.9 MPa (St. dev. 107.1 MPa) and 0.08 (St. dev. 0.054) respectively. It can be seen that the mean modulus of elasticity along the fiber direction is approximately double that of the lateral direction.

Table 3.1: Elastic moduli (E_1 and E_2), shear modulus (G_{12}) and Poisson's ratio (ν_{21}) for the delaminated bicomponent sheets.

Sample	E_1 (Pa)	E_2 (Pa)	G_{12} (Pa)	ν_{21}
bicosheet1	0.28	2058213290	4.85E+08	7.15E+08
bicosheet2	0.27	2267352698	1.96E+09	7.6E+08
bicosheet4	0.28	2241652915	6.44E+08	8.53E+08
bicosheet5	0.29	2384351181	7.17E+08	5.34E+08
bicosheet6	0.28	2053423984	3.38E+08	6.32E+08
bicosheet7	0.3	2138321398	5.62E+09	7.6E+08
bicosheet8	0.28	2208815709	5.31E+08	8.72E+08
bicosheet9	0.28	2101562799	4.21E+08	8.23E+08
bicosheet10	0.3	2052960928	9.41E+08	7.51E+08
bicosheet11	0.28	2172788550	4.89E+08	6.81E+08
bicosheet12	0.3	2047234038	3.85E+08	7.68E+08
bicosheet14	0.28	2205937772	4.23E+08	7.67E+08
bicosheet15	0.29	2384351181	7.17E+08	5.34E+08

Prior to implementation of the model described in Section 3.2.2, the mean moduli obtained in tension for the constituent lamina were combined by means of a rule of mixtures:

$$E_p x_p = E_m x_m + E_b x_b \qquad \text{Eq. 3.37}$$

where: E_i = Longitudinal modulus of elasticity

x_i = Thickness fraction of each composite lamina

p, m, b = Laminate, wood component and bicomponent sheet component, respectively

The mean longitudinal modulus calculated for the laminate was then compared with the mean longitudinal modulus obtained from on axis tensile tests conducted with t-rosette strain gauges. The mean calculated laminate modulus was found to be 950 MPa (St. dev. 68 MPa), while a mean longitudinal modulus of 923 (St. dev. 21 MPa) was measured.

The values listed in Table A3.1 and 3.1 for each sample were then used as inputs in the model described in section 3.2.1. By multiplying the inverse of the ABD matrix with the applied stress, the resultant strain at that stress level can be determined for the wood-bicomponent panels. These values were compared with the measured strain values obtained from on-axis tensile tests of the bicomponent panels. In order to control for the time dependent effect on the elastic properties of the material, it was decided to use stress and strain values taken at least 2 minutes after sample loading commenced in the MTS. Table 3.2 lists the stress and Poisson's ratio (ν_{12}) used for the calculations. It also gives the experimentally measured ε_1 and ε_2, as well as values calculated from the model.

Table 3.2: Comparison of the strains measured during on axis tensile tests with the strains calculated at arbitrary stresses for each of the bicomponent panels tested.

Sample	Stress (Pa)	Poisson's Ratio	Measured ε_1	Calculated ε_1	Measured ε_2	Calculated ε_2	Percent deviation between measured and modeled dimensions ε_1	Percent deviation between measured and modeled dimensions ε_2
bicopanel1	309753	0.29	0.000333	0.000337	-0.000096	-0.000097	-1.14	-1.16
bicopanel2	320260	0.31	0.000335	0.000321	-0.000097	-0.000084	4.31	13.03
bicopanel4	300042	0.28	0.000344	0.000320	-0.000102	-0.000087	6.96	14.98
bicopanel5	306759	0.30	0.000333	0.000302	-0.000090	-0.000083	9.34	8.33
bicopanel6	319734	0.30	0.000335	0.000334	-0.000099	-0.000090	0.43	8.88
bicopanel8	314643	0.33	0.000335	0.000319	-0.000113	-0.000087	4.73	23.44
bicopanel9	281739	0.29	0.000316	0.000310	-0.000098	-0.000090	1.85	8.58
bicopanel10	323574	0.30	0.000333	0.000352	-0.000097	-0.000106	-5.85	-8.86
bicopanel12	304836	0.29	0.000333	0.000319	-0.000108	-0.000095	4.12	12.10
bicopanel14	300992	0.29	0.000337	0.000330	-0.000131	-0.000101	2.00	22.71
bicopanel15	307918	0.30	0.000335	0.000312	-0.000101	-0.000091	6.82	10.49
Mean	308204	0.30	0.00033	0.00032	-0.000103	-0.000092	4.32	12.05
St. dev.	11794	0.01	0.00001	0.00001	0.000011	0.000007	2.79	6.48

T-tests conducted to compare the means of the measured and calculated strains for the 1 and 2 directions showed no significant difference, indicating that the model discussed in section 3.2.1 fit the experimental values well. A mean stress of 308204 Pa resulted in a mean calculated microstrain of 323 (St. dev. 12) in the x direction. Measured values for microstrain had a mean of 334 (St. dev. 15).

It can be seen from Table 3.2 that the model under predicts the strain in the x direction 4.32 percent (St. dev. 42.79). The model over predicts the strains for bicopanel1 and bicopanel10.

The under prediction can be attributed to interactions caused by the fibers passing through the thickness direction as a result of needlepunching not incorporated by the model.

In the y direction, a mean microstrain of -92 (St. dev. 7.00) was predicted by the model, with a microstrain of -103 (St. dev. 11) measured. The model under predicts the strain in the y-direction by 12.05 percent (St. dev. 6.48). The large standard deviation can be attributed to bicopanel8 and bicopanel14, both of which showed deviations from the measured values of greater than 20 percent. As was the case for longitudinal strain, the model over predicted the strains for bicopanel1and bicopanel10.

To further investigate the effect of the various parameters on the results obtained from the model, a sensitivity analyses was conducted. Parameters investigated were the bicomponent moduli (E_1,and E_2), the wood fiber core modulus (E) and the wood fiber core Poisson's ratio (ν). The mean values obtained for each of the parameters were used as initial inputs in the model to calculate the longitudinal and lateral strains. The parameters were then adapted according to the standard deviation approach employed by Skaggs and Bender (1992), who changed the input values by two standard deviation increments up to 6 standard deviations from the mean. The values calculated using this approach was then expressed as a percentage deviation from the values calculated using the mean inputs.

Figure 3.3 illustrates variation from the mean when the parameter E_1, the longitudinal elastic modulus of the reinforcement, is changed. It can be seen that increasing the longitudinal stiffness by 2 standard deviations from the mean results in a 4 and 3 percent reduction in the calculated ε_1 and $\varepsilon 2$.

The reduction is expected, seeing that an increase in elasticity will result in lower strains if the stress is kept constant. The inverse occurs when the modulus is decreased by two standard deviations. When taken into account with the fact that model calculate strains deviated from the measured strains by 4.32 percent, the importance of correctly identifying E_1 becomes apparent.

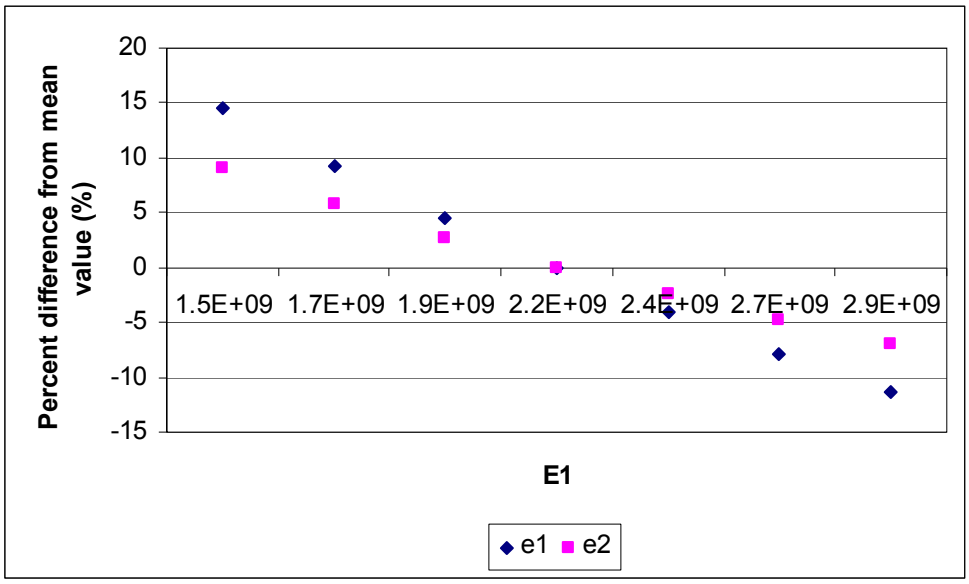

Figure 3.3: Strains calculated with the macromechanical model by varying the mean longitudinal elasticity of the bicomponent fiber (E_1) by 2 standard deviation increments, expressed as a percentage of the values obtained using the mean elasticity. A standard deviation of 1.19E+08 Pa was used.

Figure 3.4 shows the effect on calculated strains of a change in the lateral stiffness of the bicomponent fiber sheets, while Figure 3.5 illustrates the effect on calculated strains due to a variation in the Poisson's ratio of the wood fiber core. The mean value was again adjusted by 2 standard deviation increments.

As expected, an increase in lateral elasticity (Figure 3.4) and the Poisson's ratio (Figure 3.5) has a negligible effect on ε_1. They have, however, a stronger effect on lateral strains. A $\pm$2 standard deviation change in lateral stiffness results in 4.5% reduction and a 5 % increase in ε_2 from the mean. A 4 standard deviation increase in lateral stiffness results in an 8 percent decrease in lateral strain, while a 4 standard deviation decrease results in a 13 percent increase in ε_2. Varying the Poisson's ratio of the wood fiber core by $\pm$2 standard deviations results in a 15 percent variation in lateral strains. These effects are significant when taking into account that the elastic constants of the bicomponent fiber sheets and the Poisson's ratio of the core are obtained by a set of three experiments and an extensive series of calculations. Experimental and measurement errors in obtaining the lateral strains and the Poisson's ratio are therefore magnified by the model. The 12 percent difference in the lateral strains calculated with the model from the measured values might therefore be accounted for by these factors.

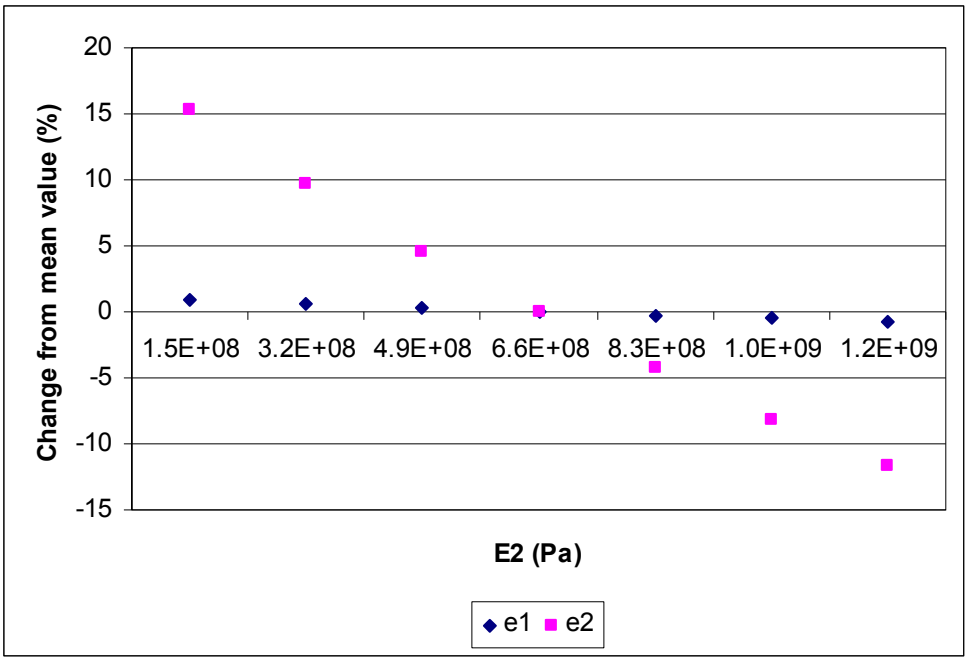

Figure 3.4: Strains calculated with the macromechanical model by varying the mean lateral elasticity of the bicomponent fiber (E_2) by 2 standard deviation increments, expressed as a percentage of the values obtained using the mean elasticity. A standard deviation of 8.66E+07 Pa was used.

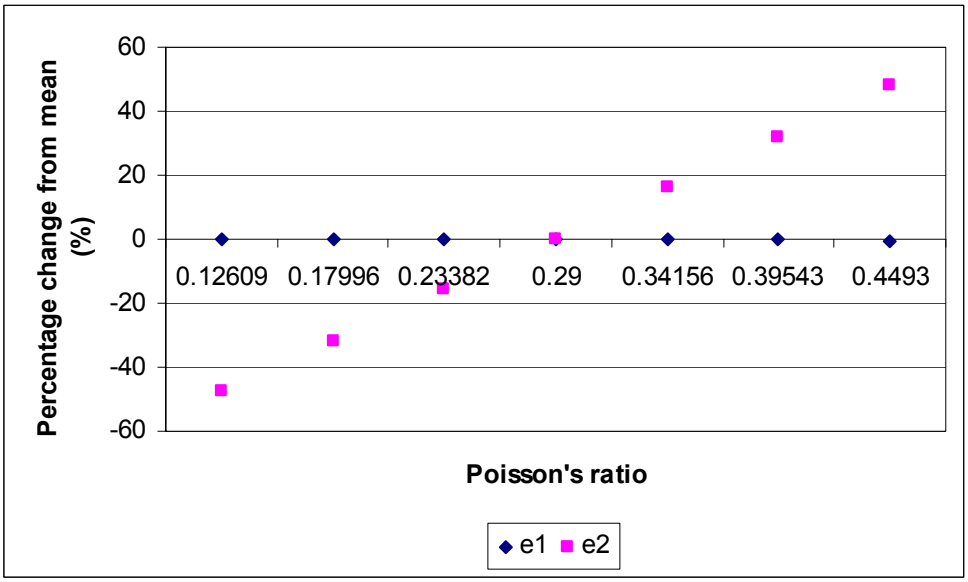

Figure 3.5: Strains calculated with the macromechanical model by varying the mean Poisson's ratio of the wood fiber core (ν) by 2 standard deviation increments, expressed as a percentage of the values obtained using the mean elasticity. A standard deviation of 0.03 was used.

Figure 3.6 illustrates the effect on calculated strains of a change in the elastic modulus (E) of the wood fiber core. It can be seen that a 2 standard deviation increase in E results in a 10 percent increase in ε_2 and ε_1. A 4 standard deviation decrease in E resulted in a 12 percent increase in ε_2 and ε_1. As expected, the model is highly sensitive to the properties of the wood fiber core, due to the fact that the core accounts for approximately 80 percent of the volume of the material. In combination with the results shown in Figure 3.5, care needs to be taken in obtaining the properties of the core material when attempting to determine the tensile properties of the laminate.

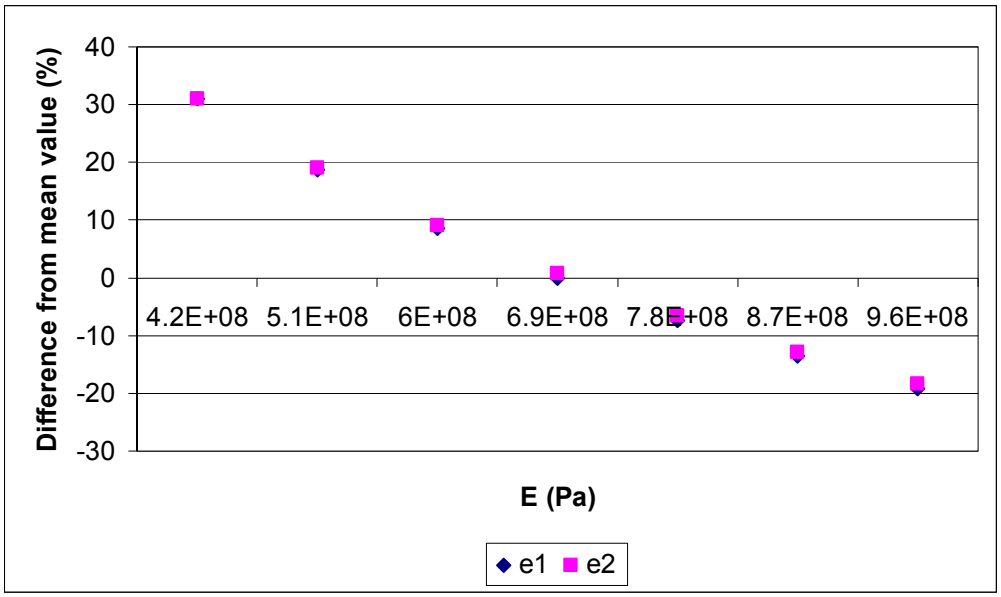

Figure 3.6: Strains calculated with the macromechanical model by varying the mean elasticity of the wood fiber core (E) by 2 standard deviation increments, expressed as a percentage of the values obtained using the mean elasticity. A standard deviation of 4.50E+07 was used.

To further investigate the effectiveness of the model in describing the elastic behavior of the composite, a sensitivity analyses was conducted on the thickness of the bicomponent fiber reinforcement. The thickness was varied by from the mean value (0.2 mm) by 0.1 mm increments (Figure 3.7). Changing the thickness of the reinforcement resulted in substantial variation from the mean strains. It was also found that the lateral strains are more sensitive to changes in bicomponent fiber sheet reinforcement thickness, which provides more evidence for the statement made previously that the difference observed between the model calculated and measured strains might be due to measurement error, and not an error in the model.

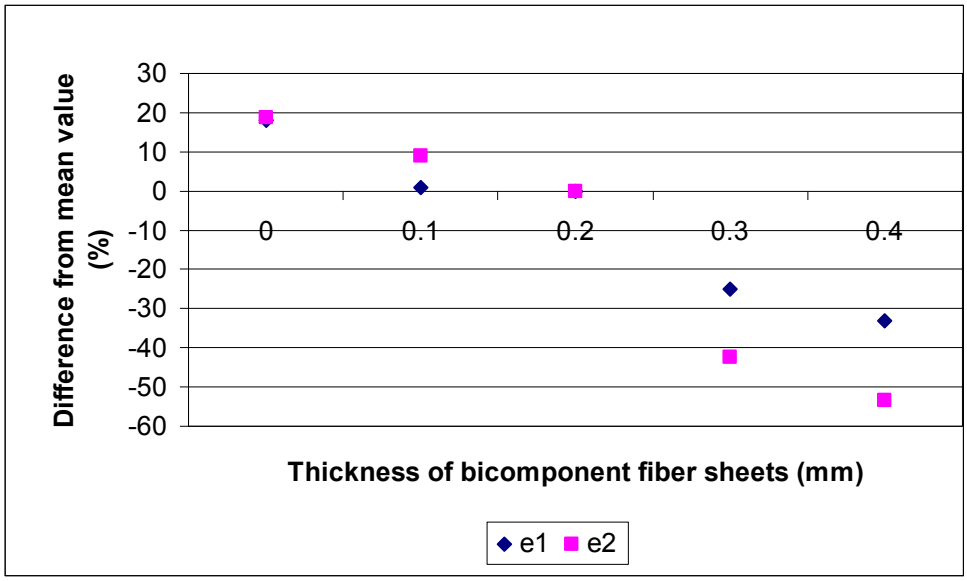

Figure 3.7: Strains calculated with the macromechanical model by varying the mean thickness of the bicomponent fiber reinforcement by 0.1 mm increments, expressed as a percentage of the values obtained using the mean elasticity.

Further assessment of the model was conducted by determining the input parameters (E_1, E_2, E and ν) needed to converge the model calculated strains to the mean measured strains shown in Table 3.2. This was done by changing each input parameter separately until the calculated strains were equal to the mean measured strains. Figure 3.8 illustrates the value for E_1 needed to converge the measured and calculated longitudinal strains. It can be seen that the convergence value of 1961 MPa is marginally less than 2 standard deviations from the mean value of E_1 and can therefore not be considered significantly different. The relatively large deviation from the mean needed for convergence, however, means that care needs to be taken when determining the value of E_1 used as input in the model. This provides further evidence that the measured and calculated strains in Table 3.2 are not significantly different.

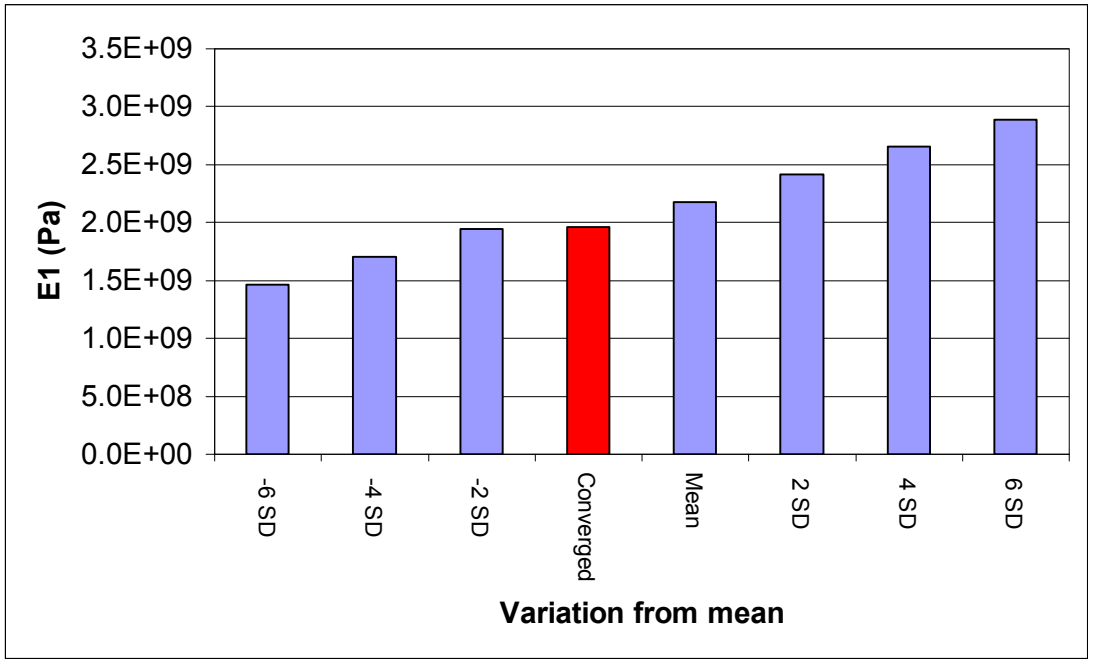

Figure 3.8: Value of E_1 where the measured and calculated longitudinal strain converges. The convergence value is indicated as in the figure as Converged. The mean modulus, as well as the moduli 2, 4 and 6 standard deviations from the mean are also shown.

Figure 3.9 illustrates the value for E needed to converge the measured and calculated longitudinal strains. The convergence value of 632 MPa is slightly more than 1 standard deviation lower than the mean. As was the case with E_1, the convergence value is not significantly different from the mean. When taking into account the results displayed in Figures 3.3, 3.6, 3.7 and 3.8, the deviation of the calculated longitudinal strain from the measured longitudinal strain of 4.32 percent can be attributed to an underestimation of E_1 and E, or a combination of the two, in the model. Furthermore, the fact that only a 1 standard deviation adjustment in E is needed to account for the deviation in the measured and calculated values shows that the core has a more dominant effect on the composite properties.

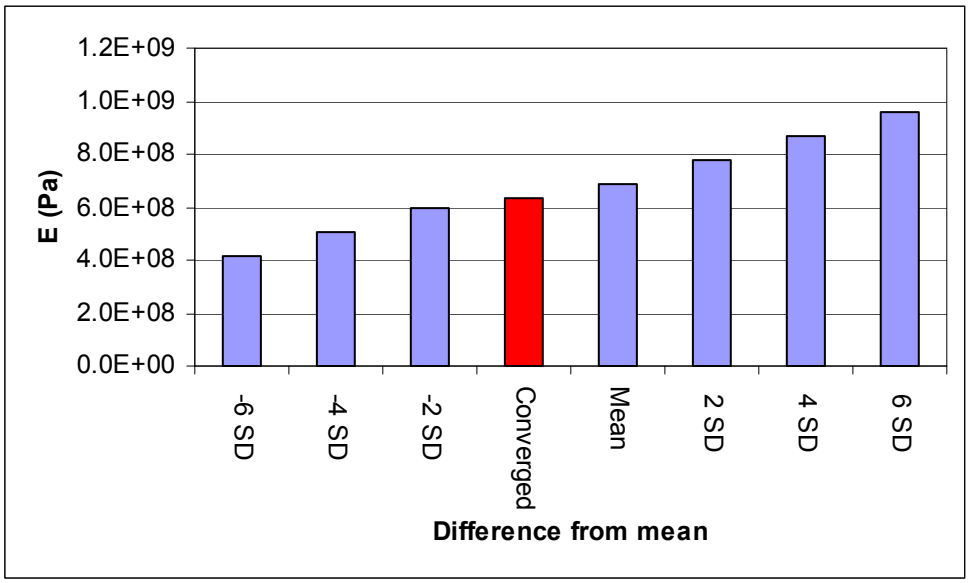

Figure 3.9: Value of E where the measured and calculated longitudinal strain converges. The convergence value is indicated as in the figure as Converged. The mean modulus, as well as the moduli 2, 4 and 6 standard deviations from the mean are also shown.

Figures 3.10 and 3.11 illustrate the values of E_2 and ν needed to converge the measured and calculated lateral strains. As was the case for E_1, the convergence value is approximately 2 standard deviations lower than the mean. A 1.5 standard deviation increase in Poisson's ratio, on the other hand, resulted in convergence of the measure and calculated lateral strain. This provides further evidence that the contribution of the core outweighs the contribution of the bicomponent fiber reinforcement in the properties of the composite.

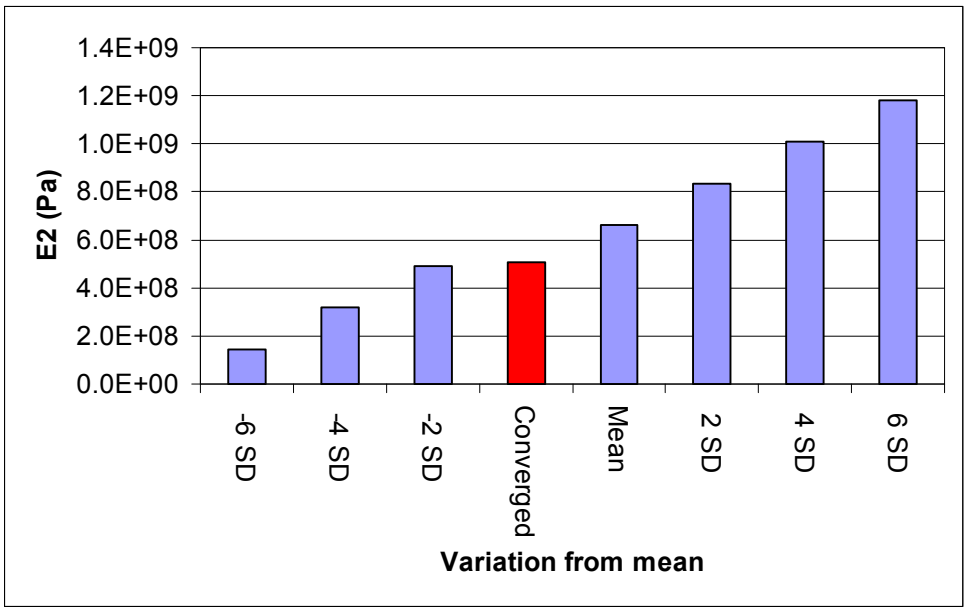

Figure 3.10: Value of E_2 where the measured and calculated longitudinal strain converges. The convergence value is indicated as in the figure as Converged. The mean modulus, as well as the moduli 2, 4 and 6 standard deviations from the mean are also shown.

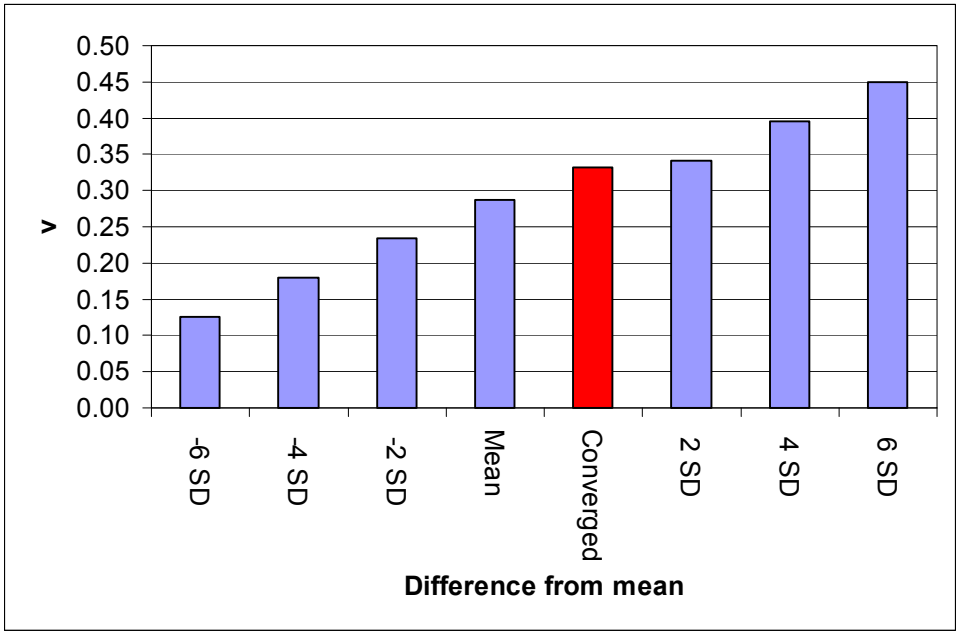

Figure 3.11: Value of ν where the measured and calculated longitudinal strain converges. The convergence value is indicated as in the figure as Converged. The mean modulus, as well as the moduli 2, 4 and 6 standard deviations from the mean are also shown.

To investigate the effect of needle punching on the tensile properties of the material, an on-axis tensile test was conducted on a non-needlepunched wood fiber board with previously established tensile properties which was reinforced with bicomponent fiber sheets. The sample was prepared by thermally bonding the bicomponent fiber sheets to the surfaces of the wood fiber board. Paper sheets were placed between the sample and the caul plates to facilitate removal from the press. Tensile tests were conducted as described previously. The modulus of elasticity of the non-needlepunched wood-bicomponent fiber board was 889 MPa. The mean modulus of elasticity obtained from on-axis tensile tests conducted on the needlepunched wood-bicomponent fiber panels was found to be 923 MPa (St. Dev. 21 MPa).

The E of the non-needlepunched wood-bicomponent fiber board was therefore slightly more than 1 standard deviation lower than that of the needlepunched wood-bicomponent fiber boards, and can not be considered significantly different. Furthermore, the wood fiber core used for this particular experiment had an elastic modulus of 615 MPa, which is about 75 MPa less than the mean modulus of the needlepunched wood fiber core. It can therefore be concluded that needlepunching did not have a significant effect on the tensile properties in the 1-2 plane of the wood-bicomponent fiber laminate.

Further experiments were also conducted to verify the effectiveness of the model by adjusting the thickness of the bicomponent fiber reinforcement. Due to the negligible effect of needlepunching on tensile properties described previously, it was decided to conduct the tests on non-needlepunched wood-bicomponent fiber panels. The panels were made with bicomponent fiber sheet thicknesses of 0.1, 0.2, 0.3 and 0.4 mm, after which they were prepared and tested by means of on-axis tensile tests. The measured strains were then compared with the calculated strains (Table 3.4). The means of the elastic constants for the bicomponent fiber sheets shown in Table 3.1 were used as inputs, while the constants for the non-needlepunched cores were obtained from on-axis tensile tests. It can be seen that from the calculated strain values that the model is able to account for changes in thickness of the reinforcement, with an increase in thickness resulting in an decrease in strain as the effective stiffness of the composite rises.

Table 3.3: Measured and calculated strains of non-needlepunched wood-bicomponent fiber panels at a load of 304182 Pa with a change in thickness of the bicomponent fiber reinforcement.

Thickness of reinforcement (mm)	Stress (Pa)	Measured ε_1	Calculated ε_1	Measured ε_2	Calculated ε_2	Percentage difference between measure and predicted strains	
						1	2
0.1	303590	0.00038	0.00038	-0.000099	-0.000110	0.02	10.00
0.2	305275.1	0.00036	0.00032	-0.000089	-0.000092	11.75	3.26
0.3	303901.9	0.00031	0.00027	-0.000071	-0.000077	14.25	7.79
0.4	307339.9	0.00026	0.00024	-0.000054	-0.000069	8.03	21.74

3.5) Conclusion

A model for predicting the mechanical properties of composite panel which contains wood fiber in the core and a bicomponent fiber sheet used as surface reinforcement was discussed. This model was validated by means of experimental data obtained from on axis tensile tests. Furthermore, it was found that off-axis tensile tests on laminates resulted in errors when used to determine the elastic constants of the material.

A sensitivity analyses was conducted to determine which parameters has the greatest effect on strains calculated by means of the model. It was found that lateral strains are especially sensitive to changes in lateral stiffness of the bicomponent fiber reinforcement, as well as the Poisson's ratio of the wood fiber core. Furthermore, the model proved to be sensitive to changes in thickness of the reinforcement, and the ability of the model to predict strains at different reinforcement thicknesses was experimentally verified.

3.6) References

Anon. 1986. The return of anisotropy. Experimental Stress Analysis Notebook. Measurements Group, Inc. Raleigh, NC.

Bosak, D.R., A.A. Ogale and J. van Dun. 2005. Bicomponent fibers derived from immiscible polymer blends. Textile Research Journal 75(1): 50-56.

Cai, Z. 2006. Selected properties of MDF and flakeboard overlaid with fiberglass mats. Forest Products Journal, 56(11/12): 142-146.

Chamis, C.C. and J.H. Sinclair. 1977. Ten-Degree Off-Axis Test for Shear Properties in Fiber Composites. Experimental Mechanics 17(9): 1-8.

Corradi, M., E. Speranzini, A. Borri and A. Vignoli. 2006. In-plane shear reinforcement of wood beam floors with FRP. Composites Part B: Engineering 37: 4-5.

Daniel I.M. and O. Ishai. 2005. Engineering Mechanics of Composite Materials - second edition. Oxford University Press, New York.

Gentile C, Svecova D, Saltzberg W, Rizkalla SH. Flexural strenghtening of timber beams using GFRP. Third international conference on advanced composite materials in bridge and structures, proceedings, Ottawa, Canada; August 15–18, 2000.

Hegde, R.R., A. Dahiya and M.G. Kamath. 2004. Bicomponent fibers. http://web.utk.edu/~mse/pages/Textiles/Bicomponent%20fibers (2005)

Lopez-Anido, R.A., L. Muszynski, D.J. Gardner, B. Goodell and B. Herzog. 2005. Performance-based material evaluation of fiber-reinforced polymer-wood interfaces in reinforced glulam members. Journal of Testing and Evaluation 33(6) 215-226.

Prian, L. and A. Barkatt. 1999. Degradation mechanism of fiber-reinforced plastics and its implications to prediction of long-term behavior, Journal of Material Science 34: 3977–3989.

Rusmee, P. 2005. High strength composites. http://www.mech.utah.edu/~rusmeeha/labNotes/composites.html#Reduction (2006)

Skaggs, S.T. and D.A. Bender. 1995. Shear deflection of composite beams. Wood and Fiber Science 27(3): 327-338.

Triantafillou, C. 1997. Shear reinforcement of wood using FRP materials. Journal of Materials in Civil Engineering ASCE 9: 65–69.

Triantafillou TC, Plevris, N. Post-strengthening of r/c beams with epoxy-bonded fiber-composite materials. Proceedings of the ASCE specialty conference on advanced composites for civil engineering structural, ASCE; 1991. 245–56.

Appendix 3

Table A3.1: Modulus of elasticity (E), Poisson's ratio (ν) and shear modulus (G), along with summary statistics, of the delaminated wood fiber core obtained from wood-bicomponent laminate panel 1 through 15.

Sample name	E (Pa)	ν	G (Pa)
MDF1	6.8E+08	0.29	2.6E+08
MDF2	7.3E+08	0.26	2.9E+08
MDF4	7.0E+08	0.21	2.9E+08
MDF5	6.0E+08	0.28	2.4E+08
MDF6	6.6E+08	0.30	2.5E+08
MDF7	7.3E+08	0.30	2.8E+08
MDF8	7.3E+08	0.33	2.7E+08
MDF9	6.6E+08	0.29	2.5E+08
MDF10	6.8E+08	0.30	2.6E+08
MDF11	7.0E+08	0.30	2.7E+08
MDF12	7.8E+08	0.29	3.0E+08
MDF14	6.9E+08	0.29	2.7E+08
MDF15	6.3E+08	0.30	2.4E+08
Mean	6.9E+08	0.29	2.7E+08
St. Dev.	4.5E+07	0.03	1.9E+07

Table A3.2: Strains, stresses and Poisson's ratios (ν_{12}) used to calculated the elastic constants of a delaminated bicomponent fiber sheet.

Sample	Strains(με)			Stress (Pa)	Poisson's ratio, ν_{12}
	ε_x	ε_y	ε_{45}		
bicosheet1	657	-120	240	1335088	0.28
bicosheet2	1565	-430	511	3502318	0.27
bicosheet4	683	-136	242	1523689	0.28
bicosheet5	912	-247	193	2059879	0.29
bicosheet6	691	-115	235	1386123	0.28
bicosheet7	701	-121	243	1513562	0.3
bicosheet8	683	-124	268	1432100	0.28
bicosheet9	683	-136	242	1523689	0.28
bicosheet10	679	-143	252	1532132	0.3
bicosheet11	721	-153	238	1535318	0.28
bicosheet12	659	-115	254	1341213	0.3
bicosheet14	657	-120	240	1432259	0.28
bicosheet15	912	-247	193	2059879	0.29

Chapter 4: Model to predict the hygromechanical behavior of a wood fiber - bicomponent fiber composite

Abstract

A hygro expansion model was developed for a wood-bicomponent fiber composite panel. The dimensional changes predicted by the model due to moisture fluctuation were compared to experimental data. No significant difference was found between the predicted and measured dimensions. However, significant differences were found between the state of strain predicted by the model and the measure state of strain in the x-direction in the panels.

4.1) Introduction

In wood products design, dimensional stability is of primary importance especially for layered wood composites where a small deformation in service can result in important value losses (Detiex et al. 2007). Wooden structures or composite boards are hygroscopic products that change in dimension as moisture content changes, irrespective of whether the moisture is due to direct contact with water or exposure to water vapor (Brauns and Raucens, 1997).

Medium density fiberboard is a hygroscopic material. Therefore, its moisture content depends on the relative humidity and temperature of the surrounding air (Ayrilmis, 2007). Linear expansion or contraction, in response to increased or decreased moisture content of the material, is one of the most important properties of fiberboards.

The in-plane movements arising from increased or decreased moisture content of the panel can cause high internal stresses due to the restraint offered by fastening such as nails in construction (Wu and Suchland, 1997). These stresses may be large enough to cause buckled panels, pushed-out nails, and separation of the panel from the structure. Expansion and contraction values of fiberboard, thus, become important design parameters.

Recent trends involve the reinforcement of a wood or wood composite product with a polymer fiber matrix. The difference in dimensional behavior between the fiber reinforced polymers (FRP's) used for reinforcement and the product being reinforced has been widely noted (Herzog et al., 2005; Barbero et al. 1994; Davalos et al. 2000, Gardner et al. 1994; Rizkalla et al. 2003; Liao and Tan, 2000). The mismatch in hygromechanical properties of the reinforcement and the wood materials build-up of residual stresses in the material and can result in deformation of the composite. Furthermore, high interfacial stresses formed due to hygro expansion issues can result in delamination of the structure (Khoshbakht et al., 2004). Consequently, methods of predicting how a composite material will behave under changing environmental and moisture conditions are essential when evaluating the end-use potential of a product.

This chapter will describe a hygro expansion model developed for a wood-bicomponent fiber composite panel, and compare strains caused by a moisture fluctuation predicted by the model with experimental data.

4.2) Model development

In the case of a lamina, moisture related changes will not result in mechanical stresses as long as the lamina is free to expand. In the case of a laminate, the lamina is not free to deform, and so residual mechanical stresses will develop. Only the strains that are different from the hygromechanical strains in the unrestrained lamina produce stresses. The hygromechanical strains can be incorporated in a transformed stress strain equation for the kth layer of a laminate as follows:

$$\begin{bmatrix} \sigma_x \\ \sigma_y \\ \tau_{xy} \end{bmatrix}_k = \begin{bmatrix} \overline{Q}_{11} & \overline{Q}_{12} & \overline{Q}_{16} \\ \overline{Q}_{12} & \overline{Q}_{22} & \overline{Q}_{26} \\ \overline{Q}_{16} & \overline{Q}_{26} & \overline{Q}_{66} \end{bmatrix}_k \begin{bmatrix} \varepsilon_x - \varepsilon_x^C \\ \varepsilon_y - \varepsilon_y^C \\ \gamma_{xy} - \gamma_{xy}^C \end{bmatrix}_k \qquad \text{Eq 4.1}$$

Where: ε_i^c = moisture induced strains

Furthermore, it was stated in Chapter 3 that the strains in a plate can be written as:

$$\begin{bmatrix} \varepsilon_x \\ \varepsilon_y \\ \gamma_{xy} \end{bmatrix} = \begin{bmatrix} \varepsilon_x^o \\ \varepsilon_y^o \\ \gamma_{xy}^o \end{bmatrix} + z \begin{bmatrix} \kappa_x^o \\ \kappa_y^o \\ \kappa_{xy}^o \end{bmatrix} \qquad \text{Eq. 4.2}$$

Combining Equations 4.1 and 4.2, we get:

$$\begin{bmatrix} \sigma_x \\ \sigma_y \\ \tau_{xy} \end{bmatrix}_k = \begin{bmatrix} \overline{Q}_{11} & \overline{Q}_{12} & \overline{Q}_{16} \\ \overline{Q}_{12} & \overline{Q}_{22} & \overline{Q}_{26} \\ \overline{Q}_{16} & \overline{Q}_{26} & \overline{Q}_{66} \end{bmatrix}_k \left\{ \begin{bmatrix} \varepsilon_x^o \\ \varepsilon_y^o \\ \gamma_{xy}^o \end{bmatrix} + z \begin{bmatrix} \kappa_x^o \\ \kappa_y^o \\ \kappa_{xy}^o \end{bmatrix} - \begin{bmatrix} \varepsilon_x^C \\ \varepsilon_y^C \\ \gamma_{xy}^C \end{bmatrix} \right\}_k \qquad \text{Eq. 4.3}$$

Combining Equation 4.3 with the equation for the force resultants from Chapter 3 we get:

$$\begin{bmatrix} N_x \\ N_y \\ N_{xy} \end{bmatrix} = \sum_{k=1}^{n} \begin{bmatrix} \overline{Q}_{11} & \overline{Q}_{12} & \overline{Q}_{16} \\ \overline{Q}_{12} & \overline{Q}_{22} & \overline{Q}_{26} \\ \overline{Q}_{16} & \overline{Q}_{26} & \overline{Q}_{66} \end{bmatrix}_k \left\{ \int_{z_{k-1}}^{z_z} \begin{bmatrix} \varepsilon_x^o \\ \varepsilon_y^o \\ \gamma_{xy}^o \end{bmatrix} dz + \int_{z_{k-1}}^{z_k} \begin{bmatrix} \kappa_x^o \\ \kappa_y^o \\ \kappa_{xy}^o \end{bmatrix} z\, dz - \int_{z_{k-1}}^{z_k} \begin{bmatrix} \varepsilon_x^C \\ \varepsilon_y^C \\ \gamma_{xy}^C \end{bmatrix} dz \right\} \qquad \text{Eq. 4.4}$$

Integrating Equation 42 with respect to the z-direction, we get:

$$\begin{bmatrix} N_x \\ N_y \\ N_{xy} \end{bmatrix} = \begin{bmatrix} \overline{Q}_{11} & \overline{Q}_{12} & \overline{Q}_{16} \\ \overline{Q}_{12} & \overline{Q}_{22} & \overline{Q}_{26} \\ \overline{Q}_{16} & \overline{Q}_{26} & \overline{Q}_{66} \end{bmatrix}_k \left\{ \begin{bmatrix} \varepsilon_x^o \\ \varepsilon_y^o \\ \gamma_{xy}^o \end{bmatrix} \left(z_k - z_{k-1}\right) + \begin{bmatrix} \kappa_x^o \\ \kappa_y^o \\ \kappa_{xy}^o \end{bmatrix} \frac{z_k^2 - z_{k-1}^2}{2} - \int_{z_{k-1}}^{z_k} \begin{bmatrix} \varepsilon_x^C \\ \varepsilon_y^C \\ \gamma_{xy}^C \end{bmatrix} dz \right\} \quad \text{Eq 4.5}$$

Similarly, combining Equation 4.4 with Equation 4.5 for the moment resultants results in Equation 44.

$$\begin{bmatrix} M_x \\ M_y \\ M_{xy} \end{bmatrix} = \sum_{k=1}^{n} \begin{bmatrix} \overline{Q}_{11} & \overline{Q}_{12} & \overline{Q}_{16} \\ \overline{Q}_{12} & \overline{Q}_{22} & \overline{Q}_{26} \\ \overline{Q}_{16} & \overline{Q}_{26} & \overline{Q}_{66} \end{bmatrix}_k \left\{ \begin{bmatrix} \varepsilon_x^o \\ \varepsilon_y^o \\ \gamma_{xy}^o \end{bmatrix} \frac{z_k^2 - z_{k-1}^2}{2} + \begin{bmatrix} \kappa_x^o \\ \kappa_y^o \\ \kappa_{xy}^o \end{bmatrix} \frac{z_k^3 - z_{k-1}^3}{3} - \int_{z_{k-1}}^{z_k} \begin{bmatrix} \varepsilon_x^C \\ \varepsilon_y^C \\ \gamma_{xy}^C \end{bmatrix} z\, dz \right\} \quad \text{Eq. 4.6}$$

In compact form, Equations 4.5 and 4.6 can be rewritten as:

$$\begin{bmatrix} N_x \\ N_y \\ N_{xy} \end{bmatrix} = \begin{bmatrix} A_{11} & A_{12} & A_{16} \\ A_{12} & A_{22} & A_{26} \\ A_{16} & A_{26} & A_{66} \end{bmatrix} \begin{bmatrix} \varepsilon_x^o \\ \varepsilon_y^o \\ \gamma_{xy}^o \end{bmatrix} + \begin{bmatrix} B_{11} & B_{12} & B_{16} \\ B_{12} & B_{22} & B_{26} \\ B_{16} & B_{26} & B_{66} \end{bmatrix} \begin{bmatrix} \kappa_x^o \\ \kappa_y^o \\ \kappa_{xy}^o \end{bmatrix} - \begin{bmatrix} N_x^C \\ N_y^C \\ N_{xy}^C \end{bmatrix} \qquad \text{Eq. 4.7}$$

And

$$\begin{bmatrix} M_x \\ M_y \\ M_{xy} \end{bmatrix} = \begin{bmatrix} B_{11} & B_{12} & B_{16} \\ B_{12} & B_{22} & B_{26} \\ B_{16} & B_{26} & B_{66} \end{bmatrix} \begin{bmatrix} \varepsilon_x^o \\ \varepsilon_y^o \\ \gamma_{xy}^o \end{bmatrix} + \begin{bmatrix} D_{11} & D_{12} & D_{16} \\ D_{12} & D_{22} & D_{26} \\ D_{16} & D_{26} & D_{66} \end{bmatrix} \begin{bmatrix} \kappa_x^o \\ \kappa_y^o \\ \kappa_{xy}^o \end{bmatrix} - \begin{bmatrix} M_x^C \\ M_y^C \\ M_{xy}^C \end{bmatrix} \qquad \text{Eq. 4.8}$$

Where:

$$A_{ij} = \sum_{k=1}^{n} \left[\overline{Q}_{ij} \right]_k \left(z_k - z_{k-1} \right)$$

$$B_{ij} = \frac{1}{2} \sum_{k=1}^{n} \left[\overline{Q}_{ij} \right]_k \left(z_k^2 - z_{k-1}^2 \right)$$

$$D_{ij} = \frac{1}{3} \sum_{k=1}^{n} \left[\overline{Q}_{ij} \right]_k \left(z_k^3 - z_{k-1}^3 \right)$$

$$\begin{bmatrix} N_x^C \\ N_y^C \\ N_{xy}^C \end{bmatrix} = \sum_{k=1}^{n} \begin{bmatrix} \overline{Q}_{11} & \overline{Q}_{12} & \overline{Q}_{16} \\ \overline{Q}_{12} & \overline{Q}_{22} & \overline{Q}_{26} \\ \overline{Q}_{16} & \overline{Q}_{26} & \overline{Q}_{66} \end{bmatrix}_k \begin{bmatrix} \varepsilon_x^C \\ \varepsilon_y^C \\ \gamma_{xy}^C \end{bmatrix}_k \left(z_k - z_{k-1} \right) = \sum_{k=1}^{n} \begin{bmatrix} \overline{Q}_{11} & \overline{Q}_{12} & \overline{Q}_{16} \\ \overline{Q}_{12} & \overline{Q}_{22} & \overline{Q}_{26} \\ \overline{Q}_{16} & \overline{Q}_{26} & \overline{Q}_{66} \end{bmatrix}_k \begin{bmatrix} \beta_x \\ \beta_y \\ \beta_{xy} \end{bmatrix}_k \Delta C \left(z_k - z_{k-1} \right)$$

$$\begin{bmatrix} M_x^C \\ M_y^C \\ M_{xy}^C \end{bmatrix} = \sum_{k=1}^{n} \begin{bmatrix} \overline{Q}_{11} & \overline{Q}_{12} & \overline{Q}_{16} \\ \overline{Q}_{12} & \overline{Q}_{22} & \overline{Q}_{26} \\ \overline{Q}_{16} & \overline{Q}_{26} & \overline{Q}_{66} \end{bmatrix}_k \begin{bmatrix} \varepsilon_x^C \\ \varepsilon_y^C \\ \gamma_{xy}^C \end{bmatrix}_k \frac{\left(z_k^2 - z_{k-1}^2 \right)}{2} = \sum_{k=1}^{n} \begin{bmatrix} \overline{Q}_{11} & \overline{Q}_{12} & \overline{Q}_{16} \\ \overline{Q}_{12} & \overline{Q}_{22} & \overline{Q}_{26} \\ \overline{Q}_{16} & \overline{Q}_{26} & \overline{Q}_{66} \end{bmatrix}_k \begin{bmatrix} \beta_x \\ \beta_y \\ \beta_{xy} \end{bmatrix}_k \Delta C \frac{\left(z_k^2 - z_{k-1}^2 \right)}{2}$$

Where: β_i = transformed coefficient of moisture expansion

ΔC = moisture content change

The force and moment resultants can be rearranged as follows:

$$\begin{bmatrix} \overline{N}_x \\ \overline{N}_y \\ \overline{N}_{xy} \end{bmatrix} = \begin{bmatrix} N_x + N_x^C \\ N_y + N_y^C \\ N_{xy} + N_{xy}^C \end{bmatrix} = \begin{bmatrix} A_{11} & A_{12} & A_{16} \\ A_{12} & A_{22} & A_{26} \\ A_{16} & A_{26} & A_{66} \end{bmatrix} \begin{bmatrix} \varepsilon_x^o \\ \varepsilon_y^o \\ \gamma_{xy}^o \end{bmatrix} + \begin{bmatrix} B_{11} & B_{12} & B_{16} \\ B_{12} & B_{22} & B_{26} \\ B_{16} & B_{26} & B_{66} \end{bmatrix} \begin{bmatrix} \kappa_x^o \\ \kappa_y^o \\ \kappa_{xy}^o \end{bmatrix} \qquad \text{Eq. 4.9}$$

$$\begin{bmatrix} \overline{M}_x \\ \overline{M}_y \\ \overline{M}_{xy} \end{bmatrix} = \begin{bmatrix} M_x + M_x^C \\ M_y + M_y^C \\ M_{xy} + M_{xy}^C \end{bmatrix} = \begin{bmatrix} B_{11} & B_{12} & B_{16} \\ B_{12} & B_{22} & B_{26} \\ B_{16} & B_{26} & B_{66} \end{bmatrix} \begin{bmatrix} \varepsilon_x^o \\ \varepsilon_y^o \\ \gamma_{xy}^o \end{bmatrix} + \begin{bmatrix} D_{11} & D_{12} & D_{16} \\ D_{12} & D_{22} & D_{26} \\ D_{16} & D_{26} & D_{66} \end{bmatrix} \begin{bmatrix} \kappa_x^o \\ \kappa_y^o \\ \kappa_{xy}^o \end{bmatrix} \qquad \text{Eq. 4.10}$$

The force and moment resultants can be combined in compact form as follows:

$$\left[\begin{array}{c} \overline{N} \\ \hline \overline{M} \end{array}\right] = \left[\begin{array}{c|c} A & B \\ \hline B & D \end{array}\right] \left[\begin{array}{c} \varepsilon^o \\ \hline \kappa^o \end{array}\right] \qquad \text{Eq. 4.11}$$

Inverting Equation 52 and solving for the midplane strains and curvatures results in Equation 4.12.

$$\left[\begin{array}{c} \varepsilon^o \\ \hline \kappa^o \end{array}\right] = \left[\begin{array}{c|c} A' & B' \\ \hline C' & D' \end{array}\right] \left[\begin{array}{c} \overline{N} \\ \hline \overline{M} \end{array}\right] \qquad \text{Eq. 4.12}$$

Where: $\left[\begin{array}{c|c} A' & B' \\ \hline C' & D' \end{array}\right] = \left[\begin{array}{c|c} A & B \\ \hline B & D \end{array}\right]^{-1}$

And:

$$\left[C'\right] = \left[B'\right]^T$$

The global strains in any ply of the laminate can then be calculated with Equation 4.13.

$$\begin{bmatrix} \varepsilon_x \\ \varepsilon_y \\ \gamma_{xy} \end{bmatrix}_k = \begin{bmatrix} \varepsilon_x^o \\ \varepsilon_y^o \\ \gamma_{xy}^o \end{bmatrix}_k + z \begin{bmatrix} \kappa_x^o \\ \kappa_y^o \\ \kappa_{xy}^o \end{bmatrix}_k \qquad \text{Eq. 4.13}$$

4.3) Materials and methods

Samples with dimensions of 40 by 40 mm were cut from the first five bicomponent fiber panels and 10 MDF panels used for mechanical modeling in Chapter 3. Bicomponent fiber sheets were also prepared and 40 by 40 mm sections were cut from the sheets. The samples were weighed and the length, width and thickness were measured with a digital caliper prior to being placed in an environmental chamber. Temperature and relative humidity (RH) settings were selected to achieve equilibrium moisture content of 19.1% based on data published by the Forest Products Laboratory for spruce (*Picea* sp.) lumber. The samples were weighed daily, and the dimensional measurements were retaken once the samples showed no change in weight. The procedure was repeated for EMC's of 12.1% and 7.4%. Finally, the samples were oven dried at 104^{o}C until dry.

The coefficient of moisture expansion was calculated according to the techniques described by Van Houts et al. (2000). A longitudinal and cross-directional coefficient of moisture expansion in MDF was calculated for each of the three moisture conditions by

means of the following equation:

$$\alpha_{l,w} = \frac{\frac{w^i_{mc\%} - w^i_0}{w^i_0}}{\Delta M} \qquad \text{Eq. 4.14}$$

Where: i = Sample

$\alpha_{l,w}$ = Longitudinal and cross-directional coefficients of moisture expansion

$w^i_{mc\%}$ = Sample length or width at a moisture condition

w^i_0 = Oven dry sample length or width

ΔM = Moisture change from zero percent moisture content

The coefficients of hygro expansion were combined with elastic moduli, shear moduli and Poisson's ratios determined for the delaminated bicomponent fiber sheets and the delaminated fiberboard core in Chapter 3 to predict moisture induced strains (Table 4.1). These predicted strains were then compared with the strains observed in the bicomponent fiber panel samples at each moisture level.

Table 4.1: Elastic moduli (E_1, E_2, and E), shear moduli (G_{12} and G), and Poisson's ratio (ν_{12} and ν), obtained from delaminated bicomponent fiber sheets and their respective wood fiber cores .

Sample No.	Stress (Pa)	Bicomponent fiber sheets					Wood fiber core	
		ν_{12}	E_1 (Pa)	E_2 (Pa)	G_{12} (Pa)	E (Pa)	ν	G (Pa)
1	1335088	0.28	2.06E+09	4.85E+08	7.15E+08	6.8E+08	0.29	2.64E+08
2	3502318	0.27	2.27E+09	1.96E+09	7.6E+08	7.32E+08	0.26	2.9E+08
3	2266814	0.29	2.21E+09	5.31E+08	8.72E+08	7.28E+08	0.27	2.87E+08
4	1523689	0.28	2.24E+09	6.44E+08	8.53E+08	7.01E+08	0.21	2.9E+08
5	2059879	0.29	2.38E+09	7.17E+08	5.34E+08	6.03E+08	0.28	2.36E+08

Table 4.2 illustrates the overall panel thicknesses and the thickness of the lamina measured for the delaminated lamina for the panels investigated.

Table 4.2: Thicknesses of the panels and lamina obtained from delaminated bicomponent fiber sheets and their respective wood fiber cores.

Sample no.	Overall dimension (mm)	Lamina		
		1 (mm)	2 (mm)	3 (mm)
1	2.29	0.2	1.89	0.2
2	2.35	0.22	1.89	0.24
3	2.25	0.18	1.8	0.27
4	2.37	0.25	1.91	0.21
5	2.3	0.22	1.85	0.23

Equation 4.15 was used to calculate the reduced transformed stiffness matrices for the reinforcement and the core of the panel.

$$\begin{bmatrix} \sigma_x \\ \sigma_y \\ \tau_{xy} \end{bmatrix} = \begin{bmatrix} \overline{Q}_{11} & \overline{Q}_{12} & \overline{Q}_{16} \\ \overline{Q}_{12} & \overline{Q}_{22} & \overline{Q}_{26} \\ \overline{Q}_{16} & \overline{Q}_{26} & \overline{Q}_{66} \end{bmatrix} \begin{bmatrix} \varepsilon_x \\ \varepsilon_y \\ \gamma_{xy} \end{bmatrix} \qquad \text{Eq. 56}$$

The respective Qbar matrices were then used to calculate the moisture induced stress and moments using Equations 45 and 46. Moisture changes from 0 to 7.7, 10.6 and 18.4 were used for the calculations. Equation 50 was used to calculate the midplane strains and curvature, which in turn is used as inputs in Equation 51 to determine the global strains at the top and bottom of each lamina. Equation 57 was used to determine the final panel dimensions:

$$\begin{bmatrix} d_{xm} \\ d_{ym} \end{bmatrix} = \begin{bmatrix} \varepsilon_x \\ \varepsilon_y \end{bmatrix} \begin{bmatrix} d_{x0} \\ d_{y0} \end{bmatrix} + \begin{bmatrix} d_{x0} \\ d_{y0} \end{bmatrix} \qquad \text{Eq. 4.16}$$

Where: d_{im} = final dimensions

d_{i0} = oven dry dimensions

4.4) Results and discussion

Table 4.3 lists the coefficients of moisture expansion of MDF calculated by means of Equation 55 (data from Table A4.1). Of note is the fact that no significant difference between α_l and α_w. was found by means of a T-test comparing the two means. This indicates that the panels are isotropic in the x- and y- planes with regards to the expansion coefficients.

This result is reported by Genav et al. (2005) who stated that MDF is isotropic with regards to linear expansion (Genav et al. 2005). Values for linear expansion coefficients were compared to those obtained by Ganev et al. (2005) in a similar study. They reported a value of 0.00023 $mm.mm^{-1}.MC\%^{-1}$ for 650 $kg.m^{-3}$ mdf panels which is about half the values obtained in this study. The difference can be attributed to differences in fiber and resin type used. Ganev et al. utilized melamine formaldehyde resin and black spruce (*Picea mariana*) and produced boards at a marginally higher density. There is conflicting reports in the literature about the effect of density on linear expansion. Some researchers report an increase in expansion with an increase in density (Ganev et al. 2005), while others (Xu and Suchland, 1998) report no change with changing density.

Table 4.3: Longitudinal (α_l) and cross-directional (α_w) coefficients of moisture expansion in MDF at the three EMC's; standard deviation in brackets

EMC (%)	α_l(mm.mm^{-1}.MC%$^{-1}$)	α_w(mm.mm-1.MC%-1)
19.1	0.00057 (0.00014)	0.00059 (0.00014)
12.1	0.00055 (0.00015)	0.00055 (0.00010)
7.4	0.00060 (0.00018)	0.00060 (0.00016)

It was found that changes in RH did not have a dimensional affect on the bicomponent fiber sheets. This is in agreement with Wei et al. (2005), who found that water only accumulates on polyolefins by condensation after a relative humidity of 100% is reached and can therefore show no dimensional changes at lower humidity ratios.

Table 4.4 lists the predicted and measured dimensions obtained for the bicomponent fiber panels at each of the EMC's. T-tests were conducted to compare the predicted and

measured values, and no significant difference were found for each moisture condition. This therefore indicates that the model was able to accurately predict the dimensional changes of the composite panel observed due to a change in moisture condition based on the inputs used.

Table 4.4: Predicted and measured final dimensions of bicomponent fiber panels at different moisture conditions

Equilibruim moisture content (%)	Sample	Longitudinal		Cross-directional	
		Predicted Dimension (mm)	Measured Dimension (mm)	Predicted Dimension (mm)	Measured Dimension (mm)
19.1					
	1	44.94	44.90	45.23	45.13
	2	45.08	45.03	45.10	45.14
	3	40.36	40.35	39.78	39.73
	4	45.07	45.11	45.23	45.21
	5	40.05	40.15	39.50	39.61
12.1					
	1	44.81	44.79	45.02	45.12
	2	44.97	44.96	44.96	44.92
	3	40.26	40.26	39.60	39.59
	4	44.96	44.97	45.02	44.92
	5	39.96	40.05	39.34	39.41
7.4					
	1	44.76	44.74	44.94	44.93
	2	44.91	44.90	44.86	44.89
	3	40.21	40.24	39.53	39.62
	4	44.91	44.86	44.94	44.90
	5	39.92	39.95	39.27	39.26
oven dry					
	1		44.65		44.77
	2		44.8		44.69
	3		40.12		39.39
	4		44.81		44.79
	5		39.84		39.14

To further illustrate the effect of fiber orientation of the bicomponent fiber reinforcement on the behavior of the composite, the relative differences in dimensional changes due to a change in moisture content was investigated. Figure 4.1 illustrates the mean predicted and measured relative dimensional changes in the longitudinal and crossdirectional directions of the panels. The values were obtained by expressing the strains caused by a change in moisture content from the dry condition as a percentage (See Table A4.2). As mentioned previously, MDF is isotropic with regards to linear expansion (Genav et al. 2005). It can be seen from Figure 4.1 that this is not the case for the bicomponent reinforced panels constructed during the course of this research. This can be attributed to the higher modulus of elasticity of the bicomponent reinforcement along the fiber axis as compared to the lateral direction. The greater stiffness along the fiber direction has a greater restraining effect on the dimensional performance of the composite, resulting in a lower observed strain. Paired t-tests were conducted to compare the measured and predicted values for both x and y at each moisture level. No significant difference was found in both the x- and y-directions Furthermore, due to restraints imposed by panel size, the coefficients for linear expansion was obtained from MDF instead of the fiberboard cores from the panels. This could potentially demonstrate differences in linear expansion in the x and y-directions in the core due to the processing techniques used to manufacture the panels.

It can also be noted that the difference in the predicted and measured values for x and y are increasing as the moisture content of the panels increase. This can be attributed to the increased effect of the expansion of the wood fiber core.

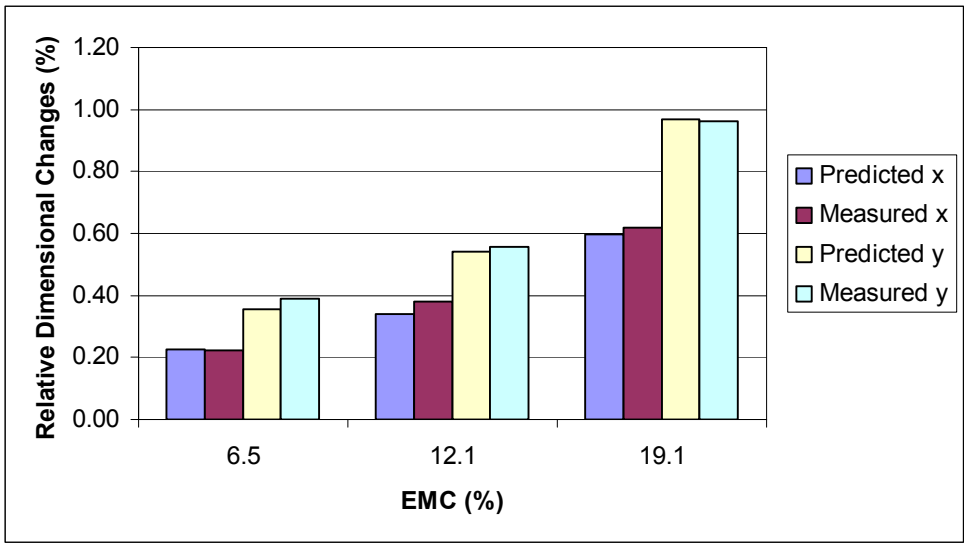

Figure 4.1: Comparison of the predicted and measured dimensional changes in the composite for the longitudinal (x) and crossdirectional (y) directions for three moisture levels

To further illustrate the effect caused by the process on the dimensional properties of the product, coefficients of linear expansion was calculated for the panels from the measured dimensions listed in Table 4.4. The values (shown in Table 4.5) were compared to the coefficients of linear expansion shown in Table 4.1 for MDF by means of t-tests. Significant differences were found between all values, except α_w at 12.1 precent. Based on these results, as well as those presented in Chapter 2, it can be concluded that the addition of a bicomponent fiber web to the surfaces of the panel in conjunction with needlepunching results in a more dimensionally stable product when compared with MDF. It does, however, introduce a degree of anisotropy into a product which normally behaves isotropically. Care should therefore be taken when using a product such as this to incorporate isotropic moisture expansion behavior into the design constraints.

Table 4.5: Longitudinal (α_l) and cross-directional (α_w) coefficients of moisture expansion in bicomponent reinforced panels at the three EMC's; standard deviation in brackets

EMC (%)	α_l(mm.mm^{-1}.MC%$^{-1}$)	α_w(mm.mm-1.MC%-1)
19.1	0.00035(0.00005)	0.00045 (0.00012)
12.1	0.00040 (0.00011)	0.00050(0.00023)
7.4	0.00033(0.00009)	0.00041 (0.00013)

4.5) Conclusions

A model was developed to predict the effects of moisture changes of bicomponent fiber panels based on the dimensional and elastic properties of each of the lamina of the composite. No significant difference was found between the values predicted by the model and the actual measured dimensions. Furthermore, the panels developed for this research also exhibited an overall improvement in linear expansion when compared to MDF.

4.6) References

Ayrilmis, N. 2007. Effect of panel density on dimensional stability of medium and high density fiberboards. Journal of Material Science 42: 8551-8557.

Barbero, E., J. Davalos, and U. Munipalle. 1994. Bond strength of FRP-wood interface. J. of Reinforced Plastics and Composites 13(9): 835-854.

Brauns, J. and K. Rocens. 1997. Hygromechanical behaviour of wooden composites. Wood Science and Technology 31(2): 193-204.

Davalos, J., P. Qiao, and B.S. Trimble. 2000. Fiber-reinforced composite and wood bonded interfaces: Part 1. Durability and Shear Strength, J. of Composites Tech. and Res. 22(4): 224-231.

Deteix, J., P. Blanchet, A. Forti and A. Cloutier. 2007. Finite element modeling of laminate wood composites : Hygromechanical behavior considering diffusion effects in the adhesive layers. Wood and Fiber Science 40(1): 132 – 143.

Gardner, D.J., J.F. Davalos, and U.M. Munipalle. 1994. Adhesive bonding of pultruded fiber-reinforced plastic to wood. Forest Prod. J. 44(5): 62-66.

Herzog, B., B. Goodell; R. Lopez-Anido and D.J. Gardner. 2005. Durability of fiber-reinforced polymer (FRP) composite-wood hybrid products fabricated using the composites pressure resin infusion system (ComPRIS). Forest Products Journal 55(11): 54-60.

Khoshbakht, M., M.W. Lin and J.B. Berman. 2004. Analysis of moisture-induced stresses in an FRP composites reinforced masonry structure. Finite Elements in Analysis and Design 42(5): 414-429

Liao, K. and Y. Tan. 2000. Influence of moisture induced stress on in-situ fiber strength degradation of a unidirectional polymer composite. Composites: Part B 32: 365-370.

Rizkalla S., T. Hassan, N. Hassan. 2003. Design recommendations for the use of FRP for reinforcement and strengthening of concrete structures. Progress in Structural Engineering and Materials 5(1): 16-28.

Van Houts, J. , D. Bhattacharyya and K. Jayaraman. 2000. Determination of residual stresses in medium density fiberboard. Holzforschung 54 (2): 176-182.

Qufu Wei, Qi Li, Xueqian Wang, Fenglin Huang and Weidong Gao, Dynamic water adsorption behaviour of plasma-treated polypropylene nonwovens. Polymer Testing: Volume 25(5): 717-722.

Wu, Qinglin, and O. Suchland. 1997 Effect of Moisture on the Flexural Properties of Commercial Oriented Strand Boards. Wood and Fiber Science 29(1): 47-57.

Appendix 4

Table A4.1: Data obtained from MDF used to determine coefficient of moisture expansion

			Dimension (mm)			Swelling (%)	
EMC	Sample	Weight(g)	Longitudinal	Crossdirectional	MC (%)	l	w
19.1							
	1	3.1	40.44	40.38	19.23	0.0052	0.0085
	2	4.1	40.52	40.52	17.14	0.0105	0.0105
	3	4.7	44.98	43.26	17.50	0.0500	0.0164
	4	3.4	43.17	43.84	17.24	0.0131	0.0113
	5	3.8	43.29	43.19	18.75	0.0112	0.0101
	6	3.4	43.66	43.42	17.24	0.0099	0.0100
	7	3.6	42.54	42.77	20.00	0.0090	0.0104
	8	3.7	42.71	43.03	19.35	0.0123	0.0091
	9	3.9	42.87	42.91	18.18	0.0101	0.0101
	10	3.1	41.83	43.15	19.23	0.0099	0.0108
	Mean	3.68	42.601	42.647	18.39	0.0141	0.0107
12.1							
	1	2.9	40.34	40.22	11.54	0.0027	0.0045
	2	3.9	40.35	40.35	11.43	0.0062	0.0062
	3	4.4	43.12	42.88	10.00	0.0065	0.0075
	4	3.2	42.95	43.64	10.34	0.0080	0.0067
	5	3.5	43.07	43	9.37	0.0061	0.0056
	6	3.2	43.49	43.24	10.34	0.0060	0.0058
	7	3.3	42.36	42.56	10.00	0.0047	0.0054
	8	3.4	42.47	42.85	9.68	0.0066	0.0049
	9	3.7	42.68	42.72	12.12	0.0057	0.0056
	10	2.9	41.64	42.94	11.54	0.0053	0.0059
	Mean	3.44	42.247	42.44	10.64	0.0058	0.0058
7.4							
	1	2.8	40.3	40.16	7.69	0.0017	0.0030
	2	3.7	40.26	40.26	5.71	0.0040	0.0040
	3	4.2	43.03	42.77	5.00	0.0044	0.0049
	4	3.1	42.83	43.54	6.90	0.0052	0.0044
	5	3.4	42.98	42.92	6.25	0.0040	0.0037
	6	3.1	43.4	43.16	6.90	0.0039	0.0040
	7	3.2	42.29	42.48	6.67	0.0031	0.0035
	8	3.3	42.37	42.78	6.45	0.0043	0.0033
	9	3.5	42.6	42.64	6.06	0.0038	0.0038
	10	2.8	41.56	42.85	7.69	0.0034	0.0037
	Mean	3.31	42.162	42.356	6.53	0.0038	0.0038

Table A4.1 (continued)

EMC	Sample	Weight(g)	Dimension (mm) Longitudinal	Crossdirectional	Swelling (%) MC (%)	l	w
dry							
	1	2.6	40.23	40.04	NA	NA	NA
	2	3.5	40.1	40.1			
	3	4	42.84	42.56			
	4	2.9	42.61	43.35			
	5	3.2	42.81	42.76			
	6	2.9	43.23	42.99			
	7	3	42.16	42.33			
	8	3.1	42.19	42.64			
	9	3.3	42.44	42.48			
	10	2.6	41.42	42.69			
	Mean	3.11	42.003	42.194			

Table A4.2: The predicted and measured relative dimensional changes in the longitudinal and crossdirectional directions of the panels when expressed as a percentage of the final dimensions

		Longitudinal		Cross-directional	
EMC	Sample	Predicted dimension (mm)	Measured dimension (mm)	Predicted dimension (mm)	Measured dimension (mm)
19.1					
	1	0.65	0.56	1.03	0.80
	2	0.61	0.54	0.67	0.54
	3	0.61	0.57	1.00	0.86
	4	0.60	0.71	0.95	0.69
	5	0.54	0.78	0.94	1.20
	Mean	0.60	0.62	0.97	0.96
	St. dev	0.04	0.11	0.14	0.25
12.1					
	1	0.36	0.31	0.56	0.78
	2	0.33	0.38	0.36	0.27
	3	0.34	0.35	0.54	0.51
	4	0.33	0.40	0.51	0.25
	5	0.30	0.53	0.51	0.69
	Mean	0.34	0.38	0.54	0.56
	St. dev	0.02	0.08	0.08	0.24
7.4					
	1	0.24	0.20	0.37	0.36
	2	0.22	0.25	0.24	0.20
	3	0.22	0.30	0.36	0.58
	4	0.22	0.16	0.34	0.20
	5	0.20	0.43	0.34	0.31
	Mean	0.23	0.22	0.36	0.39
	St. dev	0.01	0.10	0.05	0.16

Chapter 5: Creep behavior of a wood-bicomponent fiber composite

Abstract

The tensile behavior of a wood-bicomponent fiber composite under simulated long term load was studied. Short term creep tests were conducted at different temperatures and were shifted to a reference temperature to simulate long term creep tests. It was found that the shift factor used followed the WLF equation. Creep tests were conducted on bicomponent fiber sheets, MDF and the composite itself. It was observed that MDF creeped the least, with the greatest creep observed in the bicomponent fiber sheets. The wood-bicomponent fiber panel exhibited an intermediate creep.

5.1) Introduction

According to Tajvidi et al. (2004) one of the challenges in using natural-fiber/thermoplastic composites is that both phases (polymer matrix, resin and natural fiber) exhibit time-dependent properties. The long-term creep performance of these composites is of particular importance as they find increased use in structural building products.

One of the greatest constraints in studying creep behavior is the relatively long time required to complete the tests (Tajvidi et al. 2004; Bogren et al. 2006; Alwis and Burgoyne, 2006). Therefore, methods that are able to predict the long-term performance of a material from short-term data have gained considerable attention. Observation suggests that the effects of time and temperature are equivalent (Tajvidi et al. 2004).

Mechanical behaviors observed after a short time resemble those observed at cooler temperatures, whereas an increase in temperature simulates observation over greater time (Tissaoui, 1996). From these observations, numerous investigators have tried to develop equations of time and temperature.

The objective of this study was to evaluate the applicability of the time temperature superposition (TTS) principle to the prediction of the creep behavior of a wood fiber / bicomponent fiber sandwich composite panel.

5.2) Background

5.2.1) Time-temperature superposition

Viscoelastic materials exhibit behavior during deformation and flow which is both temperature and time (frequency) dependent (Anon). Applying a constant load to a polymer will, therefore, cause an increase in strain (compliance) over time. This phenomena, called creep, is caused by molecular rearrangement of the polymer in question (Anon). Commonly, the only way to accurately evaluate material performance for a specific application is to test the material under the actual temperature and time conditions the material will see in the application. However, a serious of short term creep tests conducted at different temperatures can be extrapolated to simulate long term creep tests. This treatment is known as time temperature superposition (TTS) (Anon). TTS is based on the following assumptions:

1) The processes involved in molecular relaxation or rearrangements in viscoelastic materials occur at accelerated rates at higher temperatures
2) There is a direct equivalency between time (the frequency of measurement) and temperature. This temperature effect can be described by

Temperature effects are described by altering the time scale of the response (a horizontal shift) according to (Pooler and Smith, 2004):

$$t^* = \frac{t}{a_t} \qquad \text{Eq. 5.1}$$

Where: t* = shifted time (s)

a_t = temperature shift factor

Hence, the time over which these processes occur can be reduced by conducting creep measurements at lower temperatures and transposing (shifting) the resultant data to higher temperatures. The result of this shifting is a master curve where the material property of interest at a specific end-use temperature can be predicted over a broad time scale (Anon). The amount of shifting along the horizontal (x-axis) in a typical TTS plot required to align the individual experimental data points into the master curve is generally described using one of two common theoretical models. The first of these models is the Williams-Landel-Ferry (WLF) equation:

$$\log a_t = -C_1\left(\frac{T - T_r}{C_2 + (T - T)}\right) \qquad \text{Eq.5.2}$$

Where: C_1, C_2 = Material constants,

T_r = reference temperature (in K)

T = measurement temperature (in K)

sa_t = Shift factor.

The equation is based on the assumption that, above the glass transition temperature, the fractional free volume increases linearly with respect to temperature.

The other model commonly used is the Arrhenius equation:

$$a_t = \exp\left[\frac{-\Delta E}{2.303R}\left(\frac{1}{T} - \frac{1}{T_r}\right)\right] \qquad \text{Eq 5.3}$$

Where: E = activation energy associated with the relaxation

R = the gas constant

T = the measurement temperature,

T_r = the reference temperature

The Arrhenius equation is typically used to describe behavior outside the glass transition region, but has also been used to obtain the activation energy associated with the glass transition.

5.2.2) Application of TTS on a wood-based material

One of the key assumptions behind the principle of time-temperature superposition is that the material does not undergo any chemical or physical changes as a result of the temperature change (Ferry 1980). For wood based materials two possible changes may occur. Firstly, one is a moisture content change, and the second one is a change in the crystallinity of the cellulose (Tissaoi, 1996). It was, however, suggested by Van der Put (1989) that the change in cellulose crystallinity is very small within a reasonable temperature range.

Furthermore, wood is a polymer blend with multiple transition zones: wood consists of cellulose, lignin, and hemicellulose, each of which may respond differently to temperature.

Davidson(1962) conducted creep recovery experiments in bending and concluded that time-temperature superposition should be used with caution because wood is thermorheologically complex. However, Salmèn (1984) was successful when he applied the principle to saturated wood samples at temperatures ranging from 20 to 140°C. In a study to determine the transition temperatures of the amorphous components in wood, Kelly et al. (1987) were able to apply the principle of time-temperature superposition to wood saturated with non-aqueous diluents. Gamalath (1991) superposed compliance curves obtained from creep tests in compression for southern pine samples at temperatures between 20 and 60°C.

Tissaoui conducted TTS experiments on Douglas fir and southern yellow pine and found that the shift factors followed the WLF relationship. No vertical shift was employed.

There are conflicting reports in the literature on wood / plastic composites as to the form of the shift factor used, as well as the need for a vertical shift factor accounting for changes in crystallinity. Pooler and Smith (2004) conducted TTS tests between -30^0C and 65^0C on a composite of high density polyethylene (HDPE) and wood flour and found that the WLF equation best suited their data. They also concluded that there material is thermorheologically simple, and that no vertical shift factor is needed.

On the other hand, Tajvidi et al. (2004) conducted TTS experiments on a HDPE / kenaf fiber composite between 23 and 63^0C, and concluded that the shift factor follows an Arrhenius relationship. They also employed a vertical shift factor and concluded that the material is thermorheologically complex.

5.3) Materials and methods

Bicomponent fiber panels and MDF were prepared according to the techniques described in Chapter 1. In concurrence with Chapters 3 and 4, it was decided to limit the tests conducted in this section to the 2.3 mm punched through panels. In addition to the composite panels and MDF, bicomponent fiber sheets with a thickness of 2.3 mm were prepared in the hot press.

Samples with dimensions of 60*12 mm samples were cut from the centre of each of the prepared panels (wood-bicomponent fiber composite, MDF and bicomponent fiber sheets). Samples were cut both with the fiber alignment of the bicomponent surface reinforcement parallel to the longitudinal axis of the testing beams, as well as perpendicular. Samples were oven dried prior to testing in the DMA.

Short-term creep tests were performed with a DMA analyzer. Creep tests were performed using a 50mm 3-point bending jig at 5°C for a total duration of 10 min. The tests were repeated at 5 degree increments until a final temperature of 65°C was reached. The stress level was 1 MPa. Each specimen was inserted into the chamber, and a 5 minute soak time was applied to ensure that the specimen reached temperature equilibrium after which stress was applied and held constant for 10 minutes. During the test, strain data were collected, and plotted versus time. This procedure was followed for all temperatures studied in this research. TTS was conducted by means of the TA Universal Analyses software in conjunction with the TA Rheology application.

5.4) Results and discussion

Figure 5.1 illustrates the creep compliance of a representative sample at each temperature for the duration of the load. As expected, an overall increase in compliance can be observed with an increase in temperature.

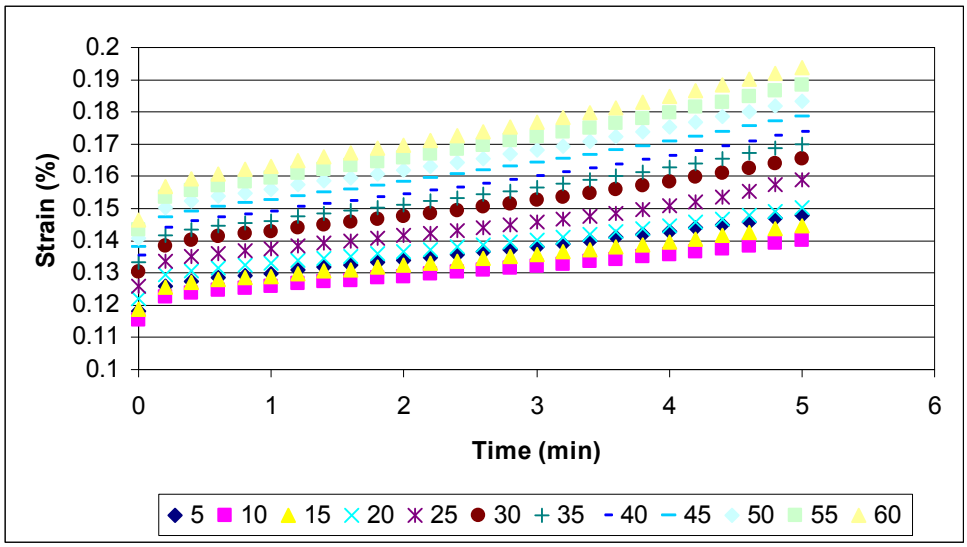

Figure 5.1: Creep strain at each test temperature for the load duration of a wood-bicomponent fiber composite.

The data is then transformed to logarithmic form and shifted to the reference temperature to create a mastercurve. The shift factor was plotted with respect to temperature, Both the Arrhenius and WLF models were fitted to the data, and it was found that the WLF equation fit the data the best (Std error 112.3 for WLF, 122.6 for Arrhenius) (See Figure 5.2 for a representative sample). The constants $C_1$and C_2 for the WLF equation are 2.09E7 and 4.125E8 respectively.

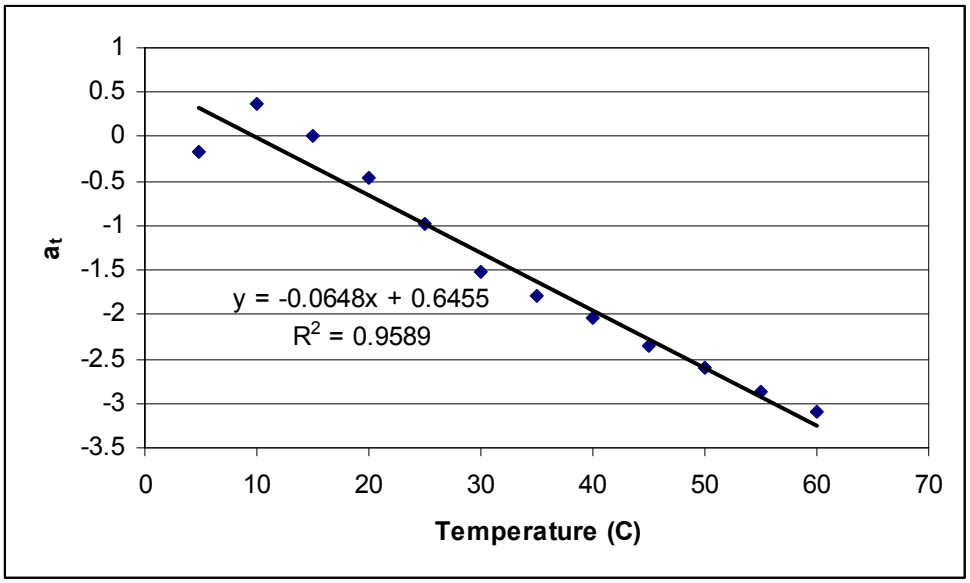

Figure 5.2: Shift factors obtained for a representative sample of a wood-bicomponent fiber composite

The reference temperature selected was 15^0C (shown in Figure 5.3). The option of applying both a horizontal and vertical shift factor was selected from the software menu. The constants for vertical shifting were determined as zero, indicating that the software did not detect the need for a vertical shift for the material. This is in agreement with results obtained by Pooler and Smith (2004), who utilized similar principles in determining whether a vertical shift is required. Single values seen below the curves are artifacts resulting from the three point bending clamp in question, according to TA Rheology Services.

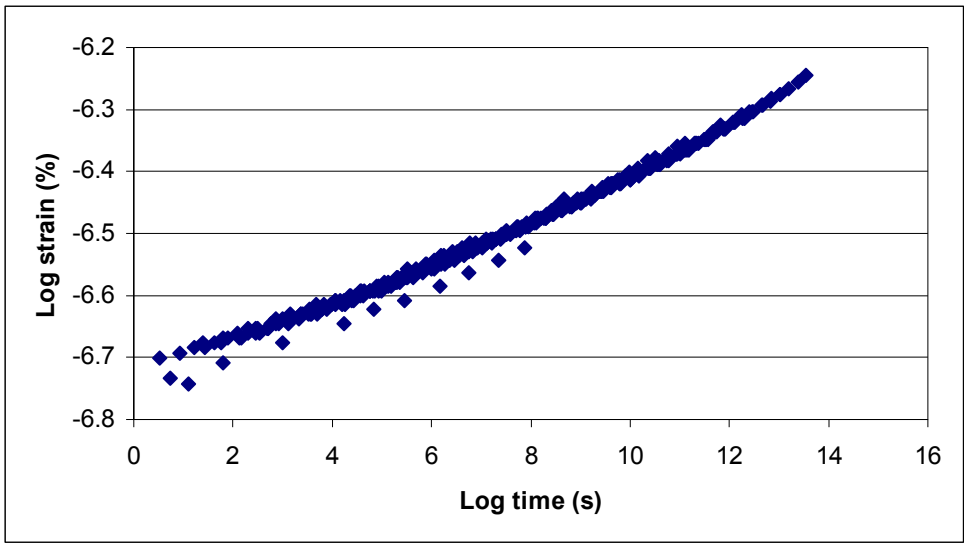

Figure 5.3: Creep mastercurve for strain data of a representative sample of a wood-bicomponent fiber composite.

The data was then transformed back to strain and time to obtain the overall creep performance of the material. Figure 5.4 illustrates the creep behavior of representative samples of the bicomponent fiber sheet and wood-bicomponent fiber composite with the fiber alignment parallel to the longitudinal axis of the testing beam (bicolong and panellong respectively), the bicomponent fiber sheet and wood-bicomponent fiber composite with the fiber alignment perpendicular to the longitudinal axis of the testing beam (bicocross and panelcross) and the creep result for MDF. The data was normalized with respect to bicocross for comparative purposes (Figure 5.5). It can be seen that the bicomponent fiber sheets has far greater initial creep, with bicolong exhibiting the highest initial creep. MDF exhibited the lowest initial creep, with the wood-bicomponent fiber composite in between.

Of note is the behavior of the wood-bicomponent fiber composite sample with the fiber alignment perpendicular to the longitudinal axis of the sample beam. Initial creep followed the behavior of the MDF. After approximately 150000 s, the creep increased before it started behaving similarly to panellong. This behavior was observed in all samples. Further investigation by means of full length creep tests is needed to describe this phenomenon, due to the fact that the assumptions for TTS might not be met for this specific configuration. The materials reached a state of steady creep after approximately 300000s. Panelcross, as mentioned earlier, displayed a secondary portion of transient creep, and only reached steady state creep after approximately 400000s.

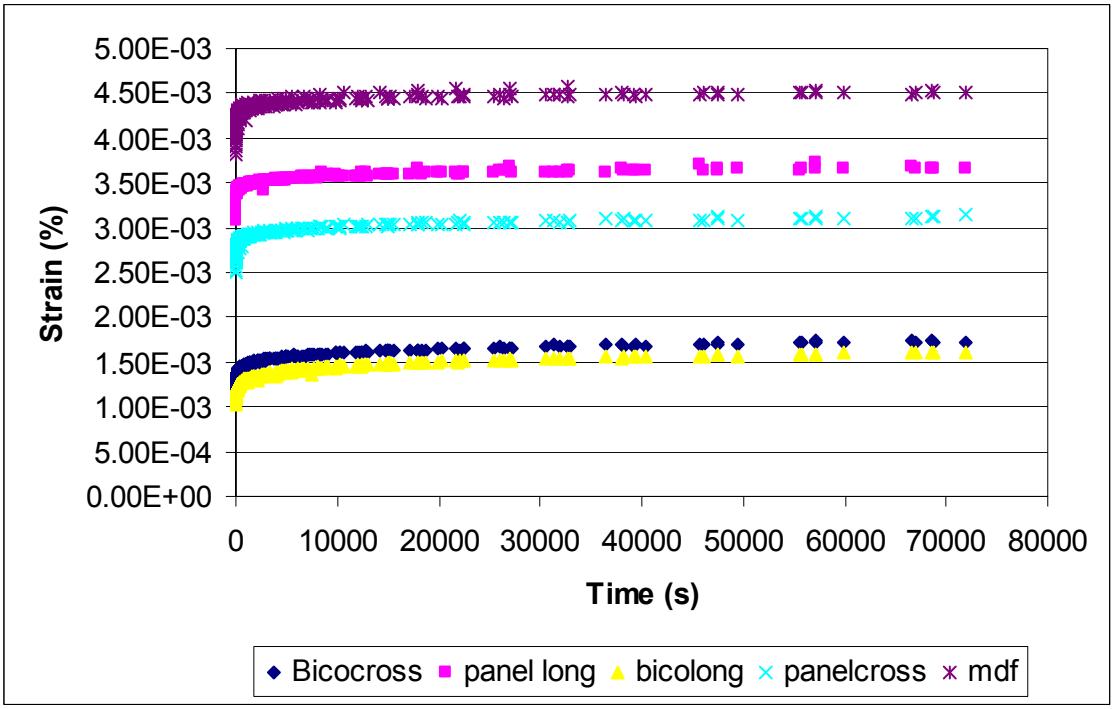

Figure 5.4: Long term creep behavior of the bicomponent fiber sheet, the wood-bicomponent fiber composite and MDF as determined by TTS.

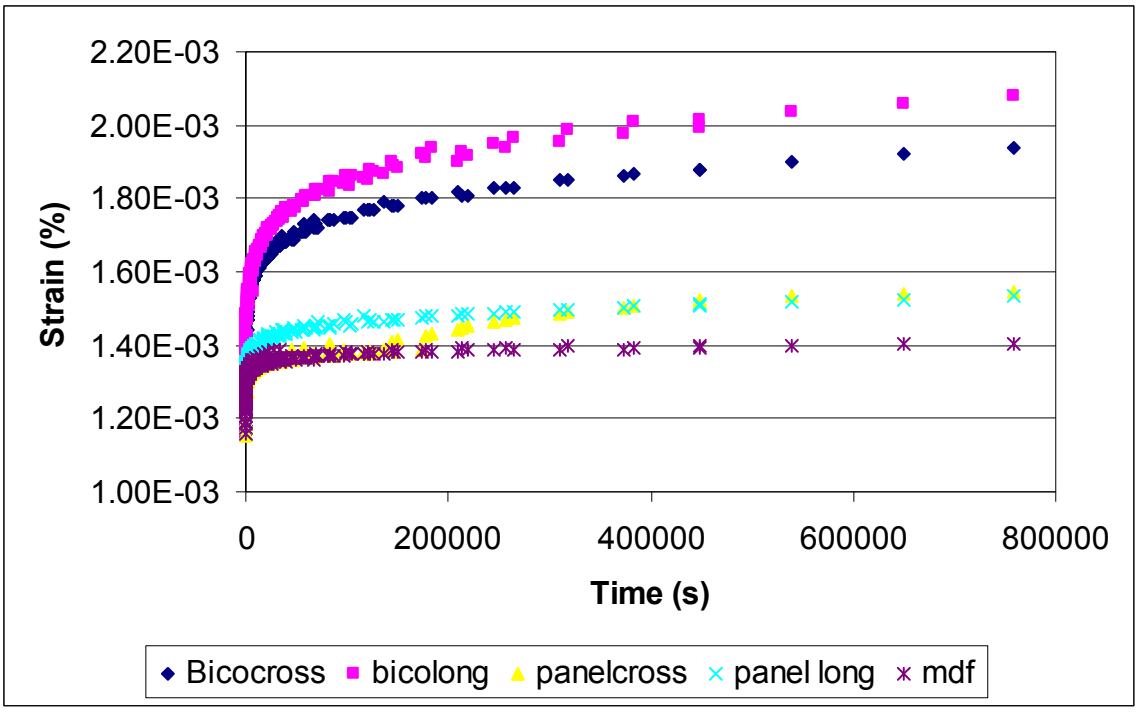

Figure 5.5: Normalized long term creep behavior of the bicomponent fiber sheet, the wood-bicomponent fiber composite and MDF as determined by TTS.

5.6) Conclusions

Short term creep tests were shifted by means of TTS to a reference temperature of 15^0C to obtain the long term creep behavior of a wood-bicomponent fiber composite. These results were then compared with the creep behavior of the constituents of the composite. Initial creep for the composite is greater than that observed in MDF as a result of the contribution of the bicomponent fiber reinforcement.

5.7) References

Alwis K.G.N.C. and C. J. Burgoyne. 2006. Time-Temperature Superposition to Determine the Stress-Rupture of Aramid Fibers. Applied Composite Materials 13: 249-264.

Anon. ??. Thermal analyses brief: Application of time temperature superposition principles to DMA. TA Instruments technical note.

Bogren, K.M., E.K. Gamstedt, R.C. Neagu, M. Akerholm and M. Linstrom. 2006. Dynamic–Mechanical Properties of Wood–Fiber Reinforced Polylactide: Experimental Characterization and Micromechanical Modeling. Journal of Thermoplastic Composite Materials, 19(6): 613-637.

Davidson, R. W. 1962. The Influence of Temperature on Creep in Wood. Forest Products Journal: 377-381.

Gamalath, S. 1991. Long Term Creep Modeling of Wood Using Time-Temperature Superposition Principle. Ph.D. Dissertation. Wood Science and Forest Products, Virginia Polytechnic Institute & State University, Virginia, USA, 1991.

Kelly, S. S., Rials, T. G. , and Glasser, W. G . 1987. Relaxation Behaviour of the Amorphous Components of Wood. Journal of Material Science (22): 617-624.

Pooler, D.J. and L.V. Smith. 2004. Nonlinear viscoelastic response of a wood-plastic composite including temperature effects. Journal of Thermoplastic Composite Materials 17: 427.

Salmèn, N. L. 1975. Viscoelastic Properties of in Situ Lignin Under Water-Saturated Conditions. Journal of Material Science 10: 3090-3096.

Tajvidi, M., R.H. Falk, J.C. Hermanson. 2004. Time–Temperature Superposition Principle Applied to a Kenaf-Fiber/High-Density Polyethylene Composite. Journal of Applied Polymer Science 7: 1995–2004.

Tissaoui, J. 1996. Effects of Long-Term Creep on the Integrity of Modern Wood Structures. Ph.D. Dissertation. Wood Science and Forest Products, Virginia Polytechnic Institute & State University, Virginia, USA, 1996.

Van Der Put, T. A. C. M. , "Deformation and Damage Processes in Wood," Delft University Press, 1989.